FOSSIL

DE#0542-8

DOE/PC/72016-T1
(DE87011194)

DEWATERING OF ULTRAFINE COAL

Final Report for the Period August 1984—December 1986

December 1986

Work Performed Under Contract No. FG22-84PC72016

For
U. S. Department of Energy
Pittsburgh Energy Technology Center
Pittsburgh, Pennsylvania

By
University of Pittsburgh
Pittsburgh, Pennsylvania

DISCLAIMER

DISCLAIMER

Available from the National Technical Information Service, U. S. Department of Commerce, Springfield, Virginia 22161.

Price: Printed Copy A07
Microfiche A01

Codes are used for pricing all publications. The code is determined by the number of pages in the publication. Information pertaining to the pricing codes can be found in the current issues of the following publications, which are generally available in most libraries: *Energy Research Abstracts (ERA); Government Reports Announcements* and Index *(GRA* and I); *Scientific and Technical Abstract Reports (STAR);* and publication NTIS-PR-360 available from NTIS at the above address.

Printed in the United States of America
USDOE Office of Scientific and Technical Information
Oak Ridge, Tennessee

DOE/PC/72016-T1
(DE87011194)
Distribution Category UC-102

DEWATERING OF ULTRAFINE COAL

Final Report

August 1984 - December 1986

Shiao-Hung Chiang
George E. Klinzing
Badie I. Morsi
John W. Tierney

Mohan Badgujar
Theresa Binkley
Yisun Cheng
Suxuan Huang
Ihtzaz Qamar
Ramraj Venkatadri

Chemical and Petroleum Engineering Department
University of Pittsburgh
Pittsburgh, PA 15261
December 1986

Prepared for the U. S. Department of Energy
Under Contract No. DE-FG22-84PC72016

TABLE OF CONTENTS

TABLE OF CONTENTS
(Continued)

SUMMARY AND DELIVERABLES

I. Particle/Filter Cake Characterization

A. Filter cakes formed with double-distilled water and washed with various wash ratios of surfactants were analyzed micrographically, and comparisons were made as to the performance of the different wash liquors.

B. Filter cakes formed with various concentrations of the collector DAH were successfully analyzed with the image analysis technique.

C. Micrographic analyses of the 10 μm coal particles were initiated using a more versatile TAS PLUS image analysis system.

II. Theoretical Modelling

A. Promising results were obtained based on the newly developed method of pore volume assignment.

B. The introduction of the concept of bond-flow correlation greatly improves the network model predicting the experimental desaturation curves.

C. Predicted results for treated cakes suggested that the effect of the presence of surface-active agents was adequately accounted for.

D. Work on modeling the two-phase flow process was initiated using two different approaches.

III. Enhanced Filtration/Dewatering

A. More electrokinetic data measurements were performed, which were used to explain the various phenomena observed in the dewatering of the treated cakes.

B. The effects of the various operating conditions on the filtration/dewatering characteristics of the 10 μm coal particles were assessed and comparisons with the -32 mesh coal were made as to its trends in response to changes in the operating conditions.

IV. Publications

A. "Dewatering of Fine Coal - Micrographic Analysis," Kakwani, R., et al., Powder Tech., 41, 239, 1985.

B. "Filter Cakes Washing with Chemical Reagents," Venkatadri, R./, and Chiang, S.-H., Filtration and Separation, 172, 1985.

C. "Effect of Surfactant Washing on Enhanced Dewatering of Fine Coal," Binkley, T., et. al., Fine Particle Symp. Ser., Hemisphere Publishing, 1986.

D. "Use of a Three-Dimensional Network Model to Predict Equilibrium Desaturation of Coal Filter Cakes," Qamar, I., et al., International Journal of Coal Preparation, 1986.

E. "Filtration/Dewatering Characteristics of 10 μm Coal Particle," presented at the 5th International Symposium on Drying, August, 1986.

V. Theses

A. "Effect of Surface-Active Agents on Filtration and Post-Filtration Characteristics of Fine Coal," Ph.D. Dissertation by R. A. Venkatadri, December 1984.

B. "Effect of Surfactant Washing on Enhanced Dewatering of Fine Coal," M.S. Thesis by T. O. Brinkley, April 1985.

C. "Application of a Three Dimensional Network Model to Coal Dewatering," Ph.D. Dissertation by I. Qamar, August, 1985.

VI. Deliverables

A. Computer Programs: programs written in standard FORTRAN language for the network model has been published.

B. Major Equipment:

1. Omnicon Alpha Image Analyzer and Accessories
2. HP-85 Mini Computer and Accessories
3. IBM PC and Accessories
4. Zeta Meter and Accessories

TECHNICAL DISCUSSION

I. Particle/Filter Cake Characterization

A. -32 Mesh Coal

1. Double-distilled Water Cake

In the previous report,[1]* micrographic data, i.e., surface-volume mean diameters of particle and pore, and porosity for washed cakes such as Triton-washed flocculated cakes and distilled water cakes washed with double-distilled water and Triton X-114 were presented. Since then, further work has been carried out with a different surfactant -- Aerosol-OT, in place of Triton X-114, in washing distilled water cakes. This serves the purpose of making comparisons of not only the dewatering performance of these reagents, but also of their influence on the cake structure.

For the series of experiments with Aerosol-OT, a different batch of coal, Batch 6, rather than Batch 4 for those with Triton X-114 and double-distilled water, has been utilized. In order to delineate any differences between batches, micrographic analyses of the dispersed sample taken from each batch have been carried out. The results are tabulated in Tables 1 and 2 with the corresponding log-normal plots in Figures 1 and 2. It should be noted that the two distributions look alike, except for the two extreme size ranges, 2 to 12.6 μm and 251.1 to 500 μm. Percentagewise, coal from Batch 6 has about two times more amount of small particles than that from Batch 4. However, coal from Batch 4 has almost five times more amount of big paricles than those found in Batch 6. Therefore, the surface-volume mean diameters come out to be 132.3 μm for Batch 4 and 81.2 μm for Batch 6.

---

*Parenthetical references palced superior to the line of the text refer to bibliography.

a. Log-normal Plots

Figures 3 to 5 depict the log-normal distribution of particles obtained by micrographic analysis in each of the five layers of the distilled-water washed cakes. It is apparent that there is a distinct segregation of small to large particles from the top to the bottom layer for the unwashed cake. This is made evidenced by the separation of the curves from one layer to another. The larger the separation of the curves, the more structured the cake, while the reverse indicates a homogeneous structure.[2] When a small amount of distilled water (WR = 2) is used to drain through the cake, no obvious change of the distribution is observed, i.e., the curves remain separated as shown in Figure 4. However, when the volume of wash liquor is increased (WR = 10), the curves seem to overlap (Figure 5), suggesting that less segregation occurs. This is substantiated by the comparison of the photomicrographs in Figures 6 and 7. For Cake D11 (WR = 10), small particles are seen to appear in the bottom layer of the cake. The same trend has been found with the surfactant-washed cakes. For example, with the same surfactant concentration, an increase in the wash ratio leads to relatively less particle segregation as seen in Figure 8 for WR = 2 and Figure 9 for WR = 10, both having a Triton concentration of 250 ppm.

Moreover, it is evident from the photomicrographs that with a small amount of wash liquor (WR = 2), some small particles are washed down only to the middle portion of the cake. But when a wash ratio of 10 is used, due to the large increase in the volume of wash liquor, a longer time is required for it to completely drain off the cake. This provides more contact between the particles and the wash liquor, causing the particles to be pushed even farther down the cake. In other words, some of the small particles that would otherwise remain in the top layer of the cake are able to reach the bottom

layer. Hence the severe stratification existing in unwashed cakes is destroyed and each layer now has more or less similar mixture of particles. The structure of the cake is thus rendered homogeneous throughout.

The log-normal plot of pore size distribution in Figures 10 and 11 substantiate the above mentioned arguments. The pores are not segregated from the top to the bottom layer. Instead, they are uniformly distributed through the cake. This phenomenon has some bearing on the filtration/dewatering characteristics of the cake, as will be discussed later.

b. Porosity

As mentioned above, washing causes the small particles to leave the top layer of the cake. Therefore, the spaces formerly occupied by these particles are replaced by pores, i.e., the narrow openings become relatively bigger. In fact, a loosely packed structure of the top layer has been observed visually in many washed cakes. As the porosity is measured by area fraction pore of the total area, this alteration in the cake structure may well be quantified by the porosity data. Table 3 lists the values of porosity obtained micrographically for the Aerosol-OT washed cakes. It is worth noting that for the same surfactant concentration, cakes washed with a larger volume of wash liquor (WR = 10), in general, give higher porosity than those washed with a wash ratio of two, particularly for the top layer. Data for the distilled water and Triton washed cakes indicate similar trend.

c. Surface-volume mean sizes

The cakes washed with Aerosol-OT have smaller particle and pore surface-volume mean sizes at each layer when compared to other cakes (see Table 4). This is attributed to the fact that Batch 6 coal has more small particles and less big particles than Batch 4 coal as mentioned above. Also, there are very slight changes in the pore size, the greatest

being less than 10 μm. When the particle and pore sizes for Aerosol-OT washed cake using WR=2 is correlated by the linear regression method, as shown in Figure 12, the correlation coefficient is found to be 0.774. In the case of Triton washed cakes, a wash ratio of 10 gives the best result, as illustrated in Figure 13. (The correlation coefficient is 0.894.)

d. Geometric-volume mean size

A linear relationship has been found to exist between the geometric volume mean sizes of particles and pores in the -32 mesh Pittsburgh coal filter cakes.[3] For washed cakes the same relationship has been observed with distilled water (Figure 14), Triton X-114 (Figures 15 and 16) and Aerosol-OT (Figures 17 and 18) washed cakes. The data are presented in Table 5. The slope of the straight line decreases from Figures 14 to 18, suggesting that the rate of change of the pore size with respect to the particle size diminishes.

2. Amine Cakes

It has been reported[1] that the addition of DAH, a cationic collector, to the coal slurry improves the filtration/dewatering characteristic of the slurry. Some of these cakes have been consolidated and analyzed micrographically. The results are presented in Table 6. The data are seen to be reproducible. There is a trend of increasing apparent mean particle size (indicating floccution) with an increase in the amine concentration. However, at an extremely high concentration (2000 ppm), the apparent mean particle size decreases.

B. 10 μm Coal

Work on the 10 μm coal has been carried out. The wet ground sample was provided by DOE in sealed plastic jars to avoid loss of fines during transport. Prior to each experimental run, the jar is rolled very slowly over

an electrically-driven roller for more than 20 minutes to assure proper mixing and uniform concentration of the sample.

1. Dispersed Particle Size Analysis

After the wet coal has been thoroughly mixed, a sample is withdrawn from the jar, placed in a dish and dried overnight in an oven. Clusters of coal particles are broken down by means of a spatula. Then the sample is dried for some more time. Now the sample is ready for analysis.

The dispersed particle size analysis has been carried out on a TASIC PLUS image analyzer coupled with a LEITZ Orthoplan microscope equipped with automatic stage movement. The result of this analysis is plotted in Figure 19. The surface-volume mean diameter is found to be 10 μm. This is plotted against the mean particle size in the cake (determined to be 5.4 μm), as in Figure 20. It can be seen that the agreement with the predicted correlation is quite good. As the particle size decreases, deviation of the dispersed particle size, as measured, from the mean particle size in the cake becomes less pronounced. This is probably due to the fact that small particles tend to lose most of the irregularities of their edges because of resolution limitation so that they can adequately be approximated by spheres. It should be mentioned here that in the dispersed particle size analysis, the diameter of each particle is taken as the longest chord cut by the boundary of the particle, while in the analysis of cakes, all the chords cut by each of the particles are used in determining the surface-volume mean size via the Cahn and Fullman technique.

2. Compressiblity of the Cake

Before proceeding to any filtration/dewatering experiment, one important problem to consider is that whether the cake made up of such tiny particles remains incompressible under the chosen operating condition. This

is important because subsequent calculations of filtration/dewatering data are based on this result. Therefore, a series of experiments were carried out under different levels of applied vacuum (67 ~ 93 kPa). The results are listed in Table 7.

II. Theoretical Modelling (Network Model)

A. Adjustment of Model Parameters

1. Bond-Flow Correlation Fraction

In the last annual report[1], a newly-developed model parameter, the bond-flow correlation fraction (FRCTN) was introduced. Its usage and effect on the resulting equilibrium desaturation curve were briefly discussed. Some results for the case of pore volumes being assigned only to the bonds were also presented. The parameter FRCTN was seen to bear a great influence especially on the initial part of the equilibrium desaturation curve. Furthermore, it was shown that use of an optimum value of FRCTN (0.4 for -32 mesh and 0.0 for -100 + 200 mesh) would yield an equilibrium desaturation curve that agrees better with the experimental data than one having no flow correlation at all (FRTN = 1.0).

Physically, the bond-flow correlation parameter provides for the presence of channels in the coal filter cakes. In fact, micrographic analyses of some of the -32 mesh coal filter cakes washed with solution showed that some of the large pores in the bottom layer contained some migrated small particles which are not present in unwashed cakes nor in some other large pores in the same layer. This indicates that migration of the small particles was not uniform and it is thus envisioned that there may exist preferential flows which are designated as channels.[4] Unfortunately, no quantitative measure of these channels has yet been developed so that the value of FRCTN is determined only

by comparing the predicted desaturation curves with the experimental curves. For example, a comparison of the curves reveals that a fraction of 0.4 for both -32 mesh coal (Figures 21 to 26) and -200 mesh coal (Figures 27 to 31) and 0.0 for -100 +200 mesh coal (Figures 32 to 35) give the lowest maximum deviation for each case, and are hence considered the appropriate values to use in predicting the equilibrium properties of the coal cakes investigated.

A smaller value of FRCTN for -100 +200 mesh coal as compared to -32 mesh and -200 mesh coals implies that there are more channels present in the former than in the latter. Note that the -100 +200 mesh coal is in a narrow size fraction in which there are no very small or very big particles. This leads to a cake structure wherein relatively large pores are uniformly distributed throughout, which in turn resembles the aforementioned channels. On the other hand, the presence of small particles in the -32 mesh coal may block some of the large pores and the channels which otherwise would have existed as in the -100 +200 mesh coal.

2. Assignment of Pore Volume

In addition to the parameter FRCTN, the three options of pore volume assignment together with their pros and cons were elucidated in the last report:[1] (a) assigning volumes to both the bonds and the nodes with the assumption that the volume of a bond is equal to the volume of the smaller adjacent node, was found to result in a relatively low final moisture content; (b) assigning the volumes only to the bonds, tends to predict a relatively high final moisture content. This option is considered as representing only an extreme case of volume assignment and its use is limited; it cannot predict very low final moisture content. And (c), the volume is assigned to the bonds and nodes by assuming that volumes corresponding to pores larger than a specified pore size are assigned to the nodes. The last

option imparts flexibility to the existing model and leads to the way of accounting for the presence of surfactant. This had also been delineated and elaboration will be presented in the next section.

A comparison of the results obtained revealed that by keeping the other variables unchanged and varying only the method of pore volume assignment, both options (b) and (c) result in similar equilibrium desaturation curves. This is because for distilled water cakes, only a small fraction of the total pore volume is assigned to the nodes. Yet option (c), when compared to option (b), provides a more uniform effect on the curve, i.e., it is not only the initial part of the curve that is drawn closer to the experimental curve, but it is the entire curve.

It is also apparent that, in general, the model does not work as good where fine coal, such as -200 mesh coal is concerned, particularly in the prediction of the final moisture content. More work is therefore necessary to achieve better results.

B. Effect of Surface-Active Agents on Equilibrium Desaturation

As mentioned above, the effect of surface-active agents on the equilibrium desaturation characteristics of the coal cakes has been accounted for in the model. It is done as follows. In the Laplace Equation,

$$P_c = 4 \gamma \cdot \cos \theta / D_e \qquad (1)$$

where P_c is the capillary pressure. The surface tension of the fluid, γ, is known experimentally. The contact angles measured are only relative values and cannot be used directly in the equation. D_e is the controlling or entry diameter of a pore and is not known either. What is measured micrographically is the equivalent diameter, D_{eq}. Therefore, by transforming Eq. (1), we have

$$P_c = 4\ \gamma/CONST \times D_{eq} \qquad (2)$$

where CONST an entry diameter constant which combines the effect of contact angle and the relationship between the entry diameter and the equivalent diameter. Its value is determined as follows. First, the model is used to calculate the capillary pressure curve by using experimental γ, micrographic distribution, contact angle of 0 and CONST as 0.5 (the same as that used for distilled water cakes). The calculated curves are then compared with the experimental curves. The capillary pressure values corresponding to a 50 percent saturation are calculated from these curves and are given in Columns 4 (model) and 5 (experimental) of Table 8. Column 6 gives the ratio of these values. Then it is assumed that the entry diameter constant for each case changes by the same ratio as those given in Column 6, so that the new CONST is obtained by multiplying 0.5 with these ratios, as listed in Column 7.

Using the modified entry diameter constants, the capillary pressure curves are recalculated with the contact angle still taken as 0. The results are plotted (Figures 36 through 41). It can be seen that the predicted curves agree well with the experimental curves. The final saturation values are also in good agreement with the experimental values. Hence it is obvious that the use of a modified entry diameter constant can adequately account for the presence of surfactants.

However, it is also clear that in order to evaluate the modified CONST, the experimental capillary pressure curve must be available. This obviously makes the use of the model very limited. Therefore, an attempt has been made to correlate the required entry diameter constant with measured data other than the actual capillary pressure curve. These are the surface tension, γ, of the fluid and the contact angle, θ. The product of γ and cos θ for each

case is listed in column 8 of Table 8 and plotted against the modified CONST in Figure 42. Thus for any new surfactant cake, if the product of γ and cos θ is known, the value of the modified CONST can be obtained from Figure 42 and the prediction of the capillary pressure curve can be made independent of the experimental capillary pressure curve.

It is interesting to note that although the correlation given in Figure 42 has been developed without using the distilled water case, when the product of the surface tension (72 dynes/cm) and the cosine of the measured contact angle (about 100 degrees) for distilled water is used in this figure, the corresponding value of CONST is very close to 0.5, which has already been obtained by comparing the curves.

Nevertheless, this correlation represents only a first approximation. More work is necessary in order to determine the real shape of the curve and thus obtain a more reliable correlation

C. Comparison of Equilibrium Final Saturations

Based on the above discussion, it should be noted that the final saturation values predicted by the model depend upon the pore size distribution and the pore volume assignment. The bond-flow correlation and the entry diameter constant have little effect on the final saturation.

Table 9 presents a comparison of the predicted and the experimental equlibrium final saturations of cakes for which the equilibrium desaturation results have been given previously. In general, the predicted values agree fairly well with the experimental data. As the prediction depends primarily on the pore size distribution and the pore volume assignment, it can be deduced that the method used in this study for the assignment of pore volume among the bonds and the nodes of the network gives reasonable results.

D. Pore Size Distribution Obtained from Dispersed Particle Size Distribution

All the equilibrium desaturation results presented so far, for distilled water cakes, have been predicted by using actual micrographic pore size distribution. However, it has been previously shown[3] that this distrubtion can be related to the dispersed particle size distribution through the following series of equations:

$$X_{gv}\ (\text{pore}) = 12.051 + 0.548\ X_{gv}\ (\text{part.}) \quad (3)$$

$$\sigma_g\ (\text{pore}) = 0.422 + 0.737\ \sigma_g\ (\text{part.}) \quad (4)$$

$$X_{gv}\ (\text{cake}) = 29.33 + 0.303\ X_{gv}\ (\text{disp.}) \quad (5)$$

where the 'X' is the size, the subscript 'gv' indicates geometric mean size (volume), 'part'. indicates particle and 'disp.' indicates dispersed. 'σ_g' is the geometric deviation.

It is interesting to note that the geometric deviation values for the dispersed particles, for the particles and for the pores in the cake do not differ greatly from one another; the average value being 2.84. Therefore, for the -32 mesh coal distilled water cakes, a representative pore size distribution can be estimated from a knowledge of the dispersed particle size distribution as follows: the dispersed particle size distribution is determined first. The geometric mean size of the particles in the cakes is then evaluated by Eq. (5) and the geometric mean pore size follows from Eq. (3). With this and taking 2.84 as the geometric deviation of pores, a pore size distribtuion can thus easily be generated using the log-normal function.

Based on the above discussion, a representative pore size distribution for -32 mesh Pittsburgh coal (Batch 1) has been computed and reproduced in

Table 10. The geometric mean size of the dispersed particle thus calculated is 84 μm, that of particle in the cake is 54.7 μm and that of the pore is 42 μm. The pore size distribution presented in Table 10 has been used to generate an equlibrium desaturation curve, which is shown in Figure 43. The agreement between this curve and the experimental one is good with a maximum absolute deviation of 11%. Furthermore, it should be noted that this curve agrees well with the predicted curve in Figure 23, which is obtained by using the actual micrographic pore size distribution. Therefore, it is possible to carry out the modeling of the equilibrium desaturation process by employing a representative pore size distribution, which in turn is obtained from the measurement of the dispersed particle size distribution. Remember that the determination of the dispersed particle size distribution is a simple task. On the other hand, micrographic analyses of a filter cake is a tedious and very time-consuming process. Consequently, it makes the model more useful and more practical to predict equilibrium desaturation characteristics of coal filter cakes.

E. Dynamic Operation

1. Single-Phase Flow

The modeling of single-phase flow is characterized by calculating single-phase permeabilities. The calculation technique has been briefly discussed in the previous report.[5] For the present work, a 15 x 15 x 15 bond-flow correlated network with simple cubic lattice, instead of a bond-correlated network with face centered cubic lattice, is used. The set of model parameters which gives the best results for equilibrium desaturation (FRCTN is 0.4 for -32 mesh and -200 mesh and is 0.0 for -100 +200 mesh) has been used. The bond average diameter constant is determined to be 0.6. Figure 44 depicts the comparison between the predicted and the experimental

single-phase permeabilities obtained with the corresponding data listed in Table 11. The dotted line in Figure 44 is obtained by a linear least square fit. It has a slope of 0.99 (cf a slope of 1.0 for a perfect fit). The correlation coefficient is 0.8. This clearly suggests that using a bond-flow correlated network not only improves the equlibrium desaturation results but also gives very good single-phase permeability predictions.

2. Two-Phase Flow

The two-phase flow behavior of a coal cake is represented by saturation versus time curves. Due to the large computing time requirements, the model dimensions used are 10 x 10 x 10. Again, a bond-flow correlated network with a simple cubic lattice has been employed together with the optimum model parameters. Two methods have been used in this work to simulate these curves.

a. Method 1 (Dynamic calculation)

Procedure:

(1) For a given cake the network is generated and the single phase flow rate is calculated. A relative flow rate of water is defined as the ratio of the water flow rate at the exit face of the partially desaturated network to that of the fully saturated network.

(2) Water in the front face nodes is displaced and a new saturation value is calculated. Pressure distribution at all the nodes are evaluated by a mass balance at each node. The driving force across a bond whose one end has been invaded by air is reduced by an amount equal to the capillary pressure of that bond. Then new values of exit-face water flow rate and relative flow rate are determined.

(3) The bonds connected to the nodes invaded by air are located. The driving force is now equal to the pressure at the invaded node minus the pressure at the other node and the capillary pressure. The bond which requires the least time is displaced and new values for saturation, pressures, and realtive flow rates are calculated.

(4) Step 3 is repeated until no bond can be displaced.

(5) The relative flow rates are converted to flow rate data, which in turn is integrated with the saturation values to yield the required time versus saturation data, viz., dewatering curve.

b. Method 2 (Using the files of paths)

This method is essentially the same as that reported previously.[3] Basically, it is assumed that the partially desaturated states of the network during dewatering can be approximated by successive equlibrium states.

Figures 45 through 48 illustrate a comparison of the model calculated dewatering curves with the experimental curves for -32 mesh and Figure 49 for -100 +200 mesh coal filter cakes. It is apparent that Method 1 gives a better agreement of the results with the experimental curves than Method 2. The major differences between the two methods are summarized as follows.

In Method 1, dynamic calculations are performed and the dewatering of the network is carried out one bond at a time. In Method 2, the dewatering is represented by successive equilibrium states and therefore the dewatering calculations are only approximate. In Method 1, the driving force is one step whereas in Method 2, it is applied in increments. In Method 1, the bond which takes the least time to empty out is emptied first while in Method 2, it is the bond with the largest diameter that is emptied first.

Method 1 is obviously more precise than Method 2 but it requires significantly greater computing time. For -32 mesh coal cakes, Method 1 gives dewatering curves which are in good agreement with the experimental curves. However, this is not so for the -100 +200 mesh cakes (Figure 49). This can be attributed to the fact that this filter cake has a high single-phase permeability and as such the experimental curve obtained is not as accurate as that obtained with other size fractions. Moreover, the dewatering curves for -100 +200 mesh coal are not enough. Therefore, more work is needed in this area.

F. Use of the Model for Other Coals

Discussions in the previous sections show that the network model presented can successfully predict the filtration/dewatering characteristics of certain size fractions of Pittsburgh Coal. Question arises as to how the model works with other types of coal. Hence the model has been used to predict the equilibrium desaturation of a -30 mesh Betteshanger coal, the capillary pressure curves of which have been reported by Gray.[6] The pore size distribution employed is that of Table 10, since the distribution for the aforementioned coal sample is not available. The results are plotted in Figure 50. It should be noted that the agreement between the calculated and the experimental curves is good, indicating that the model can in fact be used for coals other than Pittsburgh coal. However, the agreement is not as good as that obtained for Pittsburgh coal. It is speculated that a stronger bond-flow correlation is needed in this case.

III. Enhanced Filtration/Dewatering

A. -32 Mesh Coal

1. Washing Experiments

As mentioned in the first section of this report, in addition to the distilled water and Triton X-114, Aerosol-OT has been employed to wash the distilled water cakes formed under similar conditions. The results are listed in Table 12, including the data for the other wash liquor for comparison. It is clear that washing the cake with distilled water does not change its desaturation characteristic, but with a surfactant solution such as 250 ppm of Triton X-114 with WR = 10, a final moisture content of as low as 0.1 (versus a value of about 0.25 for unwashed cake) has been registered. Increasing the concentration beyond this point, however, does not effect further desaturation of the cake. In the case of Aerosol-OT, the optimum concentration is found to be 100 ppm with WR = 10. Apparently, a wash ratio of 10 consistently gives better dewatering results than a wash ratio of two. The effect of washing may be due to two factors. First, washing small particles into preferential flow paths (channels) reduce both single and two phase permeabilities of the filter cake, but increases the homogeneity of the two phase displacement. It is the increase in homogeneity that improves displacement efficiency leading to a lower residual saturation. Secondly, the surfactant changes the surface properties of the coal and thus results in a reduction of capillary forces and the final moisture content.

2. Adsorption Isotherm

a. Triton X-114

It has been previously reported that the adsorption isotherm of Triton X-114 on the Pittsburgh coal (6% ash) consists of three distinct regions[5]. However, when the same surfactant was tested on Upper Freeport

coal (35% ash), the existence of a third region has not been detected. (See Figure 51.) This indicates that hemi-micelle formation occurs in Region II and association with the hydrocarbon chains has become the prevailing mechanism for Upper Freeport Coal. On the other hand, hemi-micelle formation may have occurred to a lower extent in Region II of Pittsburgh coal, as evidenced by a lower slope of the isotherm and thus association between hydrocarbon chains begins at a much higher concentration, after the formation of the monolayer. Moreover, it is evident that the high ash coal has a greater adsorption of the surfactant except at very low dosages. Hence, reagent consumption for Upper Freeport coal is expected to be a lot more than that for Pittsburgh coal.

Let us now examine the free energy curve (Figure 52) for Triton X-114 on Upper Freeport coal. Two distinct regions are observed, which correspond favorably with the adsorption isotherm under the same conditions. In the first region, the decrease in the negative free energy has been attributed in the literature[7] to the interaction of the CH_2 groups, as suggested earlier. In this region, the Van der Waals attractive forces are large compared to the cationic repulsion of the head groups. As hemi-micelle formation begins, the free energy should be constant, as described by Fuerstenau[8], since adsorption is now occurring on a new surface: one of hydrocarbon chains. The absence of a flat region in Figure 52 indicates that the hemi-micelle formation is rapid, preventing the formation of a region of constant free energy. This further decrease in the negative free energy at higher concentrations is attributed in the literature[17] to adsorption in the bilayer, as adsorption sites are exhausted. The reverse orientation contributes to an increase in free energy of the system (i.e., a decrease in the negative free energy). This is evident at higher concentrations. The

change in the excess free energy of 5-7 kcal/g mole is typical of physical adsorption. No further attempt was made in this investigation to examine the free energy characteristics of the reagents as they were calculated values from adsorption data and not measured independently.

3. Zeta Potential Characteristics

Figure 53 represents the electrokinetic characteristics of the nonionic surfactant Triton X-114. It is apparent that the IEP is reached at a relatively low equilibrium concentration of the surfactant, after which there is virtually no change in the zeta potential value. This indicates that the charge in the Stern layer is quickly altered with the replacement of the counter-ions by the uncharged surfactant ions. A nonionic character is thus imparted to the coal surface, which results in the immobility of the particle. Therefore, it is deduced that if a nonionic reagent has adsorbed on a colloid to the extent of a monolayer and if the nonionic reagent is also predominant in the bulk phase, the resulting zeta potential would be close to the IEP[9]. Nevertheless, there is little information available in the literature about the adsorption of nonionic reagents with their effect on the colloid stability and much remains to be explored in this area.

On the other hand, the nonionic frother, MIBC, exhibits a different behavior. As shown in Figure 54, there is only little variation in the zeta potential as the MIBC concentration is increased. The slight decrease in the negative zeta potential at a high concentration has been attributed mainly to a small increase in particle size. It appears that unlike the nonionic surfactant, Triton X-114, the nonionic frother MIBC does not neutralize the charge in the Stern layer. Moreover, it has been observed that a very long time is needed for MIBC to be adsorbed on coal, which implies that MIBC molecules do not approach the double layer of the coal particles quickly

enough to replace the counter-ions in the Stern plane and hence the relatively little effect on the zeta potential. Campbell and Sun[10] have also reported very little change in the zeta potential for MIBC adsorption on coal. Klassen and Mokronsov[11] state that from this insignificant change in the zeta potential, it is difficult to say with any certainty whether or not adsorption of alcohols on the coal surface has taken place. Our data so far indicates that a short contact time has no bearing on the electrokinetic properties as it takes a long time for MIBC to be adsorbed on coal.

4. Wettability Characteristics of Reagents

Figures 55 and 56 depict the variation of contact angle with the concentration of Accoal-Floc 1201/Triton X-114 combination and DAH, respectively. Apparently, they show similar trend as Aerosol-OT and Triton X-114. There is a plateau followed by a decline in the contact angle values as the reagent concentration is increased.

In fact, a qualitative estimate of the relationship between the contact angle values and the wettability of the reagent can be obtained by implementing the method suggested by Zisman, et al.[12]. According to them, a plot of γ_{LV} versus $\cos\theta$ could be extrapolated to the value for $\cos\theta = 1$ (indicating complete wetting), at which the surface tension is termed "critical surface tension," γ_c. A typical plot is presented for MIBC in Figure 57. It is clear that the lower the γ_c value, the less wetting is the reagent. The same analysis has not been made for the other reagents because of lack of data points at low surface tension values and extrapolation is subject to error.

At a constant value of γ_{LV}, the lowering of the solid-liquid interfacial tension, γ_{SL}, is directly related to the extent of adsorption of the liquid on the solid phase. At a particular value of γ_{LV}, different reagents may adsorb

differently and yield different γ_{LV} values[13]. since it is difficult to experimentally determine γ_{SL}, an elegant and direct approach has been developed by Lucassen-Reynders[14] to relate wettability to adsorption. By combining the Gibbs' Adsorption equation and the Young-Dupre relation, it can be shown that

$$\frac{d(\gamma_{LV} \cdot \cos\theta)}{d\gamma_{LV}} = \frac{\tau_{SV} - \tau_{SL}}{\tau_{LV}} \qquad (6)$$

where τ_{SV}, τ_{SL} and τ_{LV} are the surface excess of adsorption (essentially the extent of adsorption) at the respective interfaces. For adsorption of reagents on coal, τ_{SV} can be considered negligible. The integrated form of Equation 6 indicates that a plot of $\gamma_{LV} \cdot \cos\theta$ versus γ_{LV} should be a straight line with a slope of $(-\tau SL/\tau LV)$. This is an indirect measure of the relative amount of adsorption at the respective interfaces, which in turn represents the wetting behavior of the reagents.

Figure 58 is a plot of $\gamma_{LV} \cdot \cos\theta$ versus γ_{LV} for Aerosol-OT. The data are seen to be fitted by two straight lines of different slopes. For lower surfactant concentrations (higher γ_{LV}), the adsorption is much greater, as indicted by the steeper slope of the line. It can also be seen that there is hardly any increase in the amount of adsorption when γ_{LV} is below 42 mN/M. This value corresponds to an initial concentration of about 6×10^{-6} mf for Aerosol-OT, which in turn corresponds to an equilibrium concentration of 1.4×10^{-6} mf. This is approximately the concentration at which monolayer formation occurred.

The same argument is valid for the other reagents studied. (See Figures 59 through 61.) The "break point" in the method of slopes corresponds closely to the concentration for monolayer formation as read from the respective

isotherms. This is quite remarkable, considering that the contact angles measured are not the true but only the relative values. Hence we come to the interesting conclusion that the contact angle measurement is another way of corroborating results from the adsorption experiments and that the adsorption influences the wettability of reagents in a complex manner.

It may be recalled that the adsorption isotherm of the flocculant is linear[1] and as such, does not provide a direct indication of the point of monolayer formation. Nonetheless, from the method of slopes just discussed, this point has been estimated to be at γ_{LV} = 47 mN/M, corresponding to a concentration of 1.3 x 10^{-10} mf or an adsorption density of 2.6 x 10^{-11} gmole/gm.

In the case of Triton X-114, however, because of the excessive wetting at high concentrations, as indicated by a contact angle value of 5^{o}, the above analysis cannot be carried out satisfactorily.

5. Final Moisture Content

a. Triton X-114

The adsorption of nonionic surfactant Triton X-114 on the high ash Upper Freeport coal and the relatively clean Pittsburgh coal reveals striking differences (Figure 51). A comparison of the relative lowering of the moisture content for the same equilibrium concentration in solution is revealing. At an equilibrium concentration of only 3 x 10^{-8} mf, the final moisture contents are comparable but as the equilibrium concentration is increased, Pittsburgh coal exhibits lower moisture content by at least two percentage points. At the same time, the surfactant adsorption on the Freeport coal is greater than that on the Pittsburgh coal at a given equilibrium concentration. This indicates that the clean coal, i.e. Pittsburgh coal, adsorbs less and yet reduces the moisture by a greater extent

(the moisture content for cakes formed with distilled water are comparable for both types of coal, around 0.24 kg water/kg coal). Hence the Pittsburgh seam coal can be considered to be superior to the Upper Freeport coal in terms of adsorption and dewatering characteristics.

b. Aerosol-OT

Figures 63 and 64 bring out the variation of moisture content for Aerosol-OT with respect to the adsorption isotherm and surface tension characteristics. It can be observed from Figure 63 that the correspondence between the adsorption isotherm and the moisture content regions is good. In Region I, the moisture content decreases gradually to about 0.165 kg water/kg coal. In this range of concentration, the surface tension decreases by about 9 mN/M (from 65 mN/M to 56 mN/M). According to the adsorption model proposed for Aerosol-OT, the molecule has a flat configuration at low density, which does not alter the hydrophobic nature of the coal surface. Hence, the decrease in moisture content in this case must be primarily due to a decrease in surface tension.

In Region II, there is a steeper decrease in moisture content, from 0.165 kg water/kg coal to 0.125 kg water/kg coal for a smaller change in equilibrium concentration. In this region, the surface tension decreased from 56 mN/M to about 45 mN/M. Also, by the adsorption model, the molecule will adopt an L' configuration to accommodate more incoming molecules. This will expose one hydrophobic tail group towards the aqueous phase, rendering the coal surface hydrophobic. The combined effect of a drop in surface tension and a favorable orientation contributes to the decrease in moisture content.

In Region III, the moisture content increases to about 0.17 kg water/kg coal after registering a low value of 0.125 kg water/kg coal. This is a surprising result since surface tension continues to decrease from 45 mN/M to

about 36 mN/M. Further, the adsorption model predicts that the coal surface should be rendered more hydrophobic after monolayer coverage has occurred, due to molecules adsorbing in reversed orientation. A likely explanation for this apparent inconsistency in analysis could be due to the uncertainty in determining the point of exact monolayer coverage. It is possible that monolayer coverage has already taken place before reaching the equilibrium concentration at which moisture content increases again, and not as shown in the figure for the adsorption isotherm (Figure 63). It has been well documented in the literature[15, 16] that at high concentrations of Aerosol-OT, adsorption will unfavorably affect the hydrophobicity, especially as bilayer (or hemi-micelle) adsorption takes place on coal particle surface. Hence, it must be concluded that the decrease in hydrophobicity (also implying a sharp decrease in contact angle) due to adsorption must be responsible for the increase in moisture content. This effect must be predominant enough to offset the decrease registered in surface tension of 9 mN/M.

The HLB (Hydrophile-Lipophile Balance) index system was devised to provide a way of comparing the relative hydrophobicity of pure surfactants, based on the relative contribution of various groups such as CH, CH_2, and OH in the surfactant molecules. A low HLB value indicates greater hydrophobicity and vice versa. The HLB is calculated from the following equation in the literature.[7]

$$\text{HLB} = \Sigma \text{ group values for hydrophilic groups} - \Sigma \text{ group values for hydrophobic groups} + 7 \qquad (7)$$

For the surfactant Aerosol-OT, the HLB value is low -7.6, whereas for Triton X-114, it is higher (+12.4). This suggests that Aerosol-OT should be more effective in imparting a hydrophobic nature to the coal particles than Triton X-114. However, Keller et al.[7] have cautioned that the use of HLB index may not be completely appropriate in determining the relative hydrophobicity of adsorbed monolayers. Since the group numbers are for individual components of a molecule, it is not clear how adsorption of a particular group alters their hydrophobic nature. Hence, the HLB index can only serve as a tool useful in the determination of relative hydrophobicity of surfactant molecules.

c. Combination of Flocculant/Surfactant

Let us now consider the variation of moisture content with the adsorption density and surface tension for the (50-50) weight % combination of Accol-Floc 1201 and TritonX-114. Figure 65 reveals that the moisture content decreases about four percentage points, down to 0.19 kg water/kg coal in Region 1, which corresponds fairly well with the first region of the adsorption isotherm. But the surface tension characteristics in Figure 66 show insignificant change, as it remains constant around 65 mN/M. This implies that changes in surface property produced by adsorption is the only contributing factor in this region. In accordance with the proposed adsorption scheme, strong polymeric interaction is likely at low concentrations with the coal surface. Though this has no pronounced effect, a small improvement in hydrophobicity is possible.

In Region II, there is a steep decrease in moisture content by almost ten percentage points, down to 0.095 kg water/kg coal. The surface tension decreased only from 65 mN/M to 53 mN/M in this range and is not sufficeint to warrant such a dramatic decrease in moisture content. Again referring to the

adsorption model for the combination, ploymer bridging is the most likely mechanism in Region II. The bridging proceeds rapidly, once interaction with the coal surface is established through hydrogen bonding. There is an additional effect on adsorption, as hemi-micelle formation starts occurring due to the presence of surfactant molecules. Together, these effects impart a great degree of hydrophobicity to the coal surface.

In Region III, we can observe a significant rise in moisture content, to almost 0.17 kg water/kg coal. This is surprising, considering that the surface tension declines from 52 mN/M to 35 mN/M. The adsorption model, however, predicts that bilayer formation will occur over the adsorbed monolayers and these factors decrease the hydrophobicity of the coal surface. The data appear to suggest that the effect of adsorption is so strong in the region that it more than offsets the fairly large decrease in surface tension. It is possible that the combination wets the coal surface so strongly that contact angle decreases dramatically. Further, the increase in floc size at higher concentrations could lead to entrapment of water in the flocs.

The combination of reagents brings about a slightly greater reduction in moisture content compared to the pure flocculant or the surfactant, the lowest recorded value being about 0.095 kg water/kg coal. But at higher concentrations, a high degree of hydrophillicity is introduced and at lower concentration, no significant improvement in hydrophobicity is observed. It must be concluded that since a pre-mixed combination of reagent is not signficantly more effective, it is perhaps better to utlize single reagents to improve the filtration/dewatering characteristics.

The final moisture contents for this combination are higher than those obtained with washed cakes formed with the same flocculant and then washed

with the same surfactant. For example, the maximum moisture reduction attained in the washed cake is 65.8% versus 58.2% for the combination (see Table 13). Therefore, the washing operation is highly recommended.

d. MIBC

Let us examine the moisture content characteristics of MIBC (Figure 67). No significant reduction is obtained for this reagent and it is only beyond an equilibrium concentration of 2×10^{-5} mf that the moisture content decreases to 0.17 kg water/kg coal. This suggests that the frother MIBC has little or no effect on the final moisture content indicating that no change in hydrophobicity has occurred.

Although three distinct regions were detected for the adsorption isotherm of MIBC, only two distinct regions are observed in the moisture content characteristics. Figure 68 brings out the fact that the reduction in surface tension by MIBC is insignificant. According to the postulated adsorption scheme[1], at lower concentrations, the MIBC molecule lies flat on the coal surface with hydrophobic bonding occurring between the nonpolar hydrocarbon ain and coal. This is not likely to affect the hydrophobicity of the coal surface. Further, the surface tension remains almost constant at 66 mN/M over a wide range of concentration. The combination of these factors is responsible for the almost constant value of moisture content (0.24 kg water/kg coal) at the lower concentrations.

But as adsorption sites are exhausted, the orientation of the molecule changes with the short hydrocarbon chain now being oriented towards the aqueous phase. This will render some improvement in the hydrophobicity of the coal surface, though not by a large magnitude as the hydrocarbon chain is short. The surface tension still remains largely unchanged (Figure 68). The fact that small decrease in moisture content is registered at very high

concentrations is largely due to a small decrease in surface tension as the adsorption model predicts a random oritentation with no pronounced effect on hydrophobicity.

B. 10μm Coal

1. Effect of Applied Vacuum

An increase in the applied vacuum leads to a faster filtration rate. There was about a 34% reduction in the filtration time for the -32 mesh coal when the applied vacuum was increased from 40 to 67 kPa.[4] For the 10 μm coal particle, about 30% reduction was observed for the same increase in the applied vacuum. Moreover, increasing the applied vacuum resulted in the lowering of the moisture content of the cake, as depicted in Figure 69.

2. Effect of Solids Concentration

Figure 70 shows that there is some difference between the behavior of the 10 μm and that of the -32 mesh coal in response to changes in solid concentration. For -32 mesh coal, as much as 42% reduction in the moisture content was realized when the solid concentration was increased from 0.33 to 1.0 kg coal/kg H_2O.[4] This has been attributed to the fact that a more uniform cake structure is formed when the slurry is concentrated due to less preferential settling of big particles. On the other hand, in the case of the 10 μm particles, since the sizes are so small and the size distribution so narrow, moisture content reduction is not probable by increasing the slurry concentration.

3. Effect of Reagent Pretreatment

a. Flocculant

Table 14 presents the filtration data for the 10 μm coal slurry treated with Accoal-Floc 1201. Significant reduction in the filtration time with the simultaneous improvement of permeability was observed. Flocculation

indeed effects bridging of the particles and thus reducing the specific resistance of the cake as indicated by Figure 71. It should be noted that the filtration time was reduced by more than 75% over that of the untreated slurry. However, enhancement in the desaturation of the cake was not experienced, probably due to the very high molecular weight of Accoal-Floc 1201 ($15x10^6$). It has been reported that the moisture content can even be higher in a flocculated cake than in an unflocculated cake when high molecular weight flocculant is employed.[17] This adverse effect is caused by excessive flocculation which results in a strong binding force and entrapment of moisture in the flocs.

b. Pine Oil

Only about 5% reduction in moisture content is attained when 2% (by weight of total solid in the slurry) of pine oil is added into the slurry. (See Table 15.) But the filtration time was seen to be greatly affected and the addition of 4% pine oil yields almost the same result as the slurry treated with concentrated flocculant. It is envisioned that the oil not only reduces the viscosity of the fluid, but also acts as collector which binds the small particles together and thus providing ease of flow of the fluid through the pores. Fuhrmeister[18] in filtering clay suspended in oil found a remarkable improvement in filtration rate, which was attributed to a decrease in the viscosity of the slurry.

c. Surfactant

Non-ionic surfactant such as Triton and anionic surfactant like Aerosol-OT are both very effective in reducing the surface tension of the filtrate and thus enhancing the desaturation characteristics of coal cakes (see Figure 72). For the -32 mesh coal, about 50% reduction over the distilled-water cake was attained. In the case of the 10 μm particle, only

31% reduction in cake moisture content was observed: from 1.01 for pure distilled-water cake to 0.70 kg H_2O for Aerosol-OT-treated cake. Figure 73 compares the performance of the various surfactants.

4. Washing Experiments

An additional 18% (68% overall) reduction in the cake moisture content has been reported when an untreated -32 mesh coal cake is washed with surfactant solution.[2] Further enhancement of cake desaturation was achieved through the combination of pretreatment and post-treatment techniques, e.g., treating the slurry with a flocculant prior to filtration and then washing the formed cake with a surfactant.[20] For the present work, as much as 48% reduction in retained moisture was observed when flocculated cake (the slurry was mixed with Accoal-Floc 1201) was washed with Triton X-114 (wash ratio = 4.0). Figure 74 establishes the fact that flocculated cake washed with surfactant works better than just pretreating the slurry with the same surfactant. A similar series of experiments was conducted using Aerosol-OT in place of Triton X-114 and the results compared, as shown in Figure 75. It should be noted that in the range of wash ratio and wash liquor concentration studied, Triton X-114 washed cakes resulted in a lower fluid retention than those washed with Aerosol-OT. However, in the former case, a lot more surfactant is needed to obtain the same moisture reduction. This is due to the fact that with comparable initial concentration, Triton X-114 was absorbed more strongly by coal particles than Aerosol-OT.[18]

For many industrial applications, the washing operation often aims at extracting valuables from the filtrate retained in the filter cake. In such circumstances, increasing the number of washing cycles usually tends to improve the extracting efficiency but not the moisture reduction. Indeed, in the present study, multiple washing resulted in a higher moisture retention in

the cake, as shown in Table 16. Presumably, as the wash liquor drains through the cake, flocs are broken down causing small particles to migrate into the pores. In once-through washing, this migration of small particles renders the cake structure more uniform, i.e., less stratification, which is favorable for desaturation.[2] But if the cake is subjected to a second washing, more small particles will be pushed into the small pores. As the number of times the wash liquor drains through the cake increases, more and more flocs are broken down and more and more small particles migrate down the pores. Eventually, blocking of pore spaces occurs and a higher moisture retention in the cake results.

The discrepancies in the values of fluid content obtained under exactly the same operating conditions (see, for example, Table 16) seem to be caused by the promptness of removing the paper on top of the cake. It should be removed as soon as the water just disappears from the top of the cake.

5. Premixed Flocculant and Surfactant

The preceding discussion suggests that the use of surfactant alone in pretreating the coal slurry is not sufficient to attain optimum reduction of the cakes moisture. Only when a flocculated cake is washed with a surfactant that significant enhancement of the dewatering of these coals is realized. Nevertheless, question arises on whether the same result could be obtained by premixing the two reagents (a surfactant and a flocculant) with the slurry and eliminating the washing operation. To this end, another series of experiments was carried out and the results indicate that premixing the two reagents is not an effective substitute for surfactant washing (see Table 17).

REFERENCES

1. Chiang, S.H., et. al., "Fundamental Study for Improvement of Dewatering of Fine Coal/Refuse," (DOE Project No. De-AC22-81PC42303) Annual Report, August 1984.

2. Binkley, T., "Effect of Surfactant Washing on Enhanced Dewatering of Fine Coal," M.S. Thesis, University of Pittsburgh, 1984.

3. Chiang, S.H., et. al., "Fundamental Study for Improvement of Dewatering of Fine Coal/Refuse," (DOE Project No. DE-AC22-81PC42302) Annual Report, September 1983.

4. Qamar, I., "Application of a Three Dimensional Network Model to Coal Dewatering," Ph.D. Dissertation, University of Pittsburgh, 1985.

5. Chiang, S.H., et. al., "Fundamental Study for Improvement of Dewatering of Fine Coal/Refuse," (DOE Project No. DE-AC22-81PC42302) Annual Report, July 1982.

6. Gray, V.R., "The Dewatering of Fine Coal," Journal of the Institute of Fuel, Vol. 31 (1958), pp. 96-108.

7. Keller, D.V., Stelma, G.J., and Chi, Y.M., "Surface Phenomena in Dewatering of Coal," U.S. Department of Energy Report No. FE-9001-1, January, 1979.

8. Fuerstenau, D.W. and Ragnavan, S., in Flotation, Fuerstenau,M.C., ed., AIME, New York (1976), p. 21.

9. Venkatadri, R.A., "Effect of Surface-Active Agents on Filtration and Post-Filtration Characteristics of Fine Coal," Ph.D. Dissertation, University of Pittsburgh, 1984.

10. Campbell, J.A.L. and S. C. Sun, "An Electrokinetic Study of Bituminous Coal Froth Flotation and Flocculation," Special Research Report to the Coal Research Board, Commonwealth of Pennsylvania under Contract No. CR-32 (1969).

11. Klassen, V.I. and V. A. Mokronsov, An Introduction to the Theory of Flotation, Butterworth and Company, London (1963).

12. Zisman, W.A. and M.K. Bernett, "Relation of Wettability by Aqueous Solutions to the Surface Constitution of Low-Energy Solids," Jnl. of Physical Chemistry, 63 (1959), pp 1241-1246.

13. Pyter, R.A., G. Zografi and P. Mukerjee, "Wetting of Solids by Surface-Active Agents: The Effect of Unequal Adsorption to Vapor-Liquid and Solid-Liquid Interface," Journal of Colloid and Interface Science, 89 (1982), p. 144.

14. Lucassen-Reynders, E.H., "Contact Angles and Adsorption of Solids," Journal of Physical Chemistry, 67, (1963) pp. 969.

15. Greenwood, F.G., Parfitt, G.D., Picton, N.H., and Wharton, D.G., "Adsorption and Wetting Phenomena Associated with Graphon in Aqueous Surfactant Solutions," Advances in Chemistry Series, No. 79 (1968), pp. 135-144.

16. Mukherjee, P. and Anavil, A., "Adsorption on Porous Glass," American Chemical Society Symposium, Series No. 8 (1975), pp. 107-128.

17. Mishra, S.K., "Effect of Flucculation on Moisture Reduction of Fine Coal," Coal Mining and Processing, 10, 56 (1973).

18. Fuhremeister, C., Jr., "Improving Filtration and Dewatering Rates," Chem. Eng. Prog., 46, 550 (1951).

19. Chiang, S.-H., et al., "Filter Cake Washing with Chemical Reagents," Filtrtion and Separation, May/June 1985, pp. 172-177.

20. Gala, H.B., "Use of Surfactant in the Filtration/Dewatering of Fine Coal," Ph.D. Thesis, University of Pittsburgh (1979).

APPENDIX A

TABLES

Table 1

Particle Size Distribution Analysis of Batch 4 Pittsburgh Seam Bruceton Mine -32 Mesh Coal

Particle Distribution by Omnicon Alpha Image Analyzer
-32 Mesh Batch 4 Pittsburgh Coal Size Analysis
Number of Fields Analyzed = 155

Particle Size	Particles Oversize	Number % Oversize	Weight% Oversize
2.0	29504	100.00	100.00
4.0	22040	74.70	99.99
6.3	16438	55.71	99.96
10.0	11143	37.77	99.86
12.6	8992	30.48	99.74
15.8	6631	22.48	99.49
25.1	3806	12.90	98.61
31.6	2811	9.53	97.76
39.8	2081	7.05	96.51
50.1	1506	5.10	94.56
63.1	1062	3.60	91.54
79.4	731	2.48	87.06
100.0	451	1.53	79.49
125.8	257	.87	69.04
158.4	118	.40	54.10
200.0	50	.17	39.45
251.1	24	.08	28.28
316.1	9	.03	15.47
400.0	0	0.00	0.00

Size Range	Average Size	Number % in Range	Weight % in Range
2.0-4.0	3.0	26.1988	0.006
4.0-6.3	5.2	18.604	0.022
6.3-10.0	8.1	17.404	0.083
10.0-12.6	11.3	6.700	0.085
12.6-15.8	14.2	7.560	0.191
15.8-19.9	17.9	4.523	0.455

Table 1 (continued)

Size Range	Average Size	Number % in Range	Weight % in Range
19.9-25.1	22.5	4.523	0.455
25.1-31.6	28.3	3.579	0.720
31.6-39.8	35.7	2.518	1.012
39.8-50.1	46.0	2.016	1.617
50.1-63.1	56.6	1.859	2.978
63.1-79.4	71.3	1.441	4.603
79.4-100.0	89.7	1.111	7.084
100.0-125.9	112.9	0.860	10.930
125.8-158.4	142.1	0.419	10.613
158.4-200.0	179.2	0.223	11.352
200.0-251.1	225.6	0.151	15.280
251.1-316.1	283.6	0.050	10.125
316.1-400.0	258.4	0.045	18.111
400.0-500.0	450.0	0.006	4.494

Length Mean Size = 15.4
Volume Mean Size = 48.2
Surface Mean Size = 29.3
Surface-Volume Size = 132.3
Weigth Mean Size = 208.8

Table 2

Particle Size Distribution Analysis of Batch 6 Pittsburgh Seam Bruceton Mine -32 Mesh Coal

Particle Distribution by Omnicon Alpha Image Analyzer

-32 Mesh Batch 6 Pittsburgh Coal Size Analysis
Number of Fields Analyzed = 155

Particle Size	Particles Oversize	Number % Oversize	Weigth % Oversize
7.0	63312	1001.0	100.0
4.0	49465	78.13	99.99
6.3	38228	60.38	99.93
10.0	26437	41.76	99.68
12.6	21493	33.95	99.41
15.8	15732	24.85	98.77
19.9	11904	18.80	97.93
25.1	8410	13.28	96.40
31.6	5633	8.90	93.96
39.8	3628	5.73	90.45
50.1	2292	3.62	85.78
63.1	1368	2.16	79.32
79.4	864	1.36	72.30
100.0	475	0.75	61.49
125.8	237	0.37	48.30
158.4	100	0.16	33.16
200.0	32	0.05	18.09
251.1	7	0.01	7.04
316.1	1	0.00	1.77
400.0	0	0.00	0.00

Size Range	Average Size	Number % in Range	Weight % in Range
2.0-4.0	3.0	21.871	0.014
4.0-6.3	5.2	17.749	0.059
6.3-10.0	8.1	18.624	0.246
10.0-12.6	11.3	7.809	0.275
12.6-15.8	14.2	9.099	0.635
15.8-19.9	17.9	6.046	0.838
19.9-25.1	22.5	5.519	1.533
25.1-31.6	28.3	4.386	2.437

Table 2 (continued)

Size Range	Average Size	Number % in Range	Weight % in Range
31.6-39.8	35.7	3.167	3.514
39.8-50.1	46.0	2.110	4.673
50.1-63.1	56.6	1.459	6.453
63.1-79.4	71.3	0.796	7.021
79.4-100.0	89.7	0.614	10.813
100.0-125.8	112.9	0.376	13.191
125.8-158.4	142.1	0.216	15.140
158.4-200.0	179.2	0.107	15.140
200.0-251.1	225.6	0.039	11.048
251.1-316.1	283.6	0.009	5.271
316.1-400.0	358.4	0.002	1.768

Length Mean Size = 13.9
Volume Mean Size = 34.4
Surface Mean Size = 22.5
Surface-Volume Size = 81.2
Weight Mean Size = 132.7

Table 3

Porosity from Horizontal Cut Section Analysis of Aerosol-OT
Washed -32 Mesh Coal Filter Cakes

Cake Name	Wash Ratio	Conc. PPM	Porosity by Area fraction @ X/L .000	.250	.500	.750	1.000	AVG	Final Moisture Kg Water/Kg Coal
T57	2	100	.518	.480	.463	.455	.441	.471	.174
T59	2	250	.525	.511	.479	.467	.439	.484	.165
T60	2	250	.510	.504	.462	.449	.436	.472	.161
T45	2	500	.541	.520	.493	.472	.453	.496	.148
T46	2	500	.520	.506	.478	.455	.444	.481	.151
T49	10	100	.527	.490	.478	.461	.451	.481	.144
T50	10	100	.542	.496	.471	.467	/440	.483	.143
T53	10	250	.545	.507	.478	.470	.460	.492	.135
T54	10	250	.548	.495	.467	.452	.458	.485	.136
T43	10	500	.557	.512	.493	.466	.454	.496	.148
T44	10	500	.526	.500	.478	.470	.468	.488	.124

Table 4

Particle Surface-Volume Mean Diameter from Horizontal Cut Section Analysis of Aerosol-OT Washed -32 Mesh Coal Filter Cake

Cake Name	Wash ratio	Conc. PPM	@ X/L 0.000	0.250	0.500	0.750	1.000	$\bar{X}_{sv}$	ΔX_{SV}
T57	2	100	26.12	28.55	25.76	31.91	39.48	30.36	13.36
T59	2	250	25.65	27.15	30.82	32.64	36.38	30.53	10.73
T60	2	250	24.48	28.60	35.32	35.57	38.20	32.43	13.72
T45	10	100	24.63	30.79	32.84	28.08	35.65	30.40	11.02
T50	10	100	25.61	32.18	32.05	33.05	43.74	33.33	18.13
T53	10	250	26.77	30.52	34.05	33.22	36.16	32.14	9.39
T54	10	250	26.83	30.29	30.27	34.41	34.78	31.32	7.95
T43	10	500	22.65	27.66	28.41	30.71	34.87	28.86	12.22
T44	10	500	26.62	33.18	32.17	33.33	37.78	32.62	11.16

Table 5: Average Geometric-Volume Mean Diameter of Particles and Pores for Double Distilled Water Cakes

Cake Name	Wash Ratio	Surfactant	Surfactant Concentration (ppm)	X_{GV} Particle (μm)	X_{GV} Pore (μm)
D10	0	-	-	81.69	86.84
D25	0	-	-	66.23	73.10
D12	2	-	-	60.46	69.12
D15	2	-	-	83.80	63.03
D11	10	-	-	72.06	90.88
D17	10	-	-	57.14	76.62
T5	2	Triton X-114	100	62.33	78.99
T17	2		250	77.96	76.38
T18	2		250	72.04	74.27
T39	2		500	66.77	75.37
T40	2		500	62.76	64.46
T9	10		100	47.10	68.89
T21	10		250	89.33	74.43
T24	10		250	77.89	79.98
T34	10		500	83.52	73.60
T57	2	Aerosol-OT	100	51.62	42.90
T59	2		250	52.85	44.55
T60	2		250	58.16	44.35
T45	2		500	50.15	44.40
T46	2		500	49.46	42.45
T49	10		100	53.38	45.01
T50	10		100	56.53	49.08
T53	10		250	55.02	47.03
T54	10		250	55.49	43.23
T43	10		500	47.74	44.32
T44	10		500	56.36	54.57

Table 6: Micrographic Data of -32 Mesh Amine Cakes

Cake No.	Layer	Porosity	Particle Size	Pore Size
H25AM	1	0.529	24.51	27.73
(25 ppm)	2	0.472	36.95	33.22
	3	0.469	34.84	34.49
	4	0.447	42.14	36.33
	5	0.460	36.05	34.07
	Average	0.475	34.90	33.17
H27AM	1	0.526	25.93	29.72
(25 ppm)	2	0.488	30.75	32.87
	3	0.474	36.86	34.53
	4	0.451	37.12	33.73
	5	0.417	43.64	36.95
	Average	0.471	34.9	33.56
H8AM	1	0.512	29.88	33.50
(550 ppm)	2	0.460	42.62	38.79
	3	0.426	41.10	34.45
	4	0.421	43.18	36.52
	5	0.411	49.64	36.45
	Average	0.446	41.3	35.94
H14AM	1	0.517	23.76	25.49
(500 ppm)	2	0.440	38.21	30.56
	3	0.439	35.71	29.74
	4	0.433	37.92	31.53
	5	0.418	57.16	45.66
	Average	0.449	38.6	32.60

Table 6: Micrographic Data of -32 Mesh Amine Cakes (Continued)

Cake No.	Layer	Porosity	Particle Size	Pore Size
H17AM	1	0.567	24.81	38.33
(1000 ppm)	2	0.528	35.62	42.86
	3	0.477	41.72	41.06
	4	0.438	46.70	40.33
	5	0.424	66.64	55.43
	Average	0.487	43.10	43.60
H18AM	1	0.574	22.26	31.02
(1000 ppm)	2	0.484	34.65	35.80
	3	0.479	43.02	41.59
	4	0.460	46.45	43.55
	5	0.424	62.44	53.87
	Average	0.484	41.76	41.17
H28AM	1	0.588	19.98	29.93
(2000 ppm)	2	0.502	31.72	36.14
	3	0.453	41.45	39.80
	4	0.460	39.78	40.11
	5	0.423	49.54	43.51
	Average	0.485	36.49	37.90
H31AM	1	0.586	19.31	28.97
(2200 ppm)	2	0.497	32.39	33.41
	3	0.460	34.87	32.84
	4	0.438	37.46	32.51
	5	0.432	49.01	40.24
	Average	0.483	34.61	33.59

Table 7: Effect of Applied Vacuum on Characteristics of 10μm Coal Filtration and Dewatering

Experiment No.	Applied Vacuum [kPa]	Porosity	α $10^9[\frac{m}{kg}]$	κ [mD]
U16	92.7	0.62	96.9	21.0
U15	80.0	0.62	101.3	20.2
U4	66.7	0.59	123.2	15.2

Table 8

Data Used for Surfactant Cakes

Reagent	Exptl. Surface Tension γ dynes/cm	Contact Angle θ degrees	Pcm @ 50% (model) psia	Pce @ 50% (exptl) psia	Pcm / Pce	CONST	$\gamma\cos(\theta)$
Distilled Water	72.0	100	3.760	3.735	1.00	0.50	-12.5
Trinton/Floc. 125 ppm	64.9	40	2.740	1.350	2.03	1.00	49.7
Triton/Floc. 30 ppm	58.2	89	2.984	2.300	1.29	0.64	1.2
MIBC 1000 ppm	64.0	108	2.898	3.420	0.84	0.42	-19.7
Triton 200 ppm	46.0	10	2.325	4.670	0.50	0.25	45.3
MIBC 500 ppm	68.1	110	2.960	6.050	0.49	0.24	-23.3
Triton 500 ppm	33.0	4	1.790	3.680	0.48	0.24	32.9

Table 9

Comparison of Equilibrium Final Saturations

Cake	Percent Final Saturation	
	Experimental	Model
-32 mesh (distilled water)	21	20
-100+200 mesh (dist. water)	14	17
-200 mesh (distilled water)	18	27
-32 mesh (Trinton 200 ppm)	18	18
-32 mesh (Trinton 500 ppm)	12	13
-32 mesh (MIBC 100 ppm)	13	16
-32 mesh (Trinton/Accoal-Floc 1201 30 ppm)	17	18
-32 mesh (Trinton/Accoal-Floc 1201 125 ppm)	11	19
-32 mesh (MIBC 500 ppm)	35	18

Table 10

Pore Size Distribution for -32 Mesh Coal
Obtained From Dispersed Particle Size Distribution

Pore Size (microns)	Number % Undersize
2.0	0.000
4.0	16.9484
6.3	37.1770
10.0	61.5920
12.6	72.7943
15.8	81.9237
19.9	88.9591
25.1	93.8006
31.6	96.7832
39.8	98.4692
50.1	99.3312
63.1	99.7331
79.4	99.9023
100.0	99.9674
125.8	99.9900
158.4	99.9972
200.0	99.9993
251.1	99.9998
316.1	100.0000

Table 11

Comparison of The Single Phase Permeabilities

Coal	Experimental (mD)	Predicted (mD)
-32 mesh	568	413
-32 mesh	516	471
-32 mesh	522	317
-32 mesh	191	289
-32 mesh	795	474
-32 mesh	209	288
-32 mesh	236	297
-32 mesh	208	277
-32 mesh	576	665
-32 mesh	548	703
-32 mesh	491	421
-32 mesh	634	479
-100 mesh	466	285
-400 mesh	112	151
-80 mesh	202	432
-80 mesh	271	427
-80 mesh	278	449
-100+200 mesh	1065	1620

Table 12

Effects of Surfactant Washing on the Final Moisture Content of -32 Mesh Coal Filter Cakes

Trinton X114

Wash Ratio = 2 (11 ml)		Wash Ratio = 10 (55 ml)	
Concentration PPM	Final Moisture Kg water/Kg coal	Concentration PPM	Final Moisture Kg water/Kg coal
100	0.220	100	0.080
100	0.240	100	0.194
100	0.242	100	0.191
100	0.220	100	0.184
100	0.199	100	0.205
100	0.223	100	0.109
		100	0.192
250	0.189	100	0.185
250	0.183	100	0.170
250	0.180	100	0.176
250	0.193	250	0.094
250	0.202	250	0.079
250	0.191	250	0.093
		250	0.098
		250	0.132
500	0.154	250	0.103
500	0.137	250	0.094
500	0.156	250	0.104
500	0.152	250	0.106
500	0.161	250	0.084
		400	0.079
		400	0.095
		400	0.101
		400	0.097
		500	0.091
		500	0.080
		500	0.093
		500	0.092
		500	0.098
		500	0.078
		500	0.078
		500	0.061

Table 12 (continued)

Effects of Surfactant Washing on the
Final Moisture Content of -32
Mesh Coal Filter Cakes

Aerosol - OT

Wash Ratio = 2 (11 ml)		Wash Ratio = 10 (55 ml)	
Concentration PPM	Final Moisture Kg water/Kg coal	Concentration PPM	Final Moisture Kg water/Kg coal
100	0.175	100	0.123
100	0.201	100	0.144
100	0.174	100	0.143
250	0.153	250	0.144
250	0.165	250	0.122
250	0.161	250	0.135
		250	0.135
500	0.148	500	0.133
500	0.151	500	0.148
500	0.153	500	0.124

Table 13
Comparison of Effectiveness of Reagents on Filtration/Dewatering

Reagent	Maximum % Reduction in Moisture Content	Lowest Moisture Content $\frac{\text{kg water}}{\text{kg coal}}$	Lowest Cake Formation Time (secs)	Adsorption Density at Optimum Conc. (g mole/gm)	Initial Reagent ppm for Optimum Dosage	Lb/Ton Needed (Based on ppm)	Lb/Ton Needed (Based on ppm)	BTU/Ton Saved $\times 10^{-6}$ Adsorp.
Triton X-114	42.91	0.137	12	1.4×10^{-6}	250	1.50	1.50	0.200
Aerosol OT	43.80	0.132	12	1.1×10^{-6}	150	0.93	0.92	0.210
Accoal-Floc 1201	44.60	0.130	5	2×10^{-10}	250	1.51	6.0	0.214
Accoal-Floc Triton X114	58.2	0.098	5	3×10^{-6}	510	3.09	3.05	0.276
MIBC	26.8	0.172	9	2×10^{-4}	10,000	60.30	35.3	0.132
DAH	37.5	0.153	12	7×10^{-6}	520	3.10	3.10	0.169

Table 13 (continued)
Comparison of Effectiveness of Reagents in Washing

Reagents Combination	Maximum % Reduction in Moisture Content kg coal	Lowest Moisture Content Recorded kg water	Adsorption Density g mole/gm (ppm)	Initial Wash Liquid Required	lb/ton of Reagent (based on ppm)	lb/ton of Reagent (based on Adsorption)	BTU/ton Saved $\times 10^{-6}$
Accoal-Floc/ Triton X-114	65.8	0.082	1.1×10^{-6}	350	1.20	1.17	0.207
MIBC/Tirton X-114	68.7	0.075	1.5×10^{-6}	360	1.58	1.56	0.321
MIBC/Aerosol OT	64.5	0.085	2.5×10^{-7}	250	1.1	0.22	0.301
DAH/Triton X-114	45.8	0.130	0.95×10^{-6}	300	0.96	0.95	0.214
DAH/Aerosol-OT	45.8	0.130	5×10^{-7}	245	0.78	0.532	0.212

Table 14: Filtration/Dewatering Data for Flocculated Cake

Flocculant: Accoal-Floc 1201

Expt.No.	Concentration [ppm]	Filtration Time [Sec.]	Moisture Retention [kg Fluid/kg Coal]	K [mD]
U 21	0	79.4	1.01	31.3
U 17	34.2	49.8	1.04	35.4
U 18	683.6	30.6	1.08	50.0
U 20	3280	17.9	1.11	68.0

Table 15: Effect of Pine Oil Addition

Exper. No.	Concentration [ppm]	Filtration Times [sec]	Moisture Retention kg Fluid/kg Coal
U 35	0.5	30	1.06
U 35	1.5	21	1.09
U 30	2.0	29	0.96
U 29	4.0	16	0.98

Table 16: Effect of Multiple Washing

All cakes are formed with 684 ppm Accoal-Floc 1201 prior to washing

Wash liquor used: Triton X-114
WR = 4 (66 ml)

Experiment No.	No. of Times of Washing	Fluid Retention [$\frac{\text{Kg fluid}}{\text{Kg coal}}$]
U 59	1 (66 ml/wash)	0.53
U 55	1 (66 ml/wash)	0.56
U 51	2 (33 ml/wash)	0.725
U 60	2	0.746
U 50	3 (22 ml/wash)	0.947
U 61	3	0.846

Table 17: Comparison of Performance Between Washing Operation and Pretreatment with Combined Reagents

Exper. No.	Reagents Premixed with Slurry	Wash Liquor	Cake Moisture Retention [Kg Fluid/Kg Coal]
U 25	Accoal-Floc 1201 (684 ppm)	Aerosol-OT (1000 ppm, WR=4)	0.893
U 31	Accoal-Floc 1201 (684 ppm)	Aerosol-OT (2000 ppm, WR=4)	0.787
U 41	Aerosol-OT (1000 ppm) Accoal-Floc 1201 (684 ppm)	--	1.03
U 42	Aerosol-OT (2000 ppm) Accoal-Floc 1201 (684 ppm)	--	1.05

APPENDIX B

FIGURES

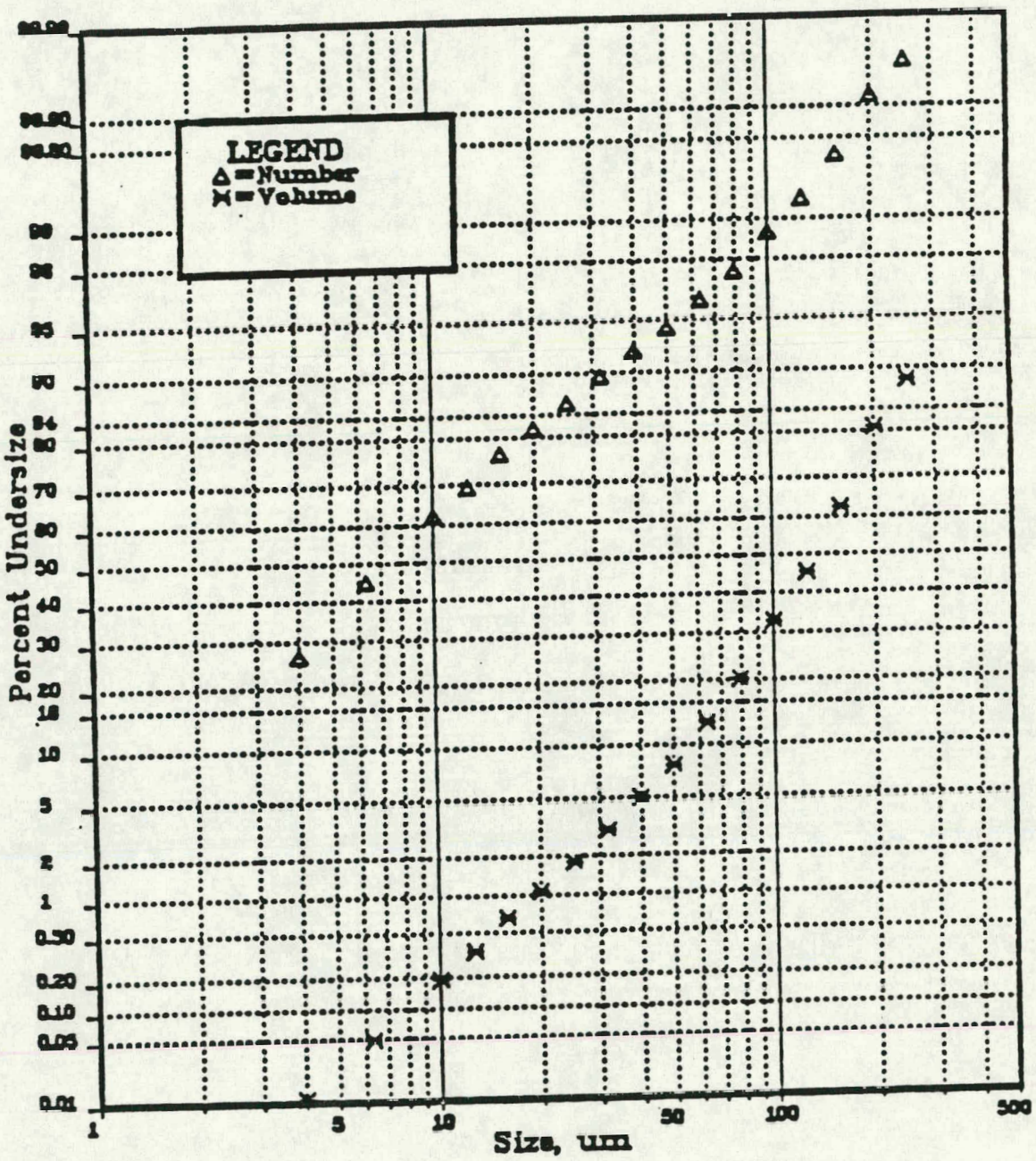

Figure 1: Log-normal Particle Size Distribution of Dispersed -32 Mesh Pittsburgh Seam Bruceton Mine Coal Batch 4

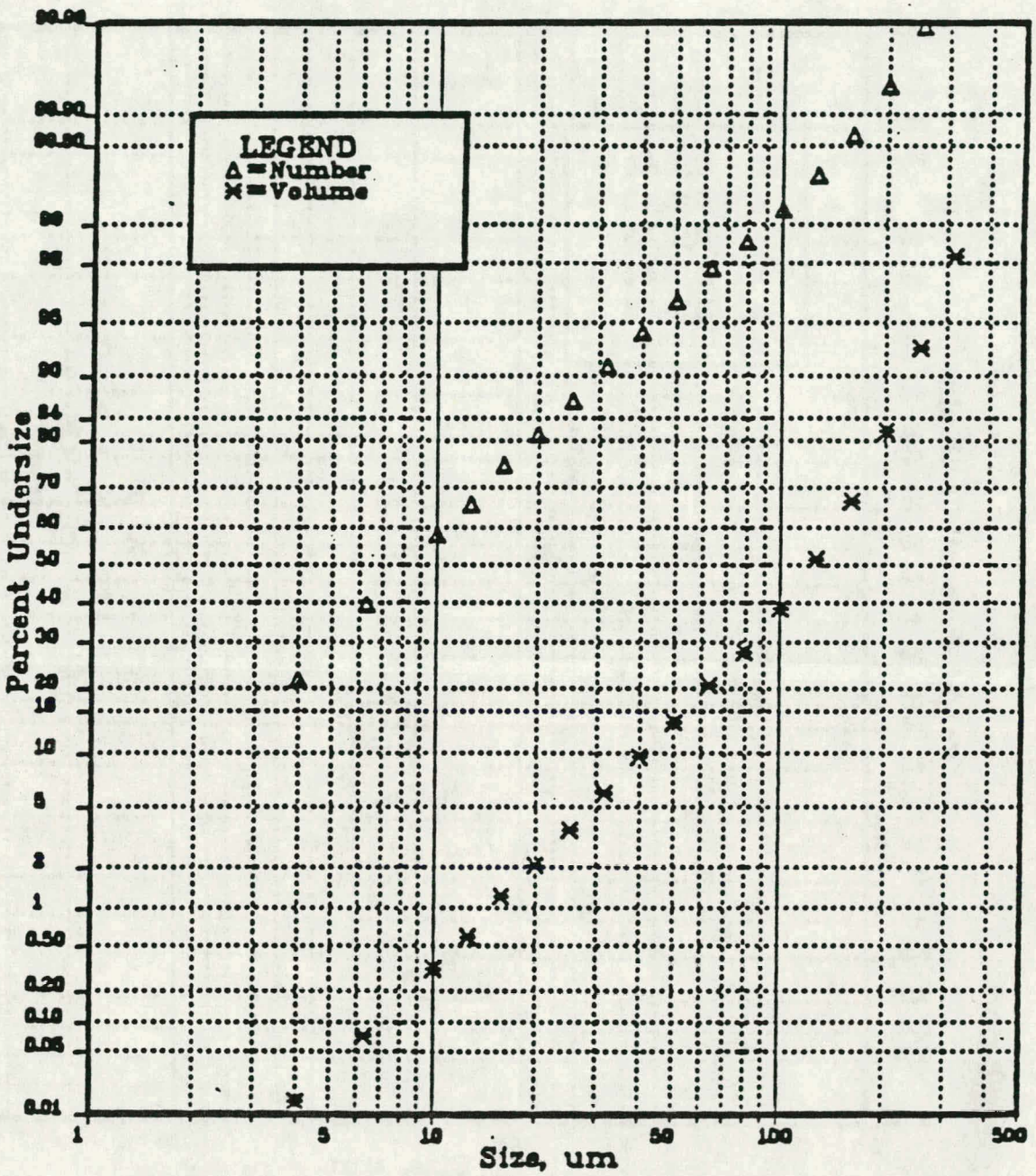

Figure 2: Log-normal Particle Size Distribution of Dispersed -32 Mesh Pittsburgh Seam Bruceton Mine Coal Batch 6

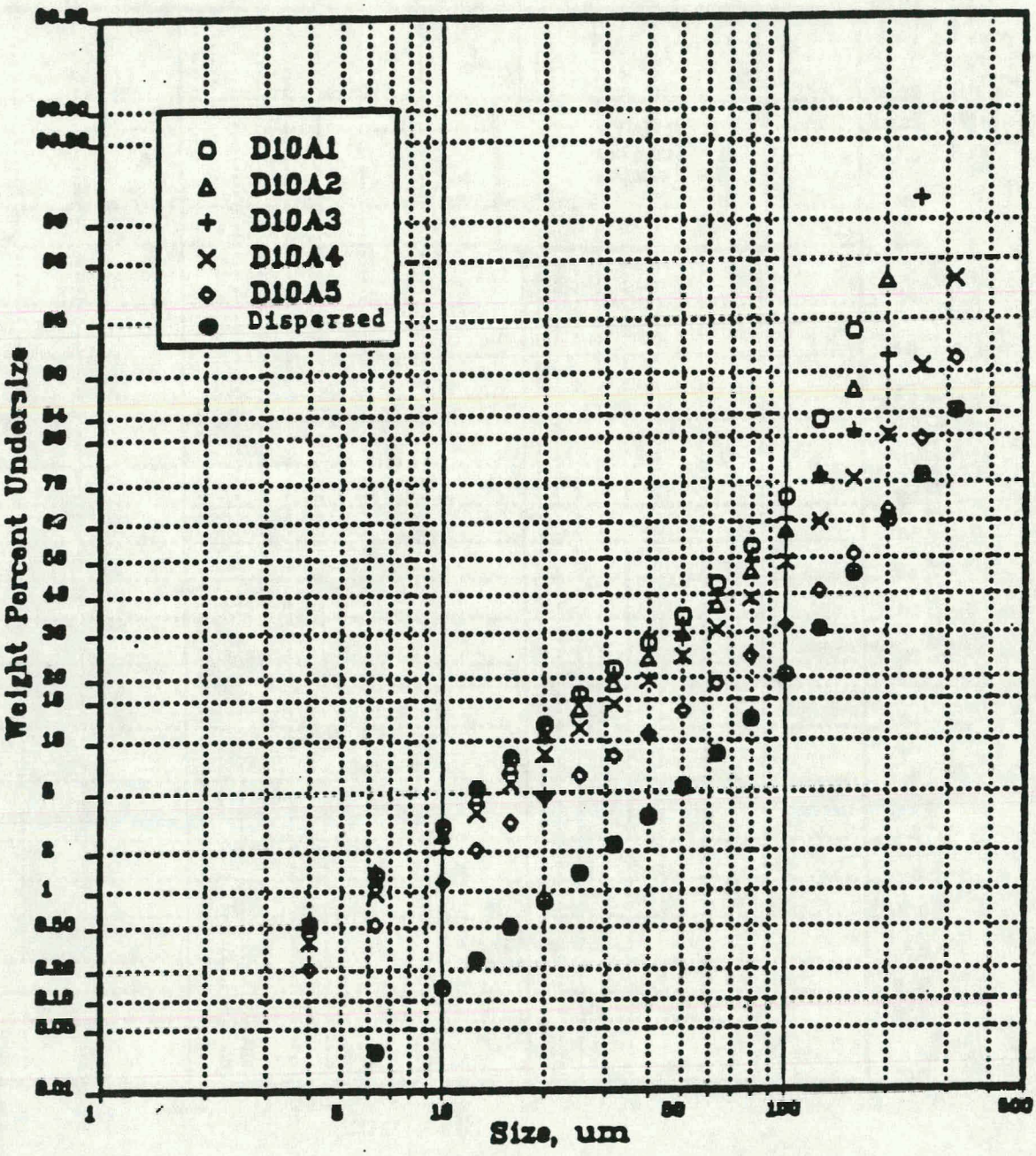

Figure 3: Comparison of the Particle Size Distribution of the Five Layers in a Filter Cake (WR=0) and the Dispersed Particle Size Distribution of -32 Mesh Coal.

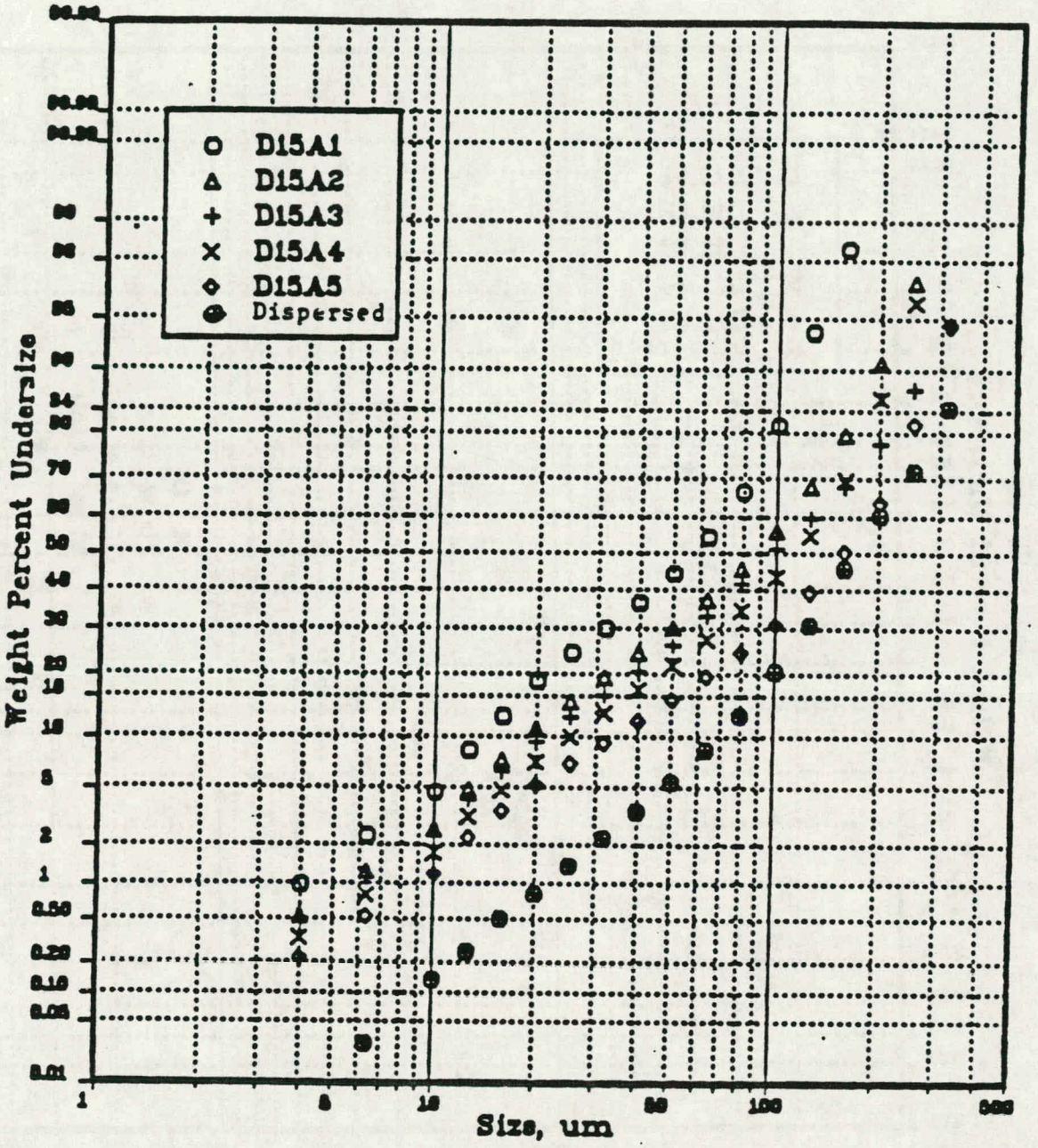

Figure 4: Comparison of the Particle Size Distribution of the Five Layers in a Double Distilled Water Washed Filter Cake (WR = 2) and the Dispersed Particle Size Distribution of -32 Mesh Coal.

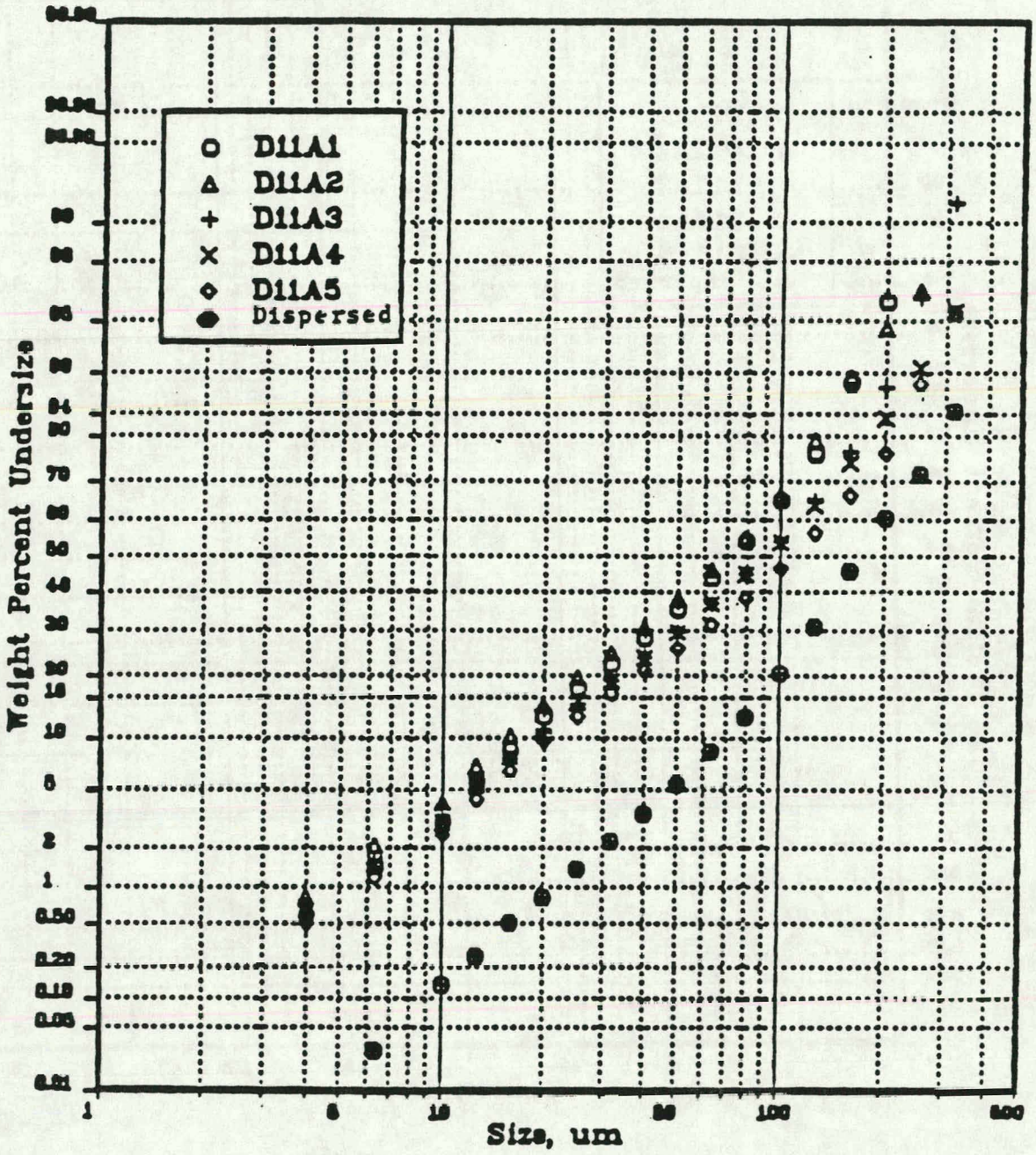

Figure 5: Comparison of the Particle Size Distribution of the Five Layers in a Double Distilled Water Washed Filter Cake (WR = 10) and the Dispersed Particle Size Distribution of -32 Mesh Coal.

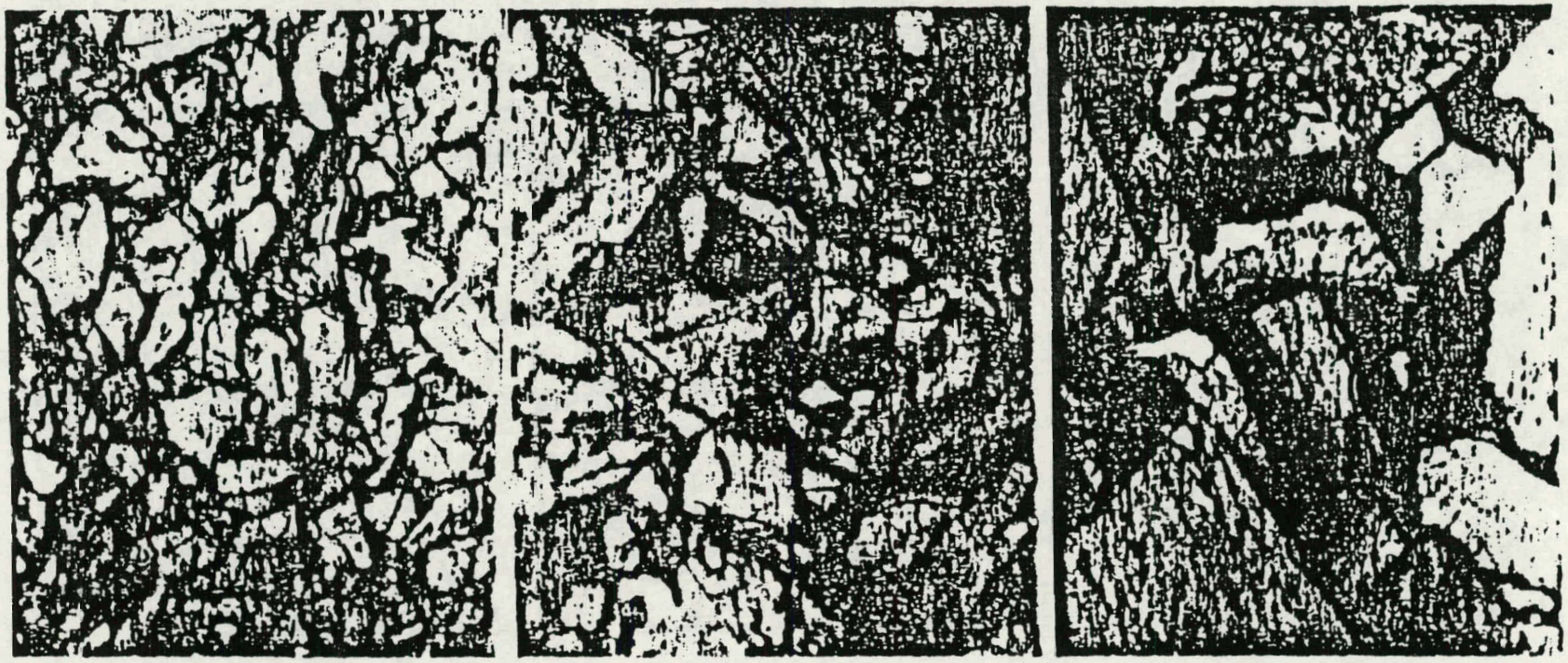

Top Layer Middle Layer Bottom Layer

Figure 6 : Photomicrographs of D10 Filter Cake, with No Washing (WR=0)

Top Layer Middle Layer Bottom Layer

Figure 7: Photomicrographs of Dll Filter Cake Washed with Double Distilled Water Using a Wash Ratio of Ten.

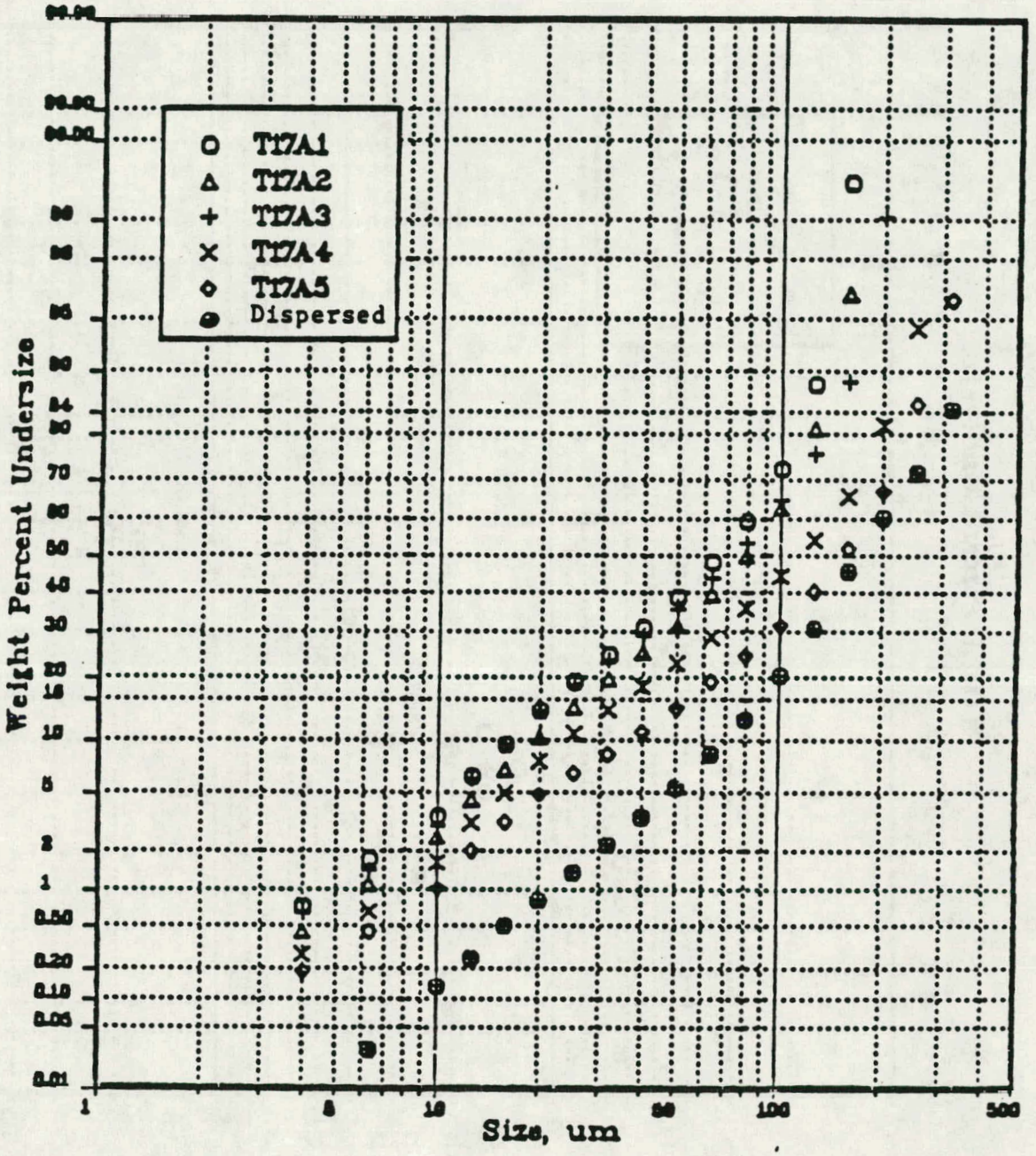

Figure 8: Comparison of the Particle Size Distribution of the Five Layers in a 250 PPM Triton X-114 Washed Filter Cake (WR=2) and the Dispersed Particle Size Distribution of -32 Mesh Coal.

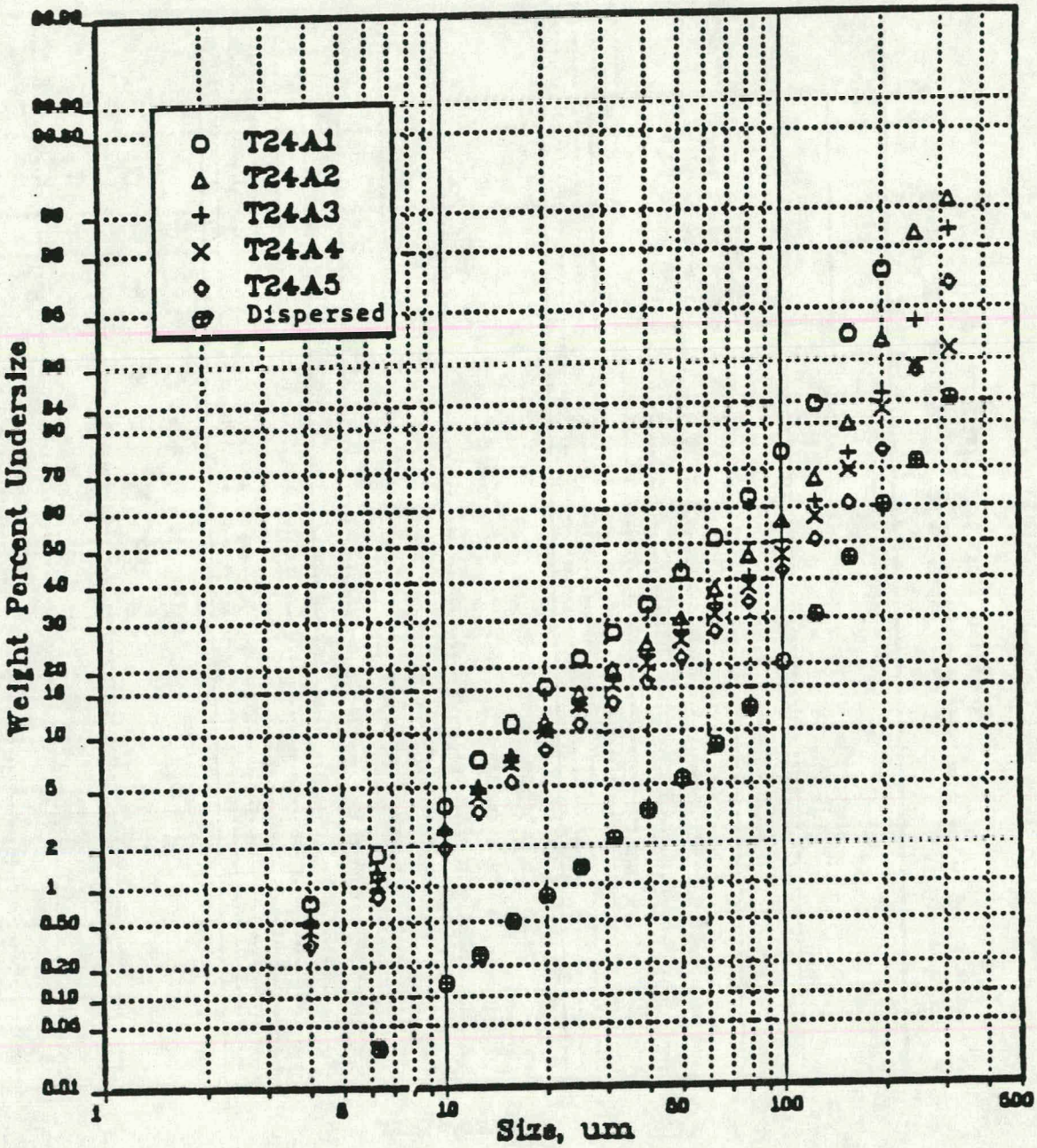

Figure 9 : Comparison of the Particle Size Distribution of the Five Layers in a 250 ppm Triton X-114 Washed Filter Cake (WR=10) and the Dispersed Particle Size Distribution of -32 Mesh Coal.

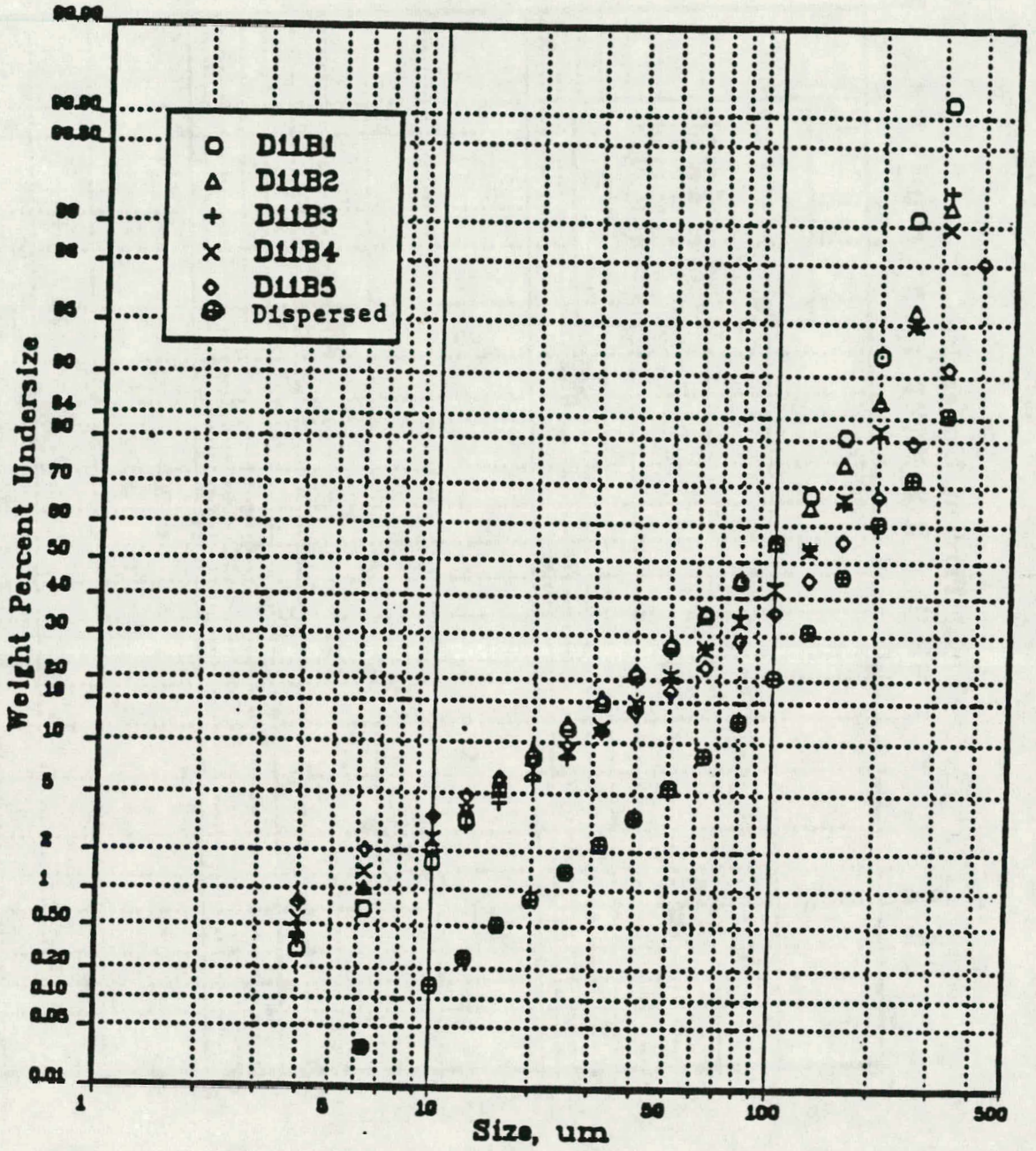

Figure 10: Comparison of the Pore Size Distribution of the Five Layers in a Double Distilled Water Washed Filter Cake (WR = 10) and the Dispersed Particle Size Distribution of -32 Mesh Coal.

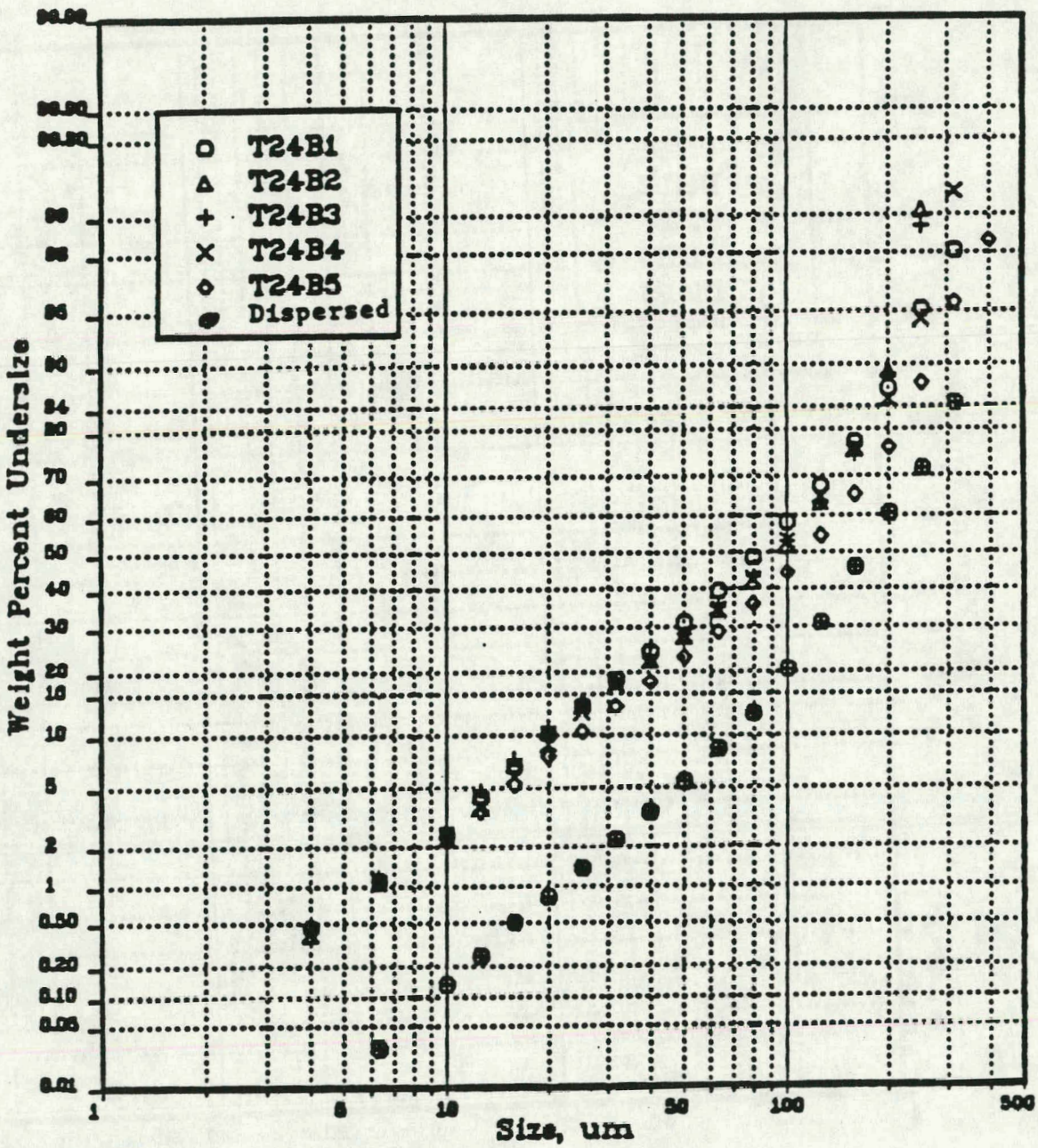

Figure 11: Comparison of the Pore Size Distribution of the Five Layers in a 250 ppm Triton X-114 Washed Filter Cake (WR = 10) and the Dispersed Particle Size Distribution of -32 Mesh Coal.

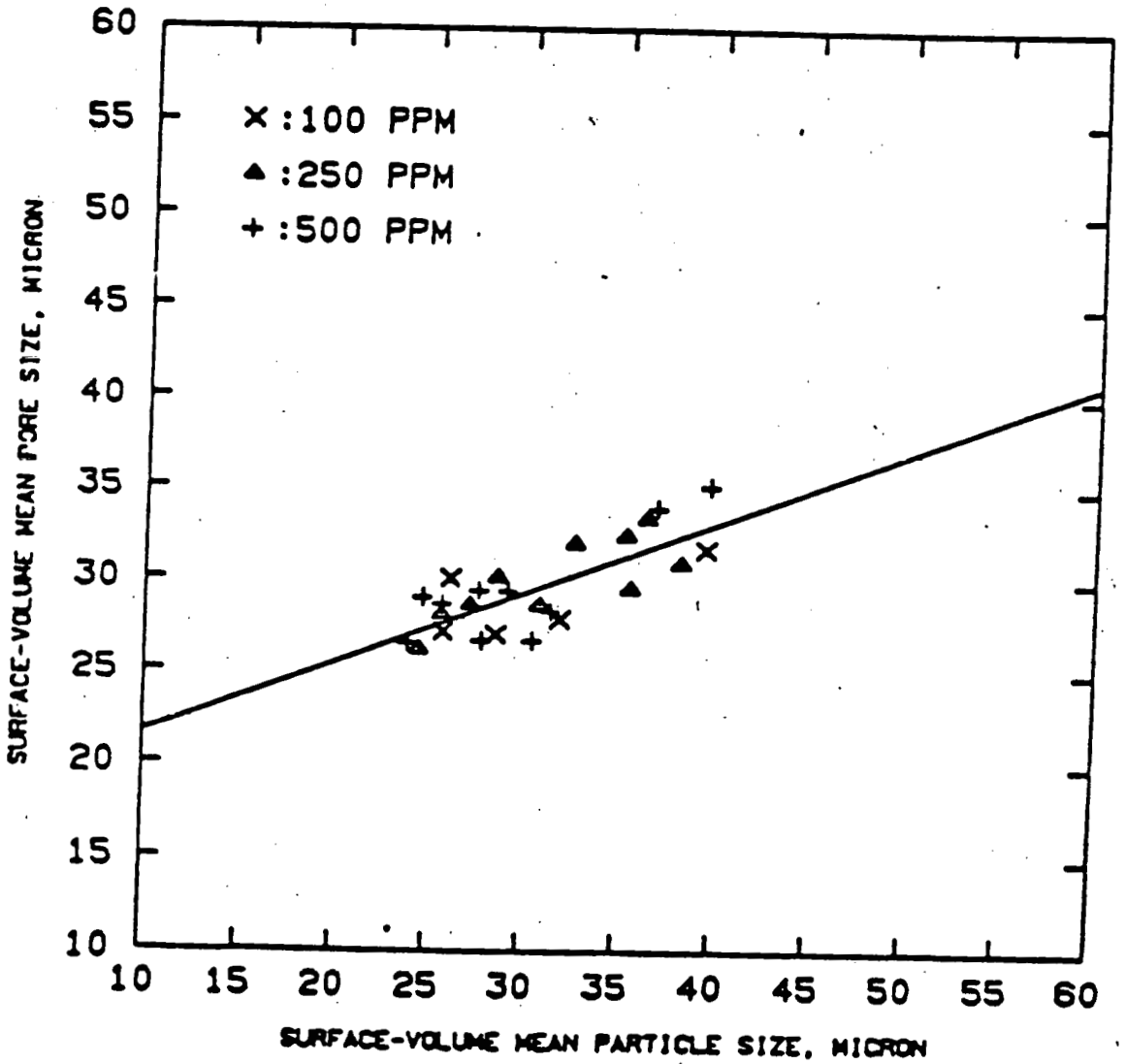

Figure 12: Effect of Surface-Volume Mean Sizes of the Particles on the Surface-Volume Mean Sizes of the Pores for All Concentrations of Aerosol-OT Using a Wash Ratio of Two.

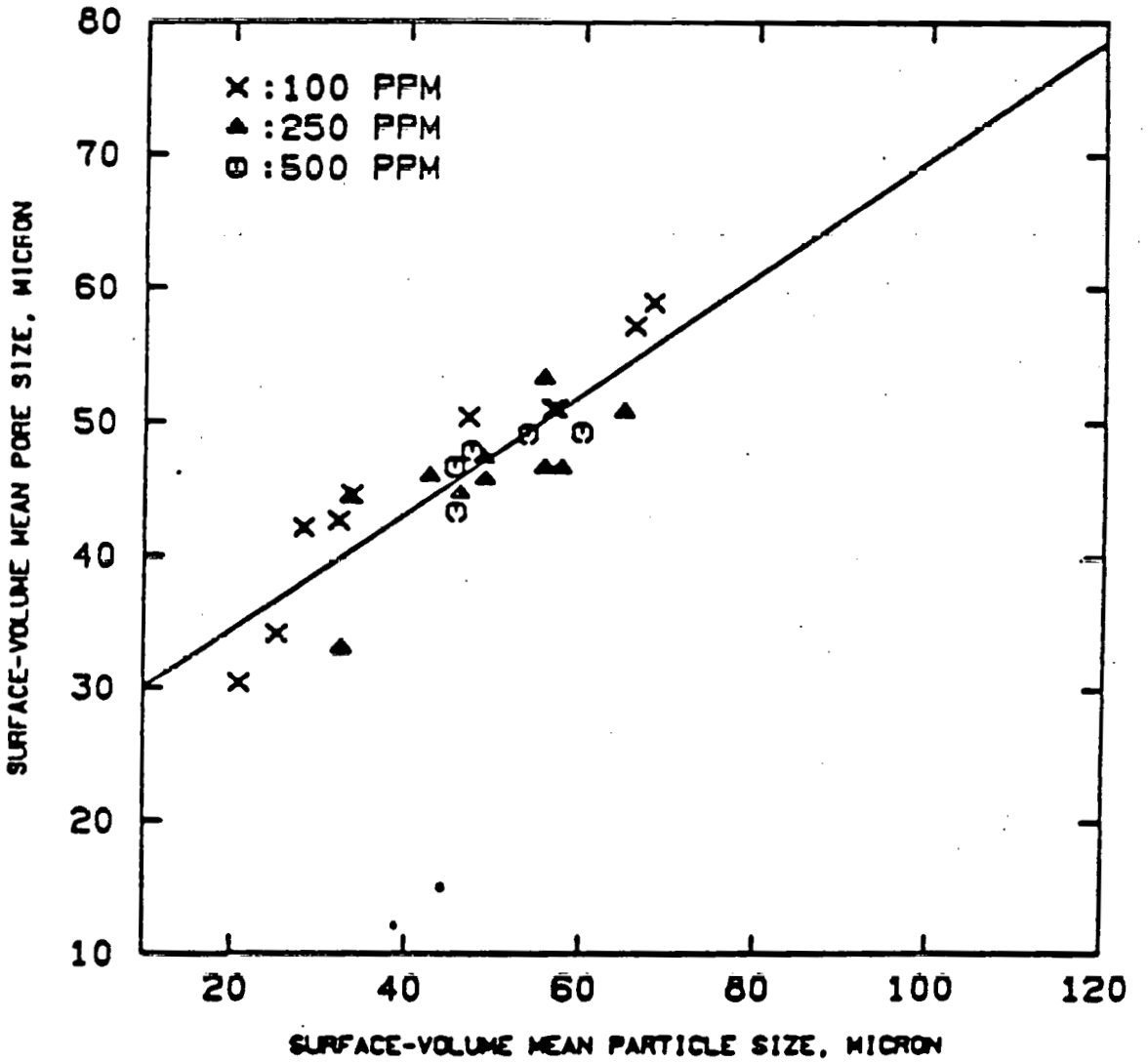

Figure 13: Effect of Surface-Volume Mean Sizes of the Particles on the Surface-Volume Mean Sizes of the Pores for All Concentrations of Triton X-114 Using a Wash Ratio of Ten.

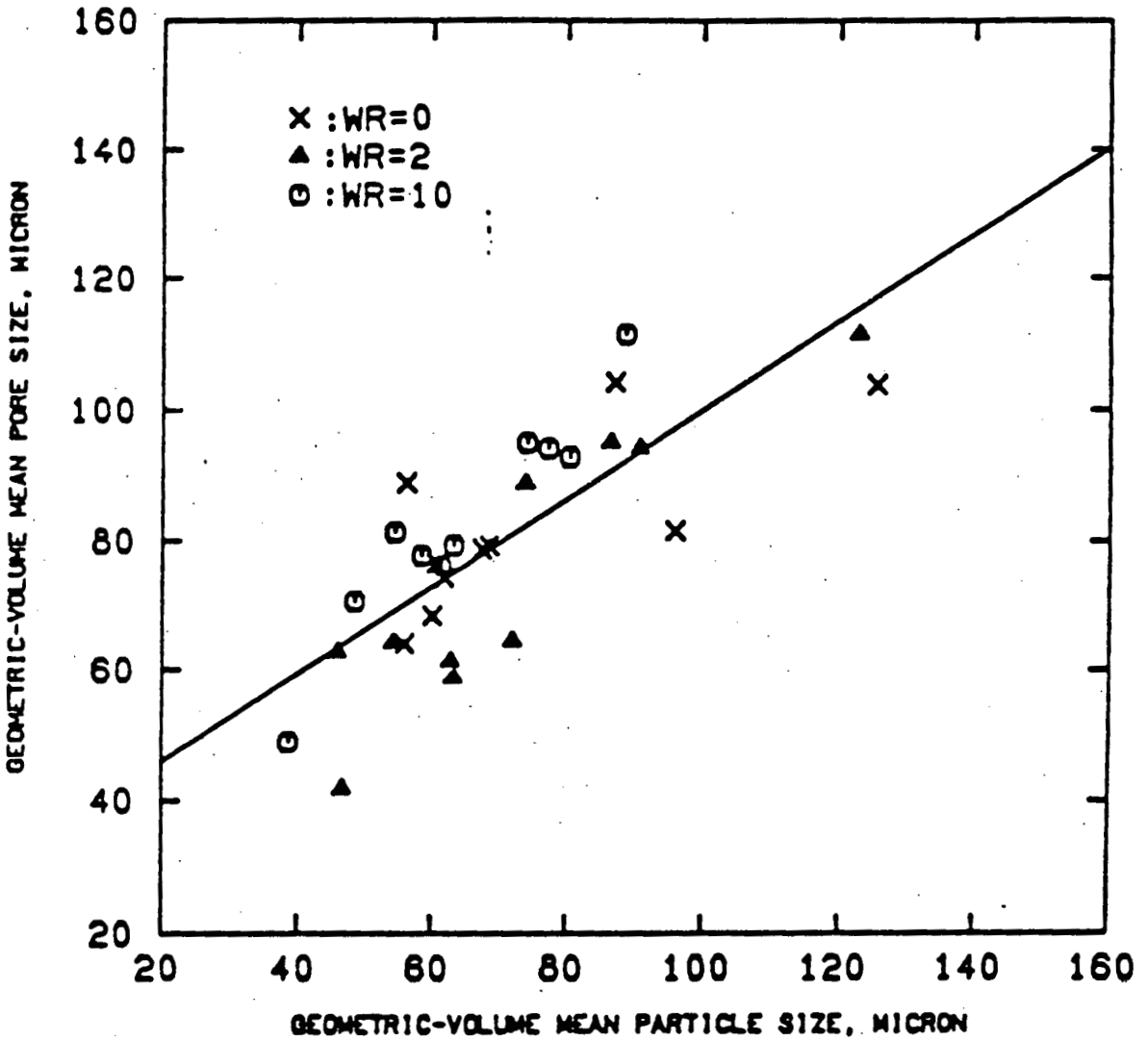

Figure 14: Effect of Geometric Mean Sizes of the Particles on the Geometric Mean Sizes of the Pores for Double Distilled Water and All Wash Ratios.

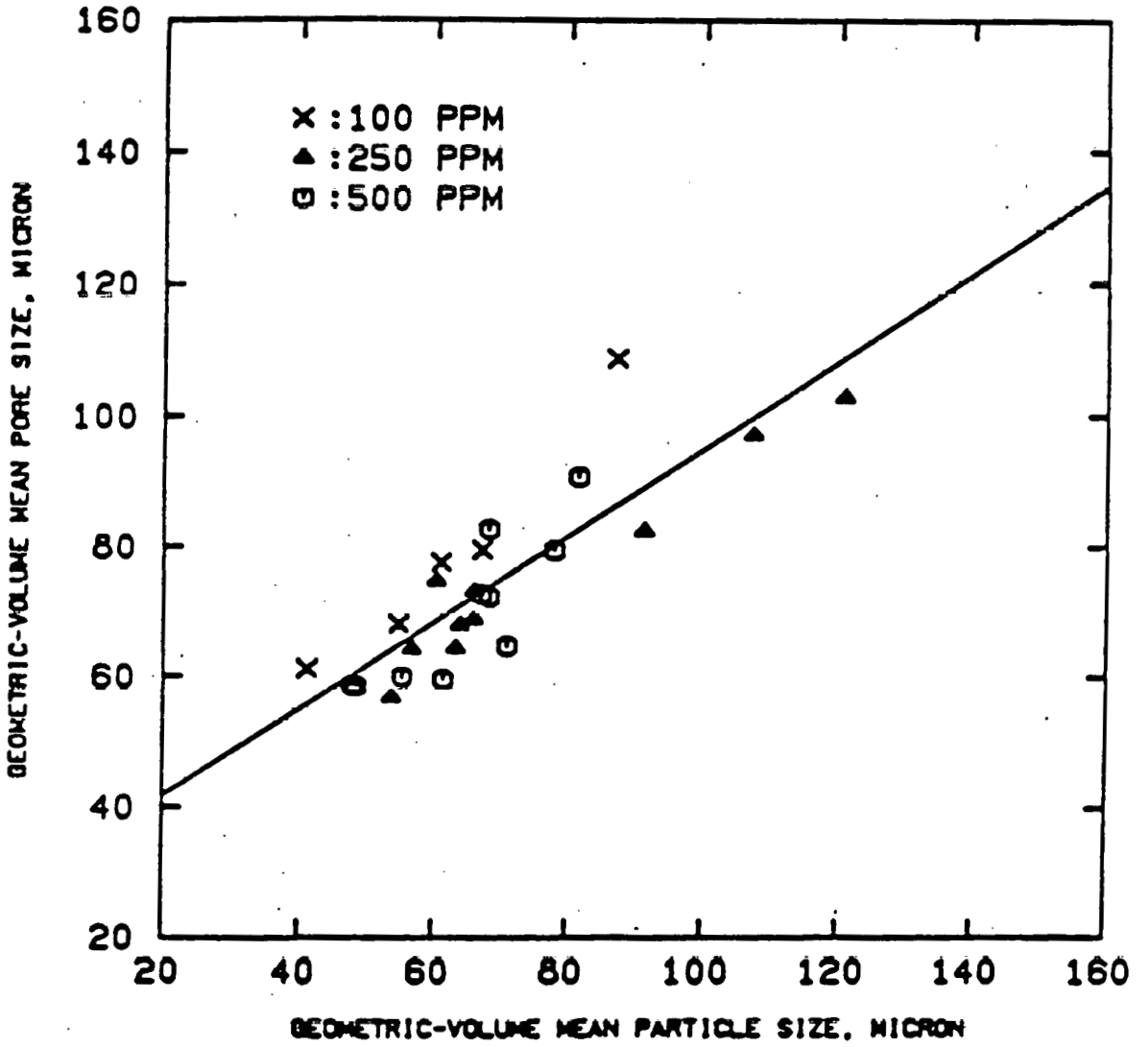

Figure 15 : Effect of Geometric Mean Sizes of the Particles on the Geometric Mean Sizes of the Pores for All Concentrations of Triton X-114 Using a Wash Ratio of Two.

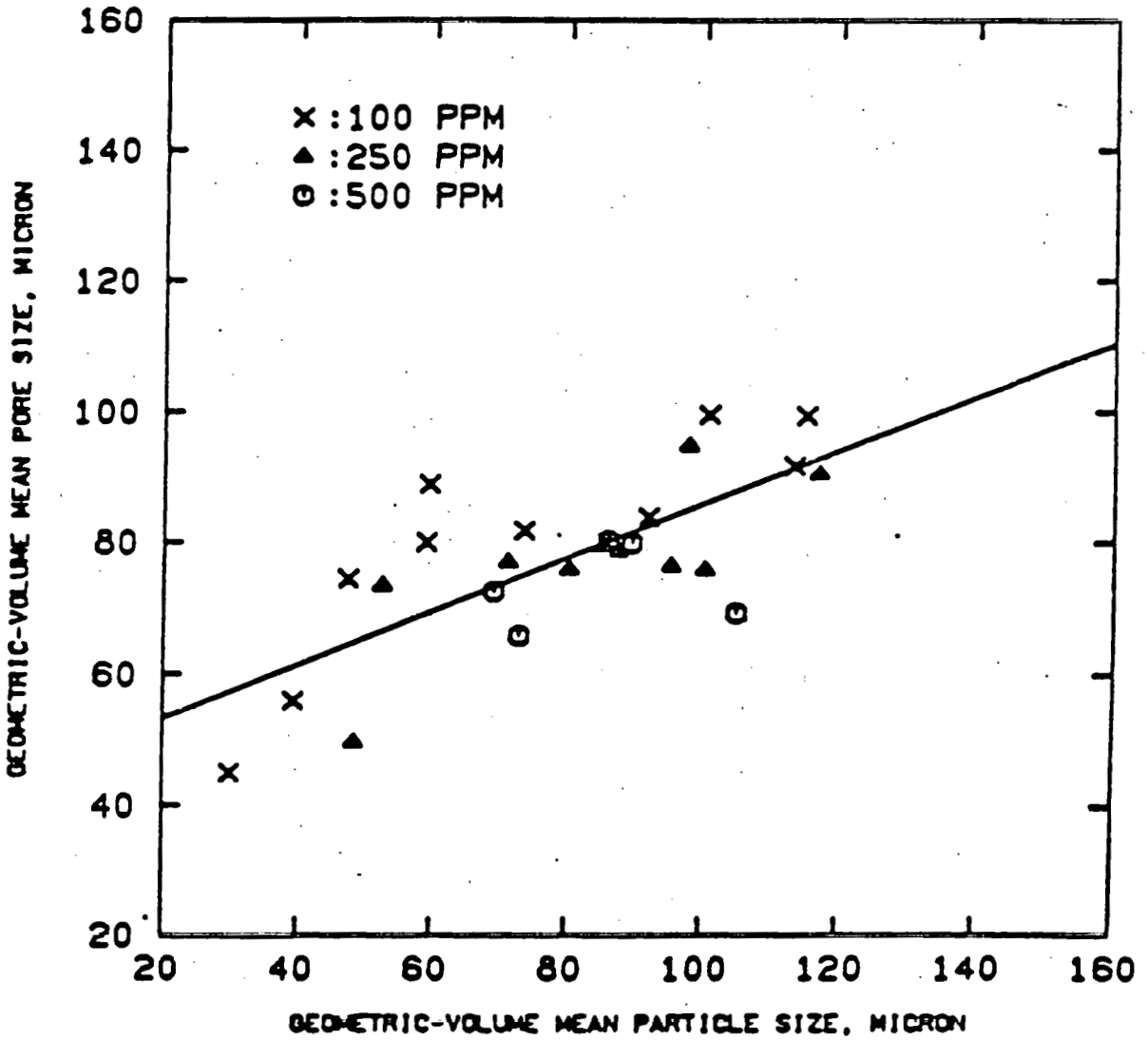

Figure 16 : Effect of Geometric Mean Sizes of the Particles on the Geometric Mean Sizes of the Pores for All Concentrations of Triton X-114 Using a Wash Ratio of Ten.

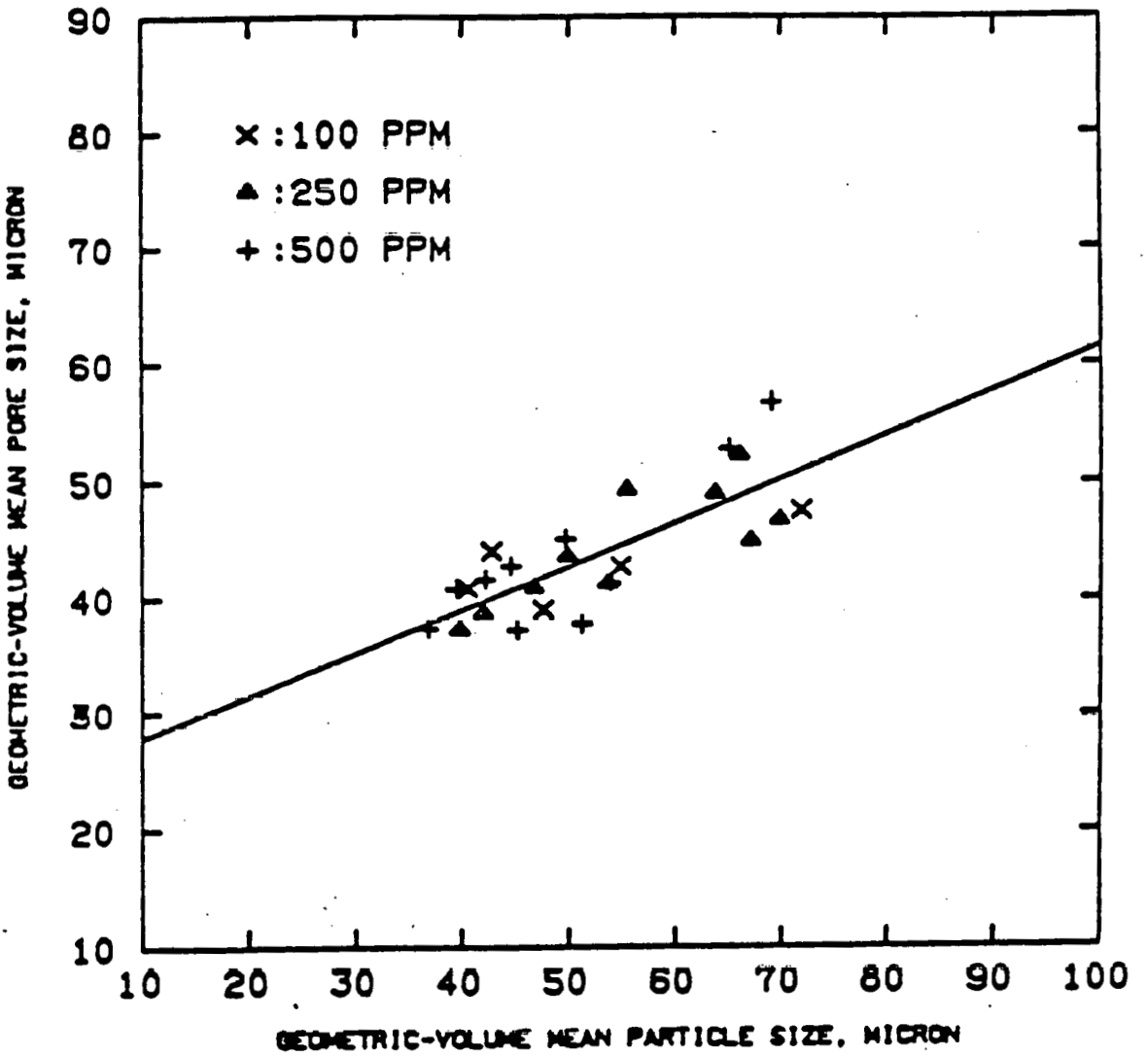

Figure 17: Effect of Geometric Mean Sizes of the Particles on the Geometric Mean Sizes of the Pores for All Concentrations of Aerosol-OT Using a Wash Ratio of Two.

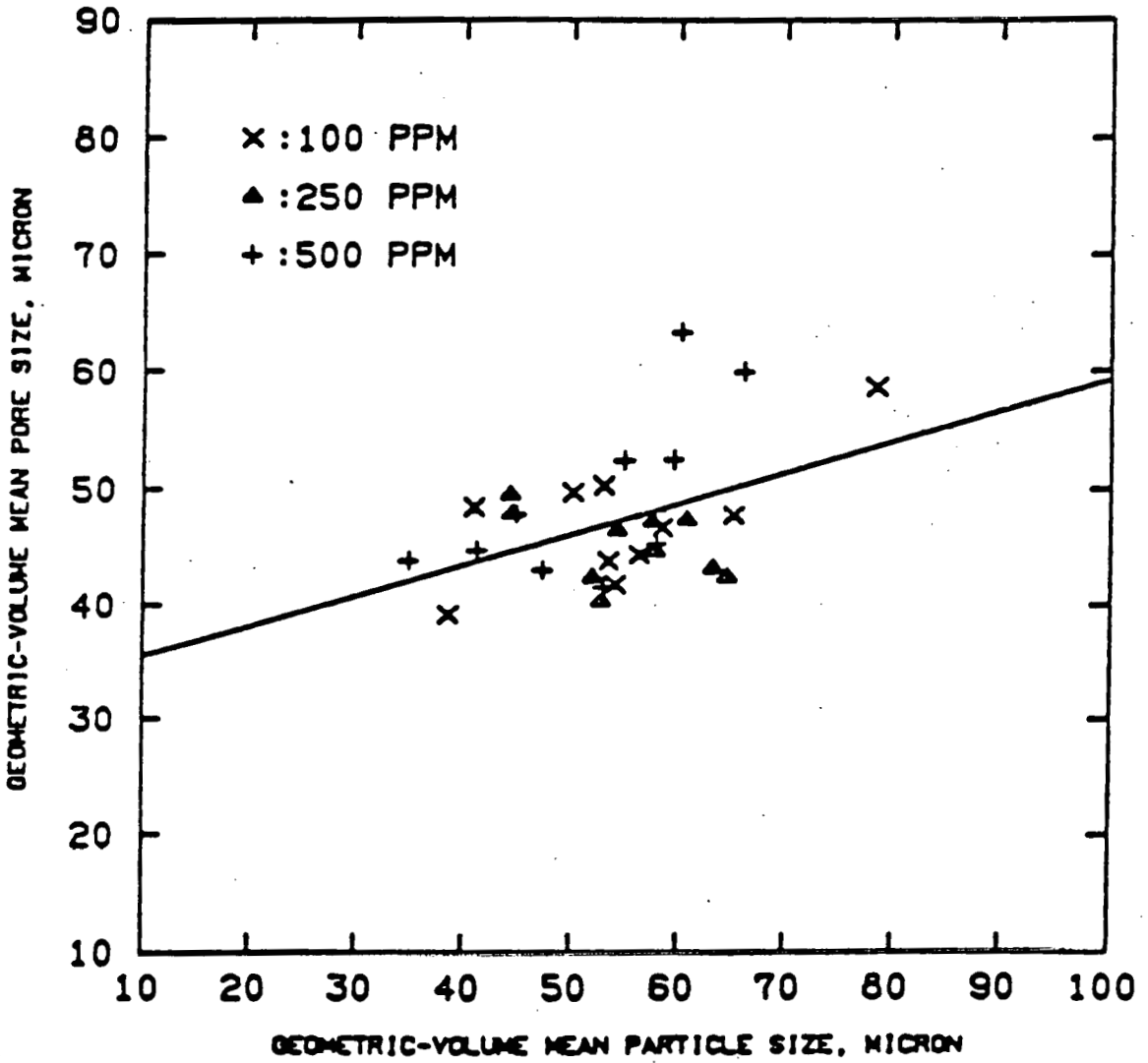

Figure 18: Effect of Geometric Mean Sizes of the Particles on the Geometric Mean Sizes of the Pores for All Concentrations of Aerosol-OT Using a Wash Ratio of Ten.

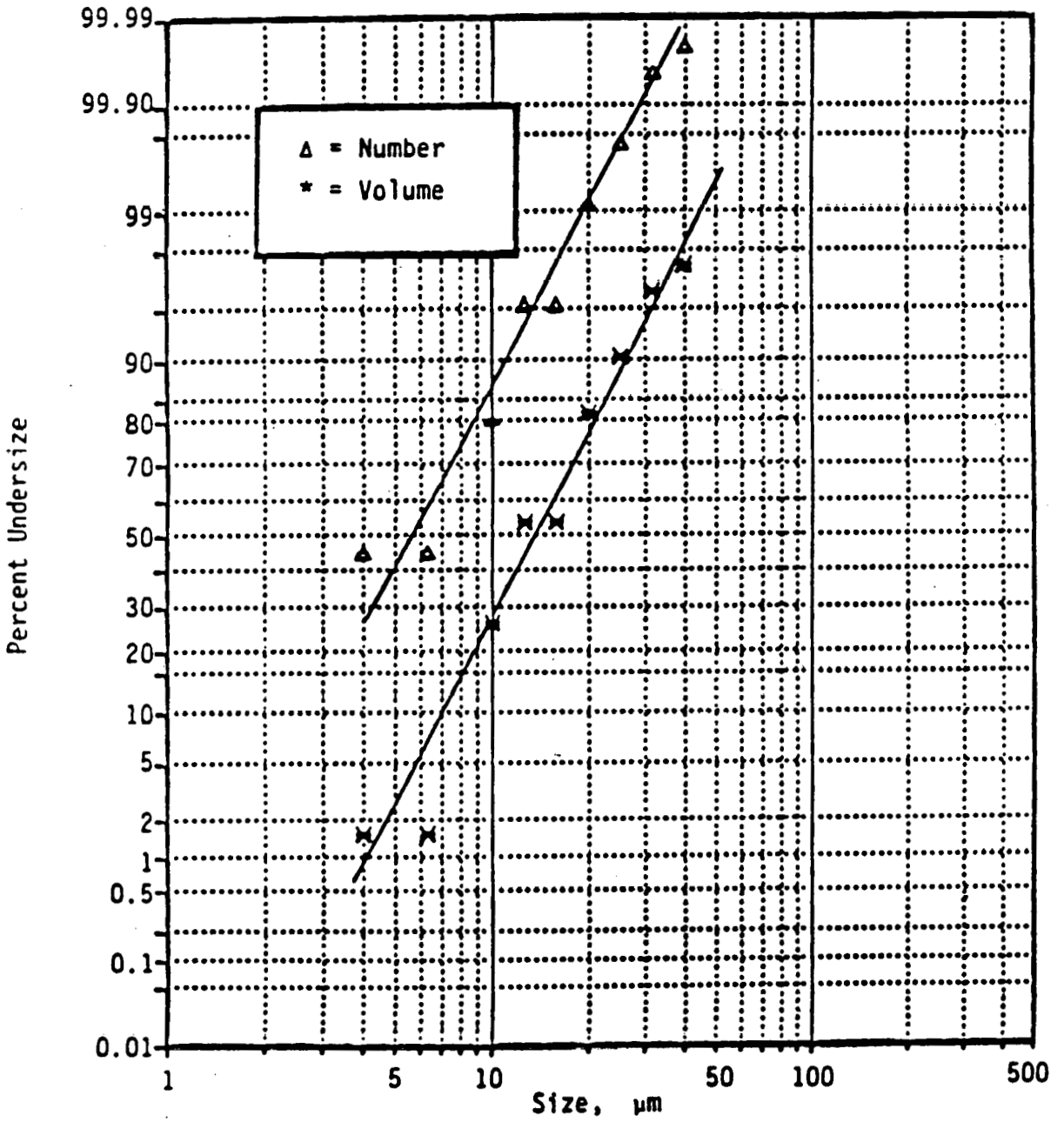

Figure19: Particle Size Distribution of the 10 μm Pittsburgh Seam Bruceton Mine Coal

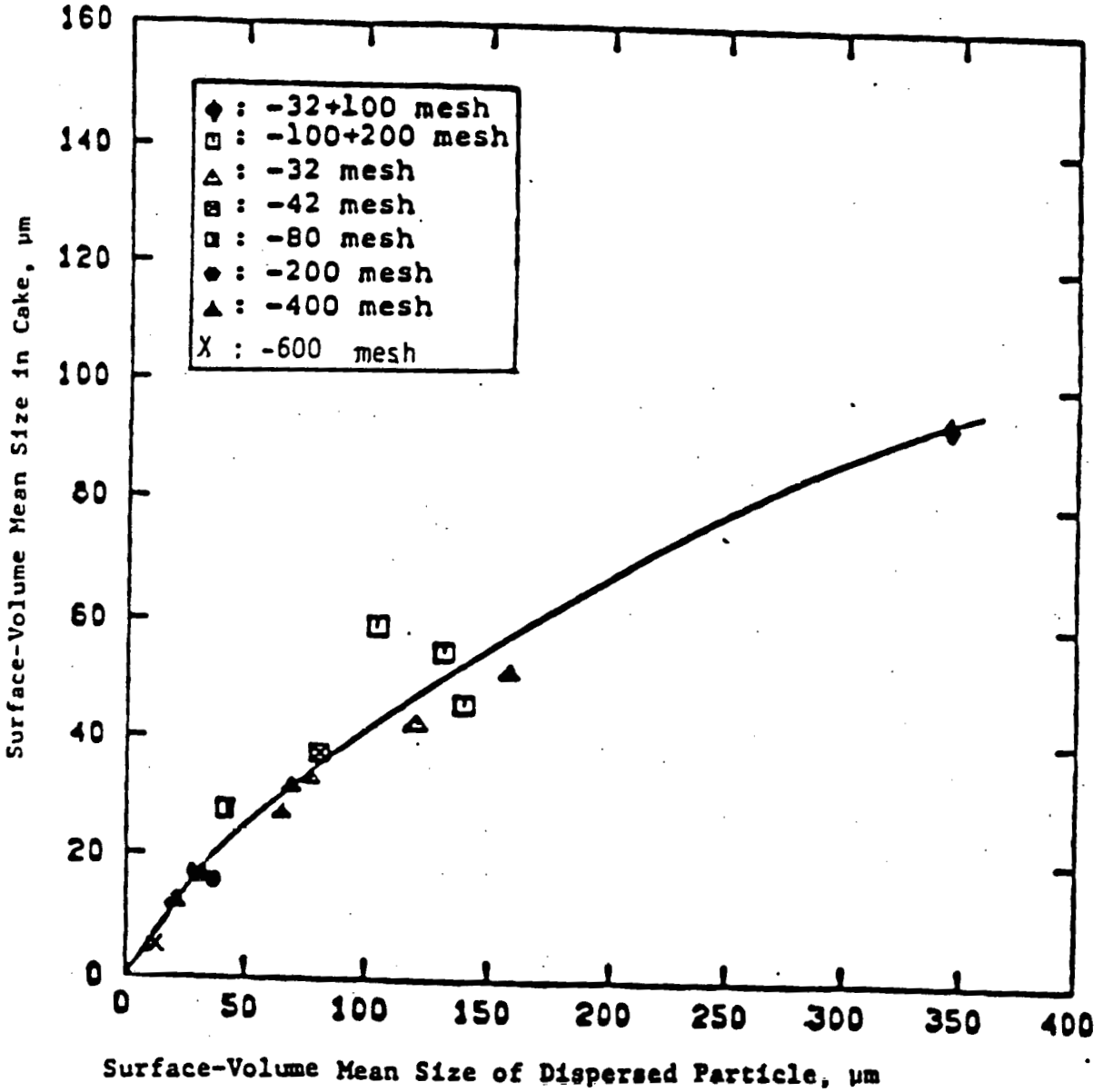

Figure 20 : Comparison of Average Surface-Volume Mean Size in Coal Cake and Surface-Volume Mean Size of Dispersed Coal Sample

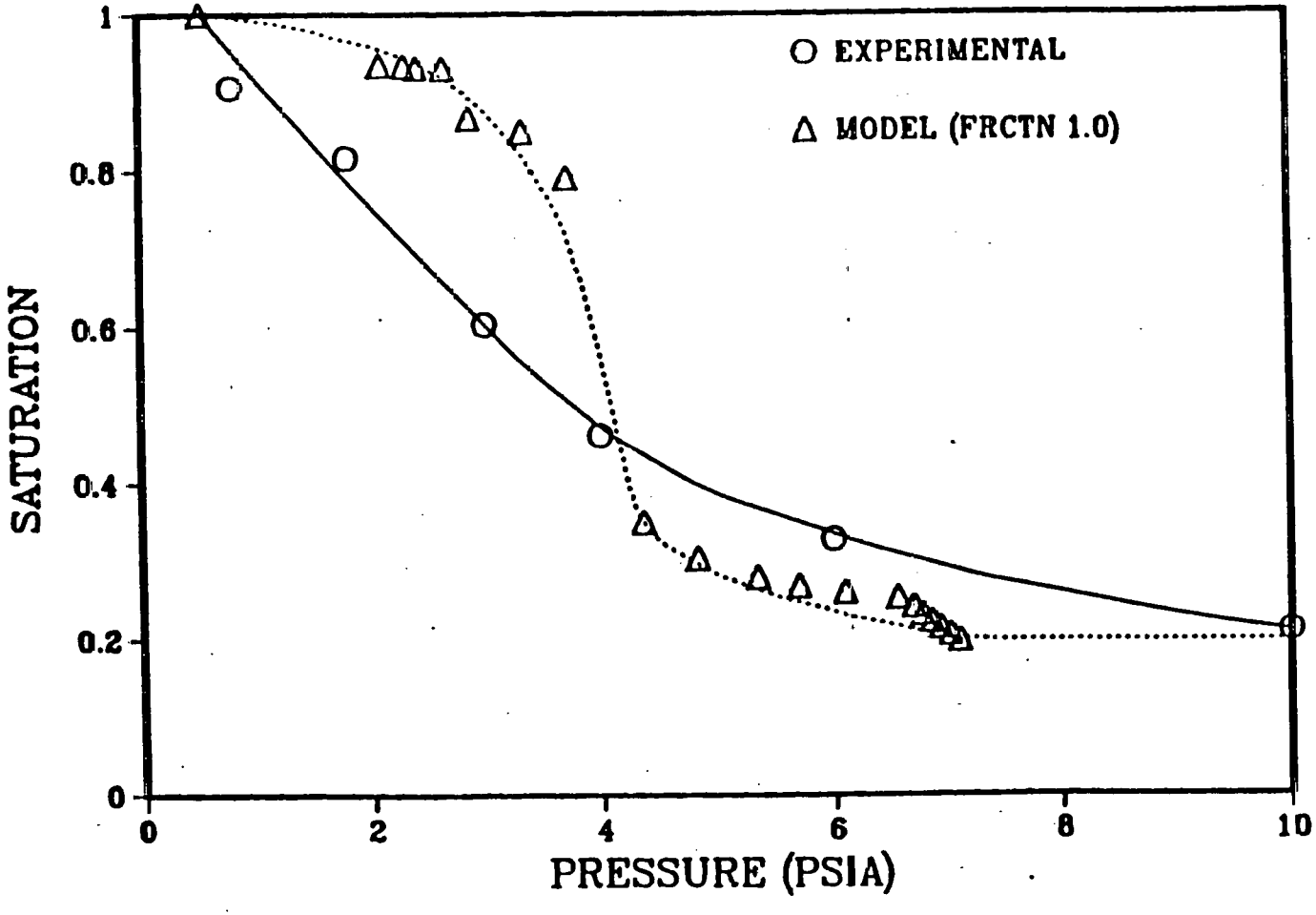

Figure 21: Equilibrium desaturation curve for −32 mesh coal

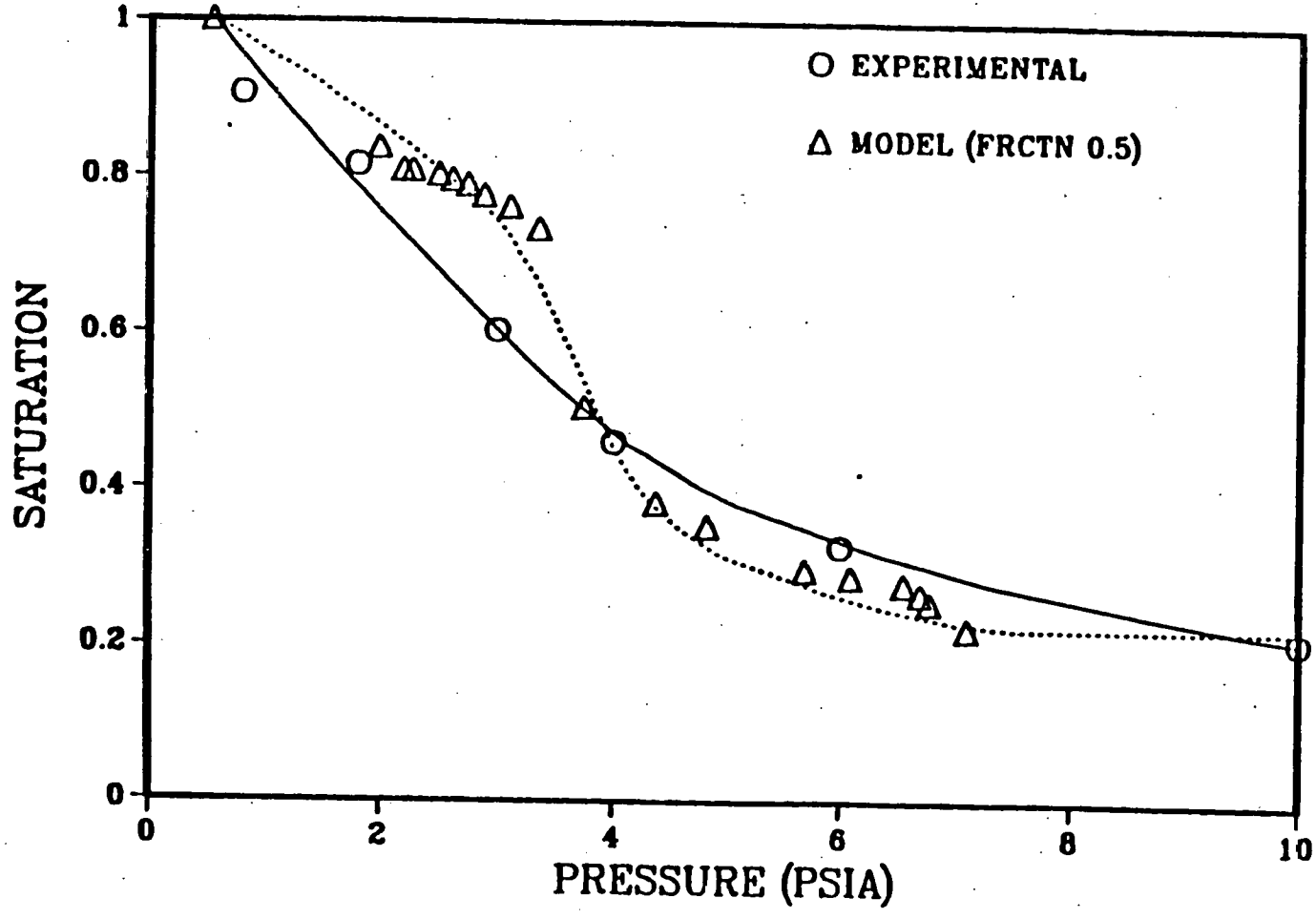

Figure 22: Equilibrium desaturation curve for −32 mesh coal

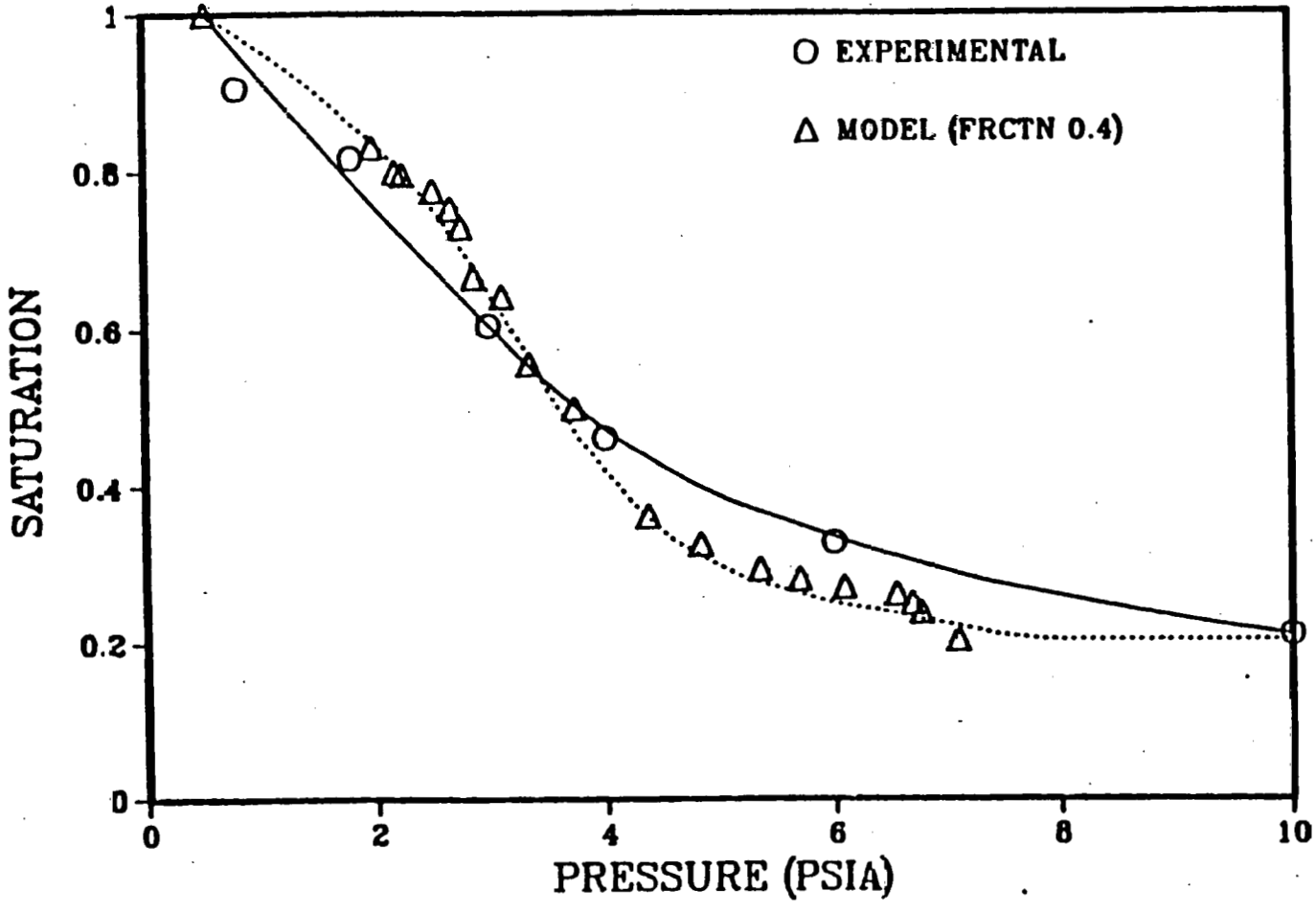

Figure 23: Equilibrium desaturation curve for −32 mesh coal

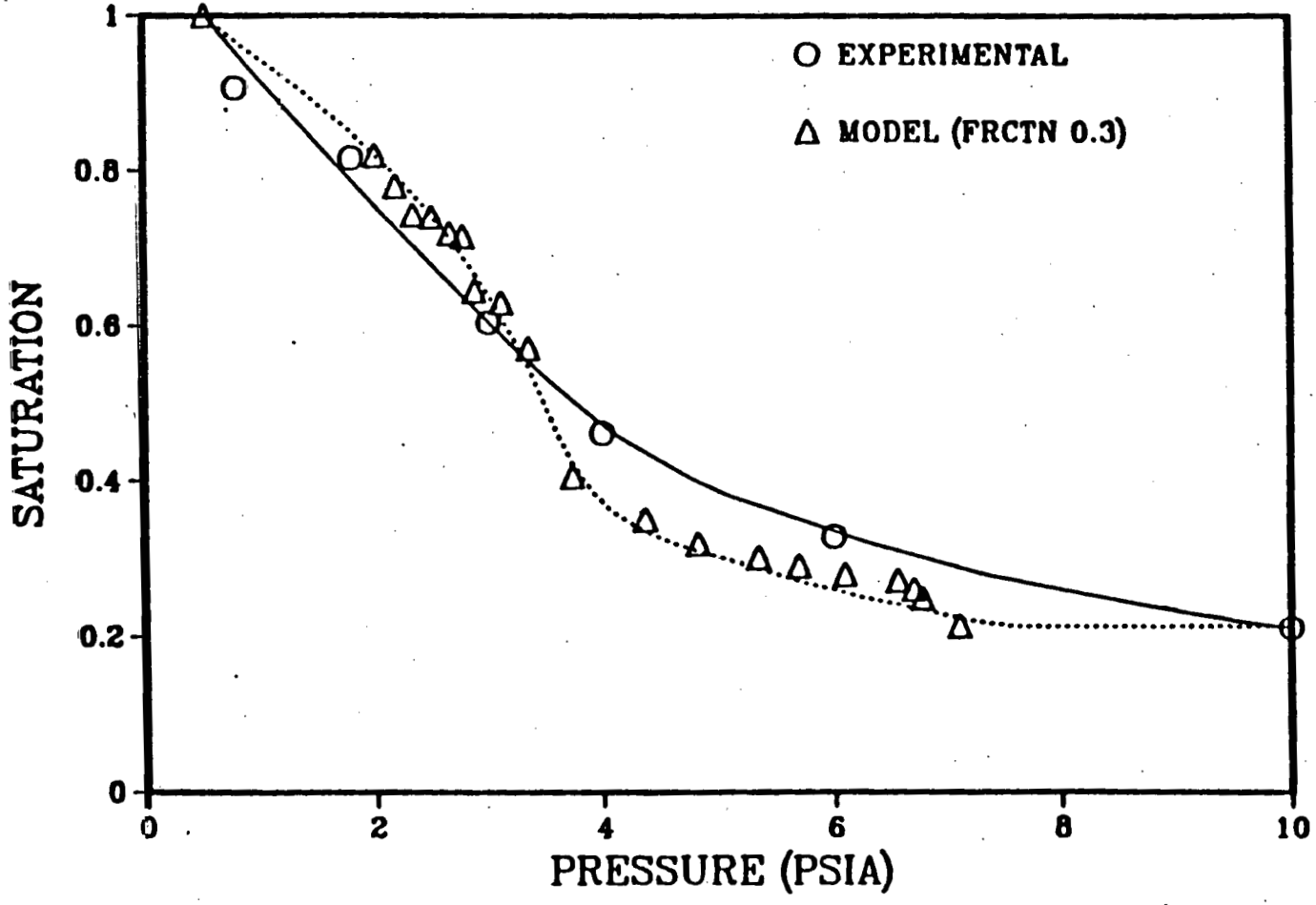

Figure 24: Equilibrium desaturation curve for −32 mesh coal

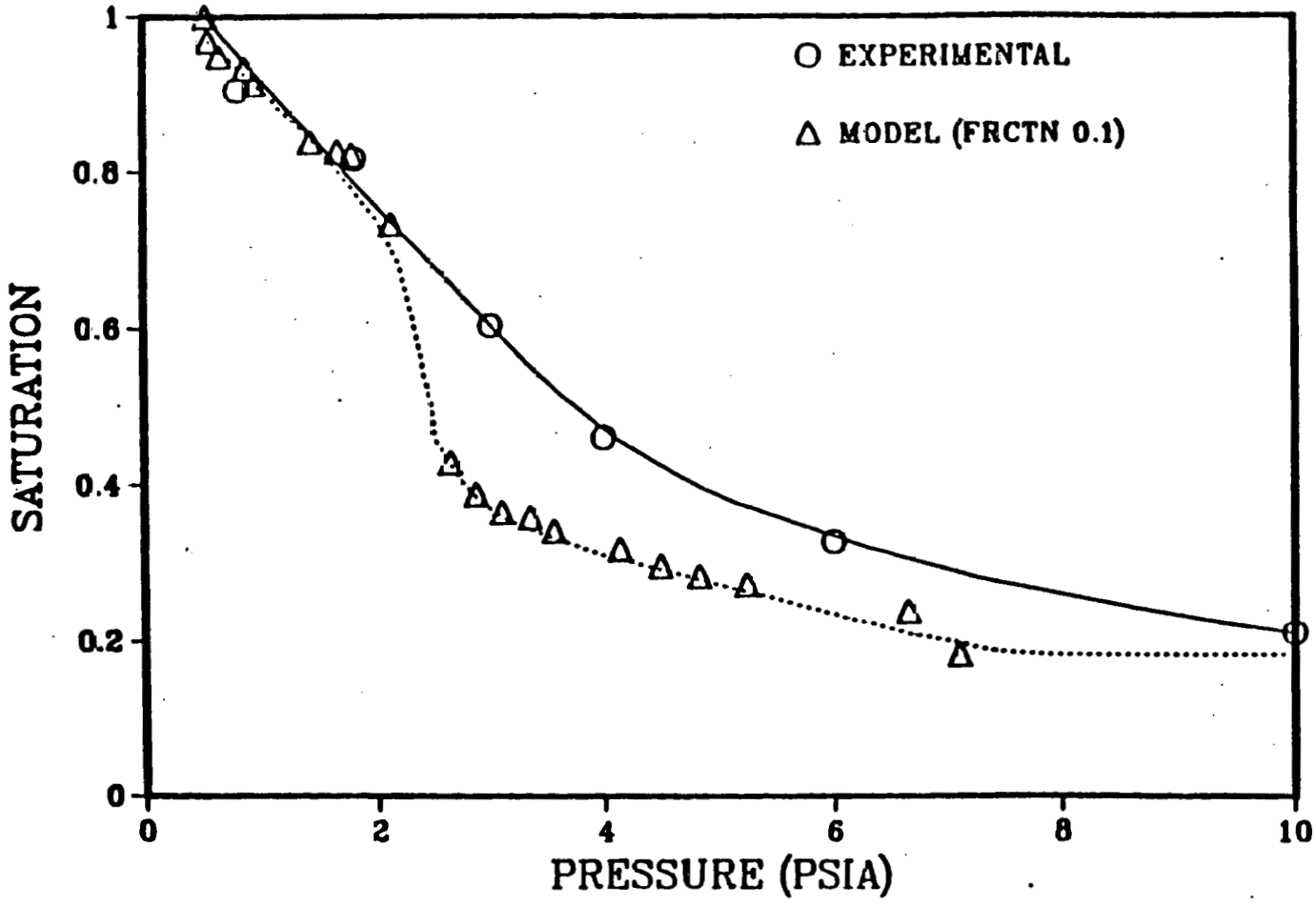

Figure 25: Equilibrium desaturation curve for −32 mesh coal

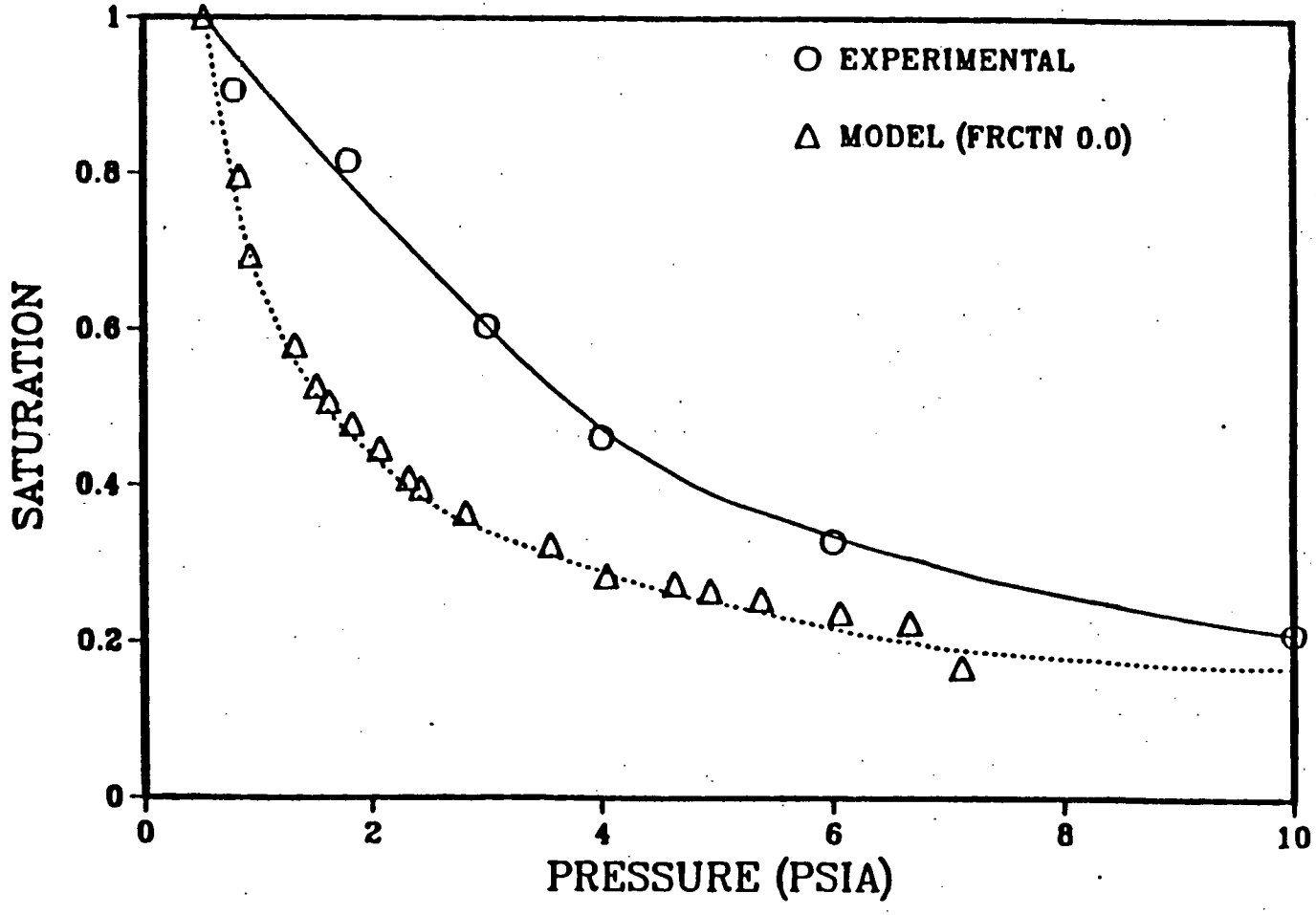

Figure 26: Equilibrium desaturation curve for −32 mesh coal

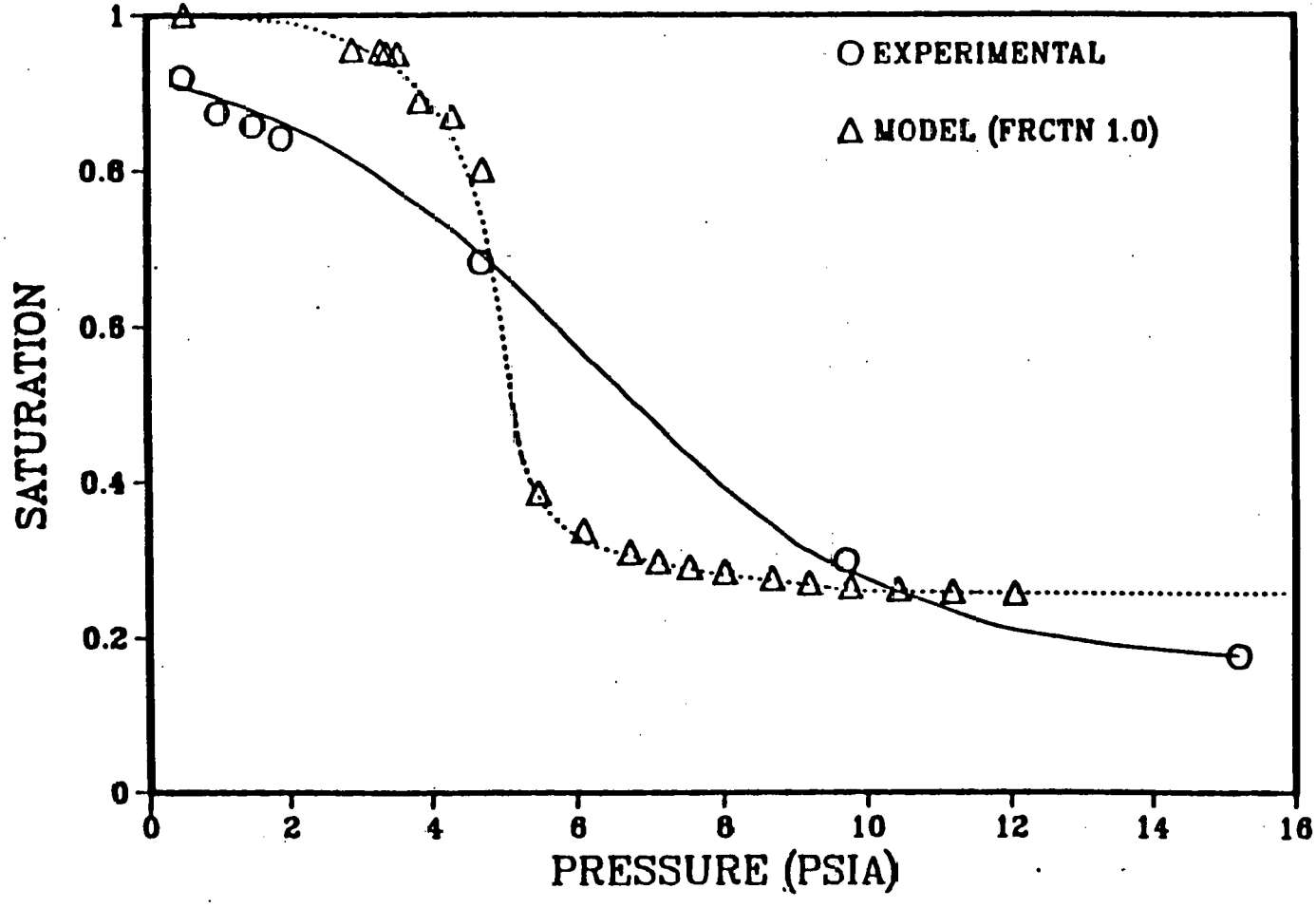

Figure 27: Equilibrium desaturation curve for −200 mesh coal

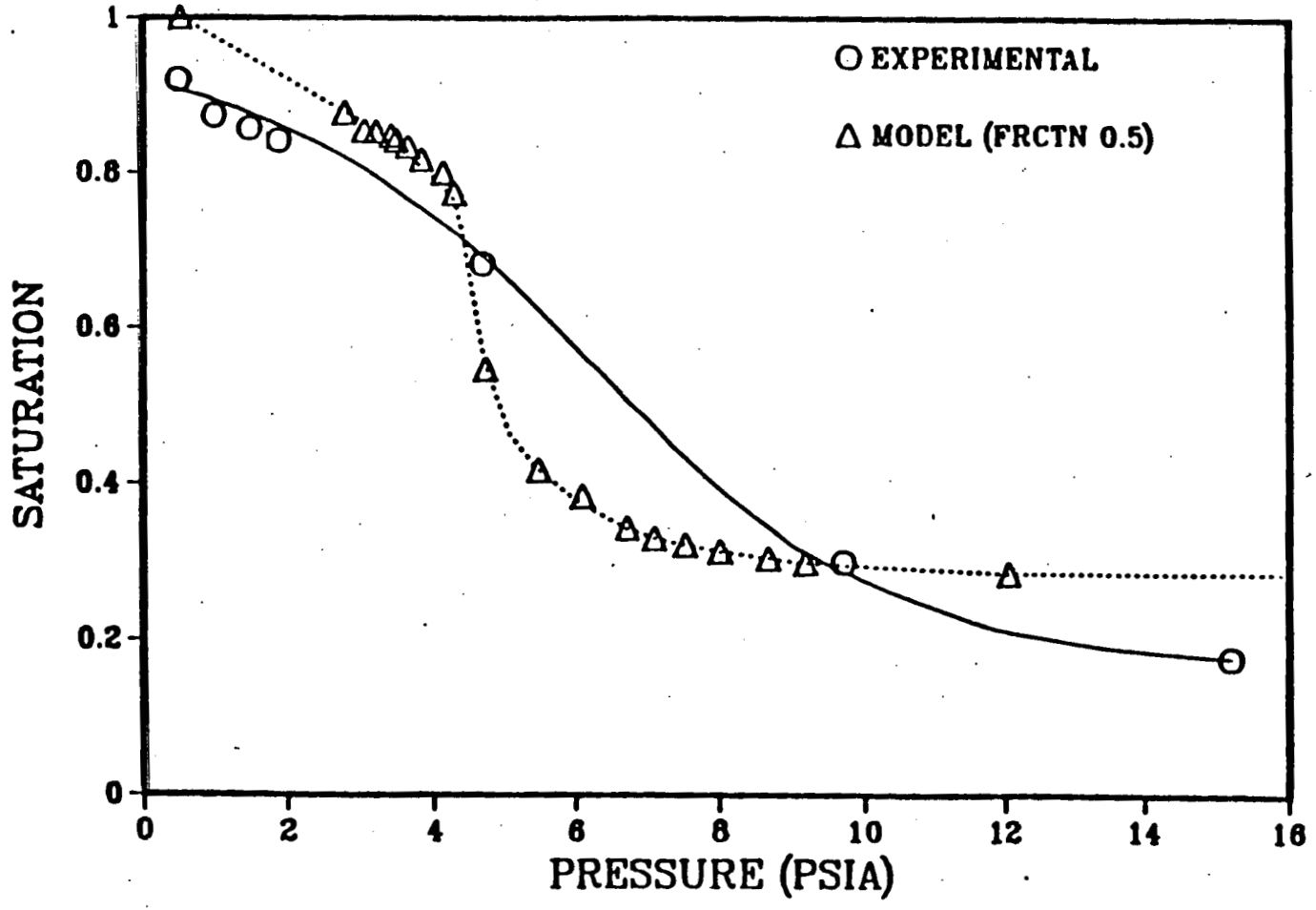

Figure 28: Equilibrium desaturation curve for −200 mesh coal

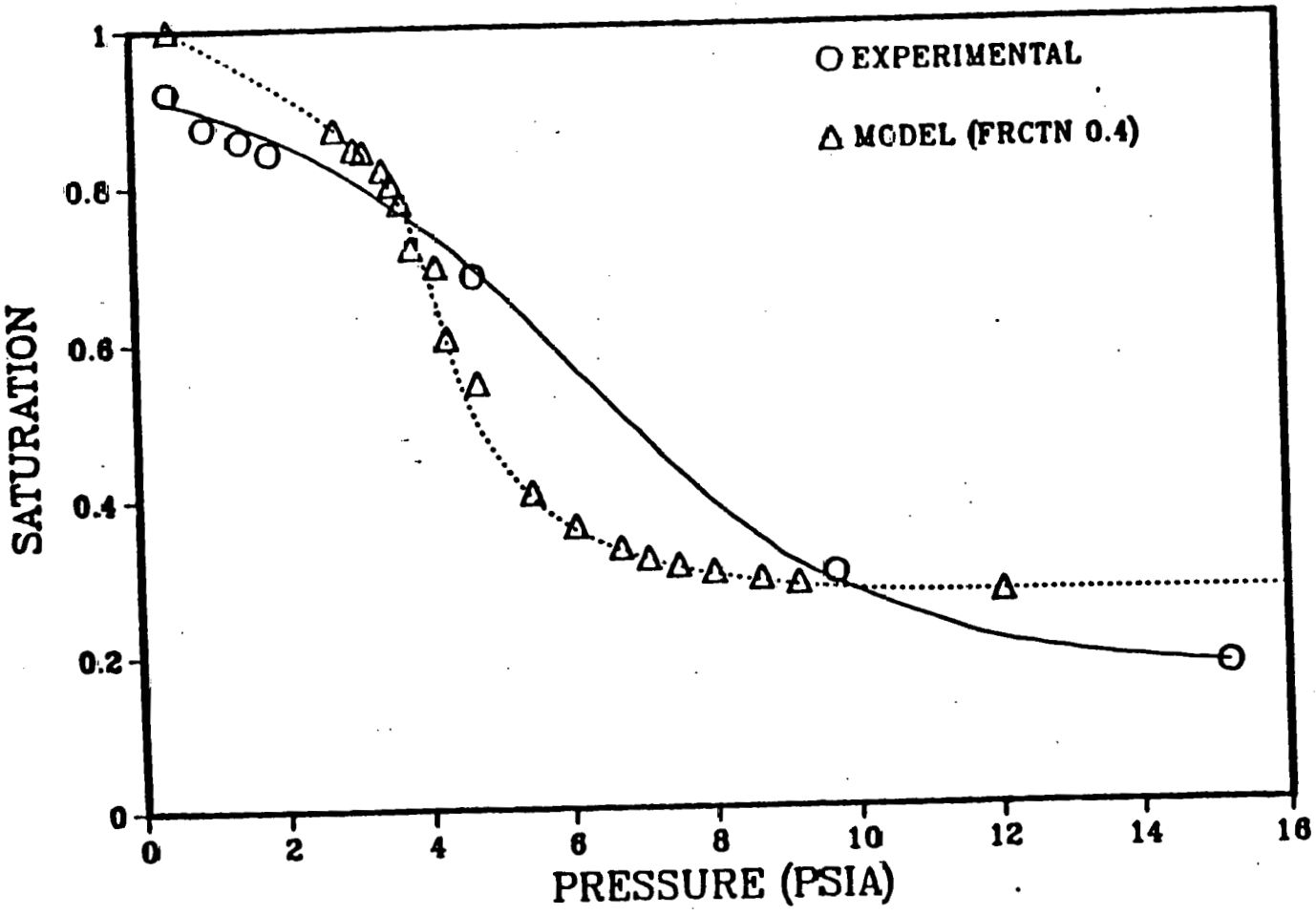

Figure 29: Equilibrium desaturation curve for −200 mesh coal

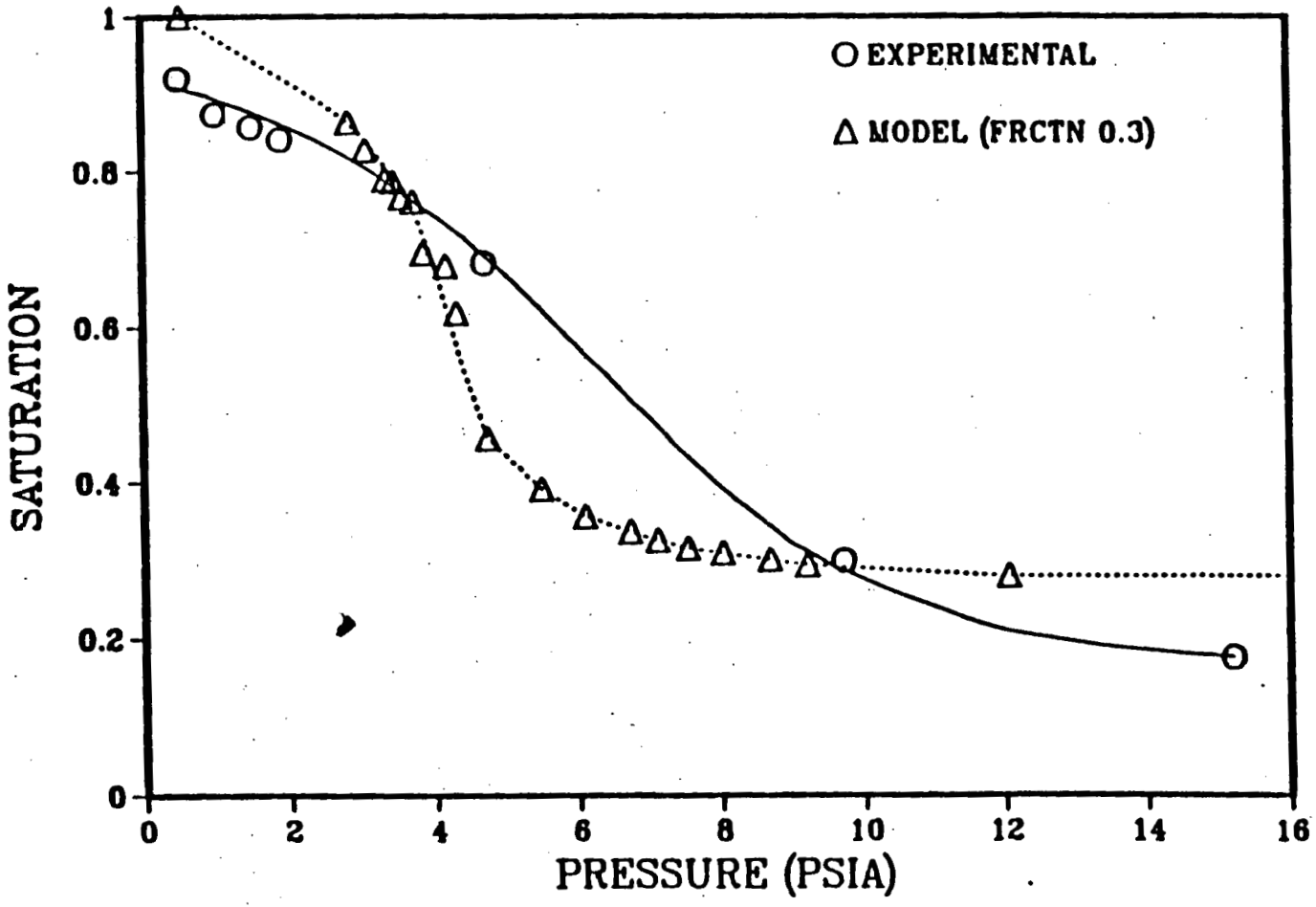

Figure 30: Equilibrium desaturation curve for −200 mesh coal

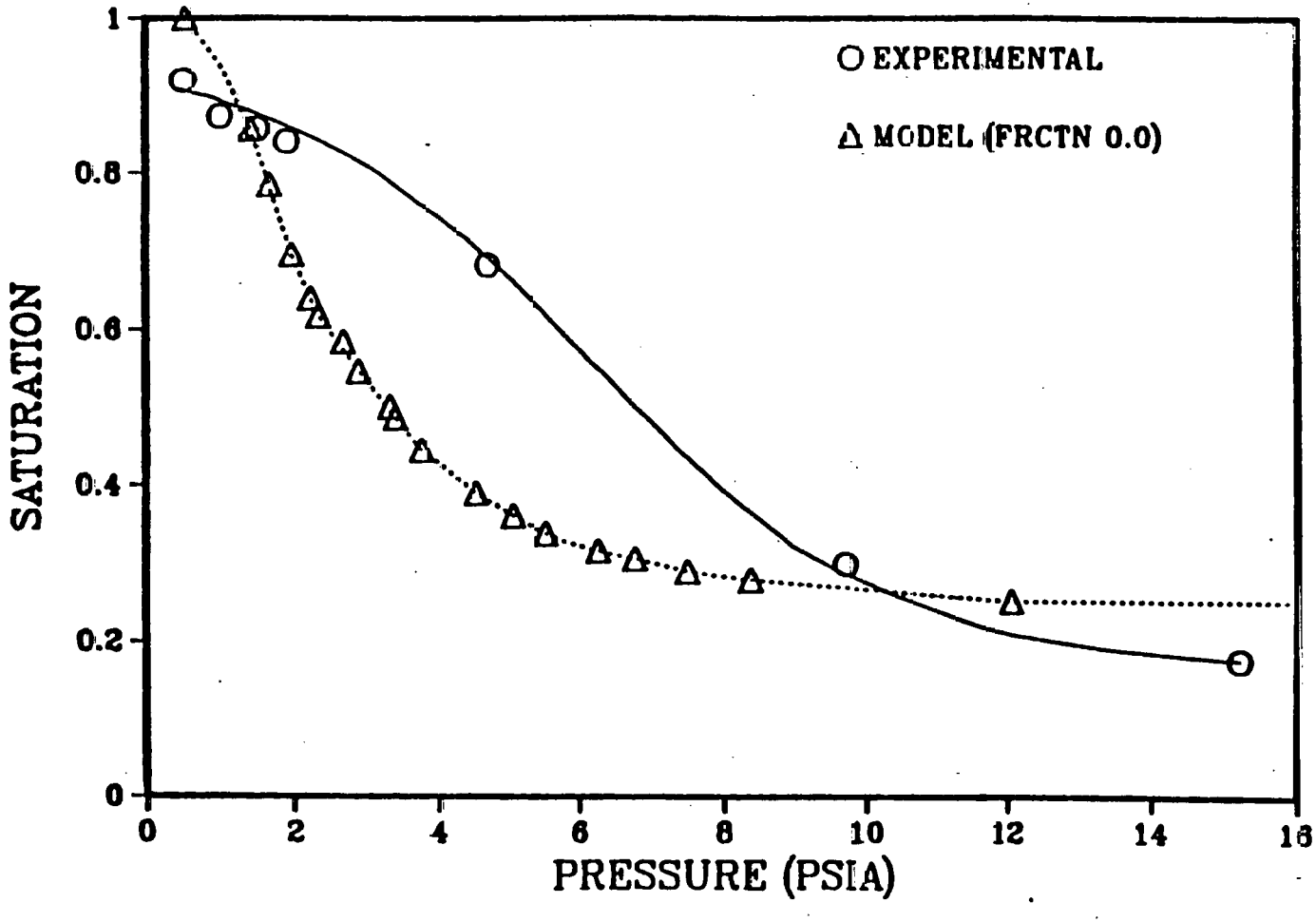

Figure 31: Equilibrium desaturation curve for −200 mesh coal

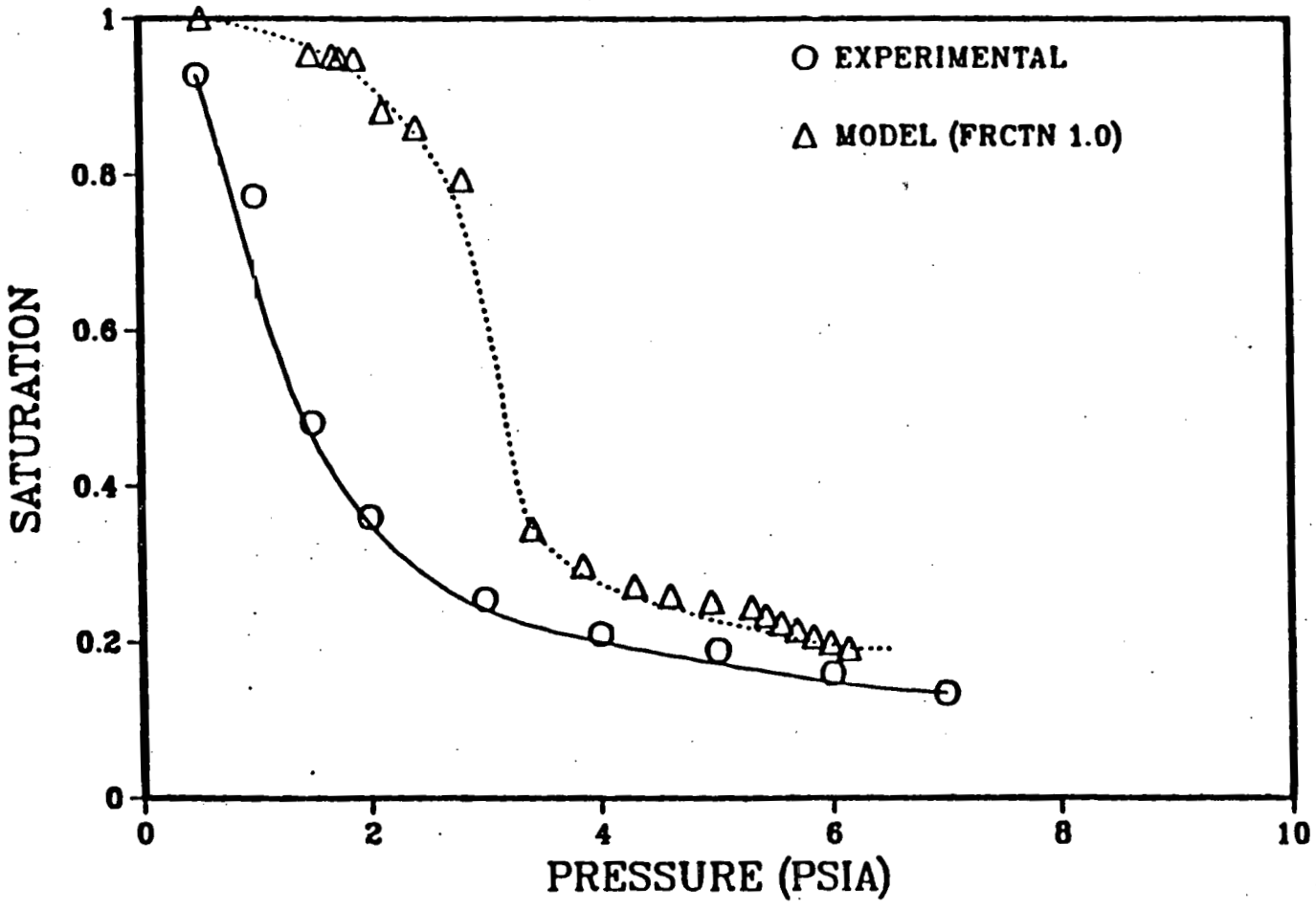

Figure 32: Equilibrium desaturation curve for −100+200 mesh coal

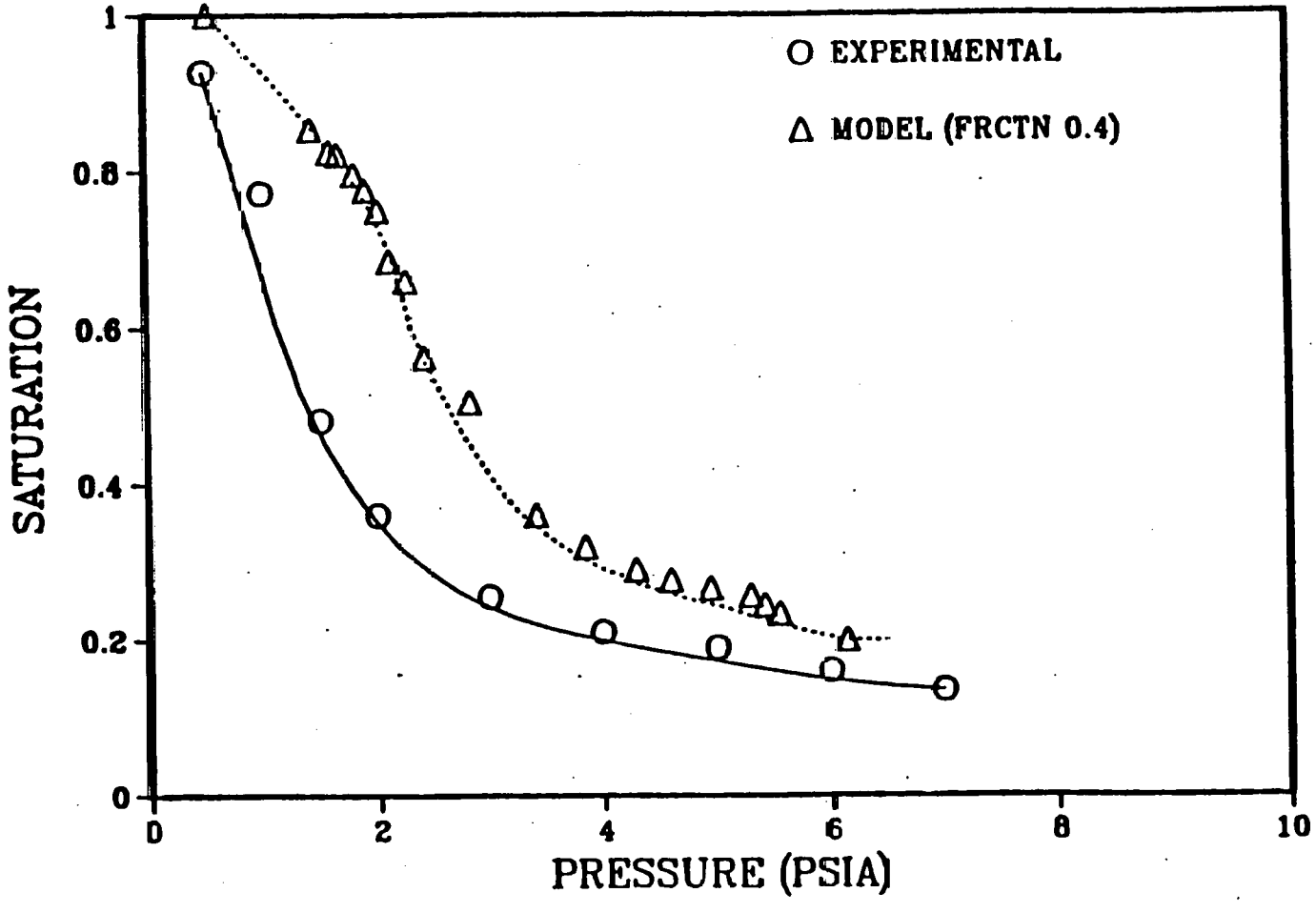

Figure 33: Equilibrium desaturation curve for −100+200 mesh coal

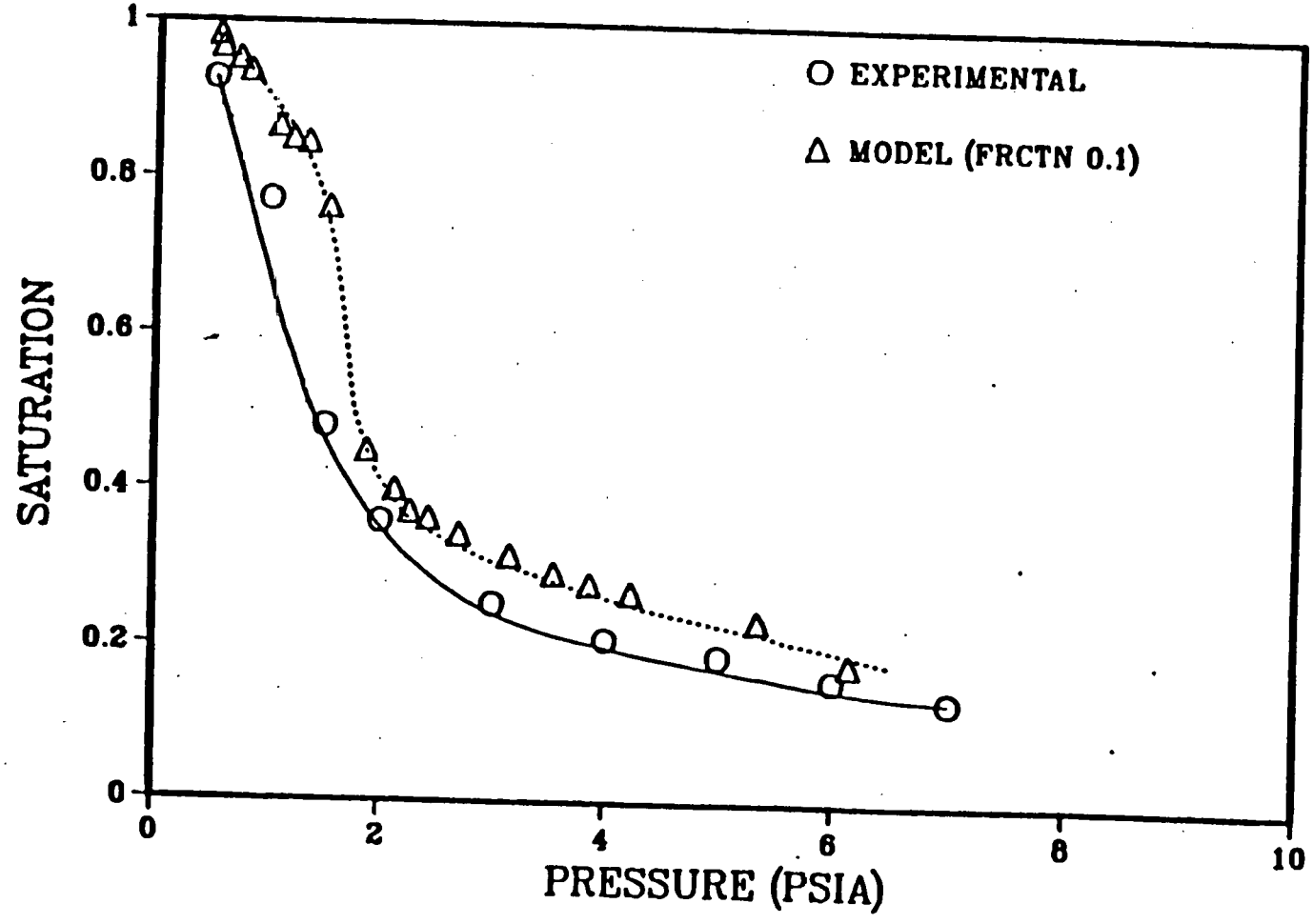

Figure 34: Equilibrium desaturation curve for −100+200 mesh coal

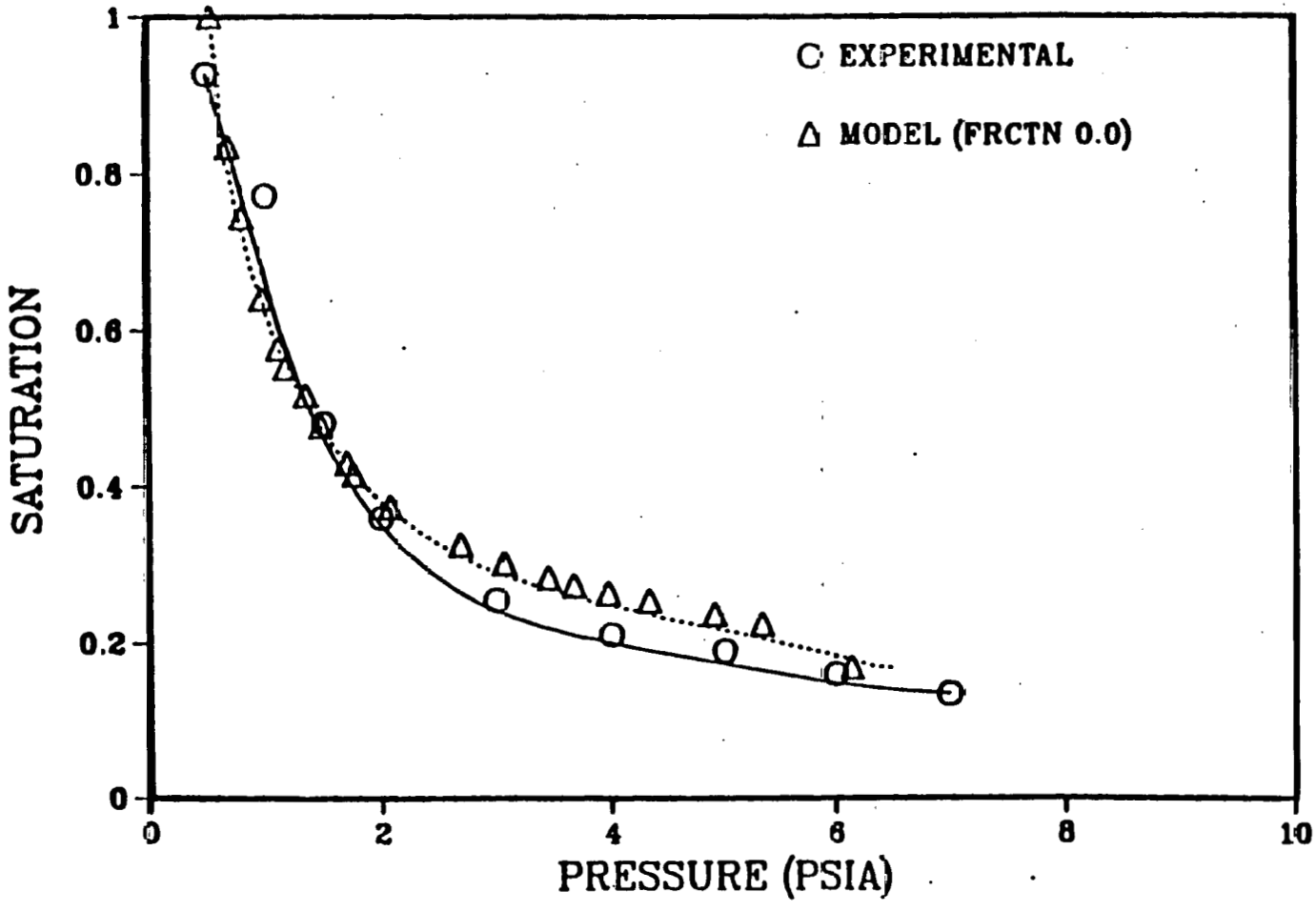

Figure 35: Equilibrium desaturation curve for −100+200 mesh coal

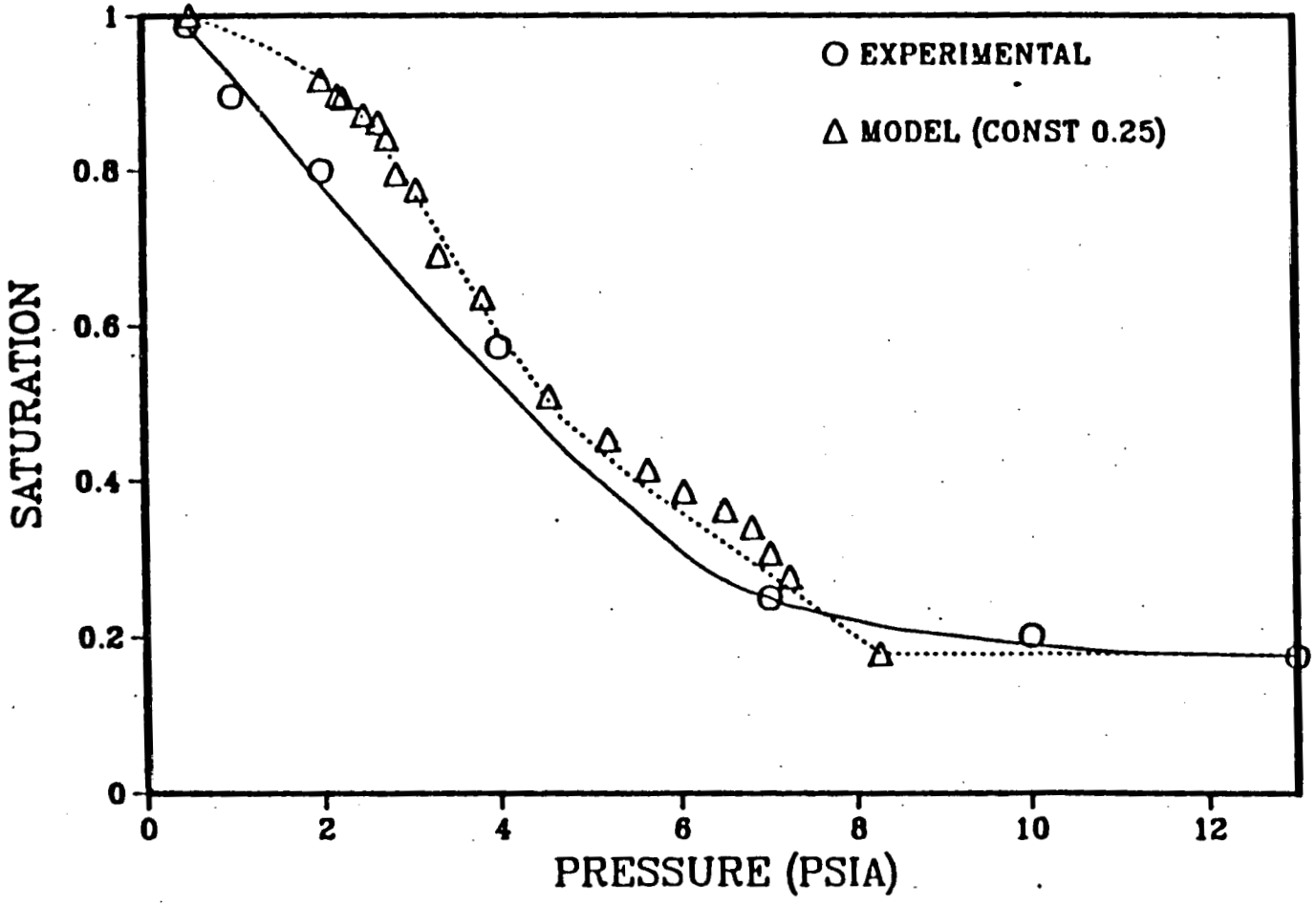

Figure 36: Equilibrium desaturation curve for −32 mesh coal Cake formed with Triton X−114 200 ppm

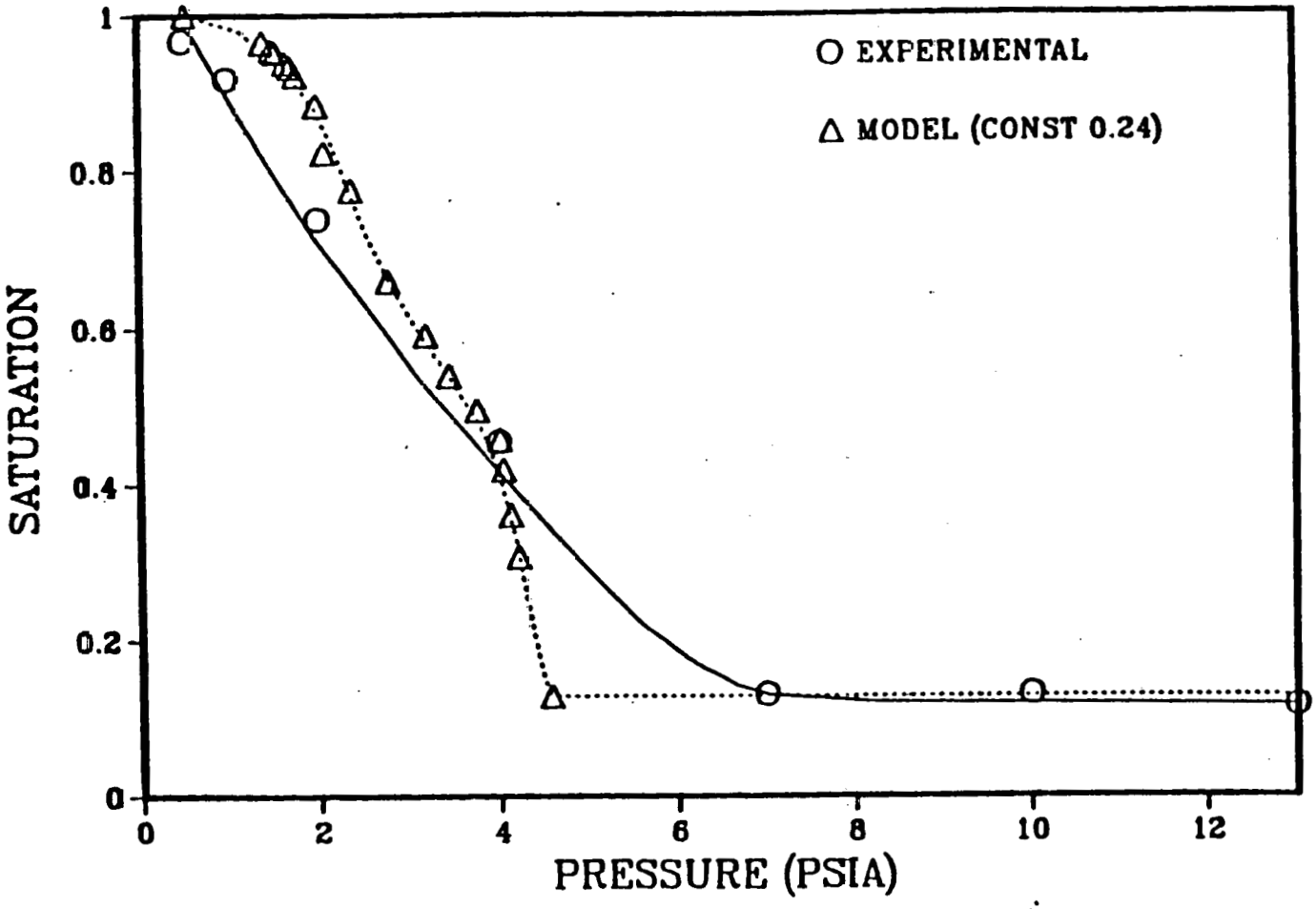

Figure 37: Equilibrium desaturation curve for −32 mesh coal Cake formed with Triton X−114 500 ppm

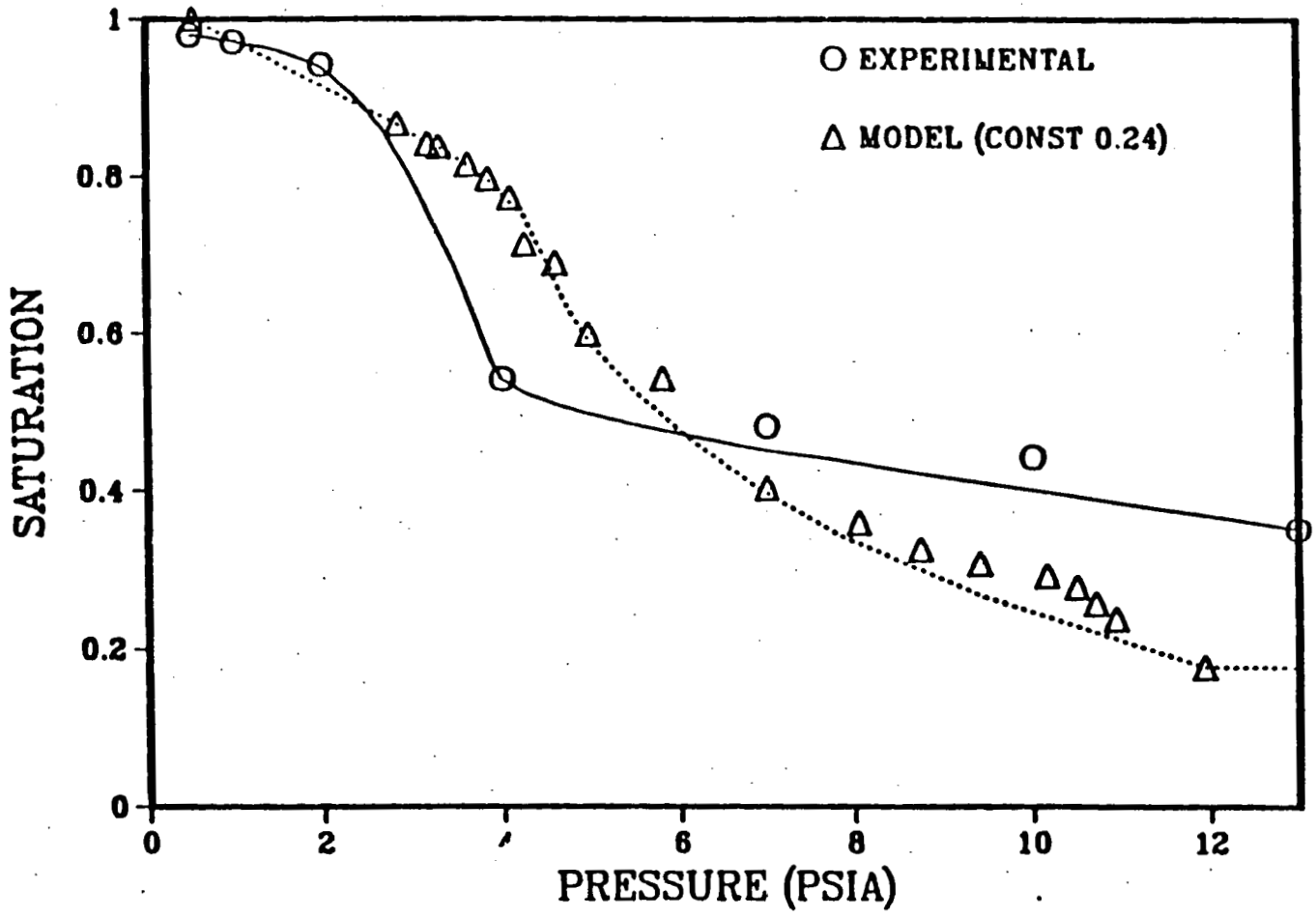

Figure 38: Equilibrium desaturation curve for −32 mesh coal Cake formed with Triton X−114 500 ppm

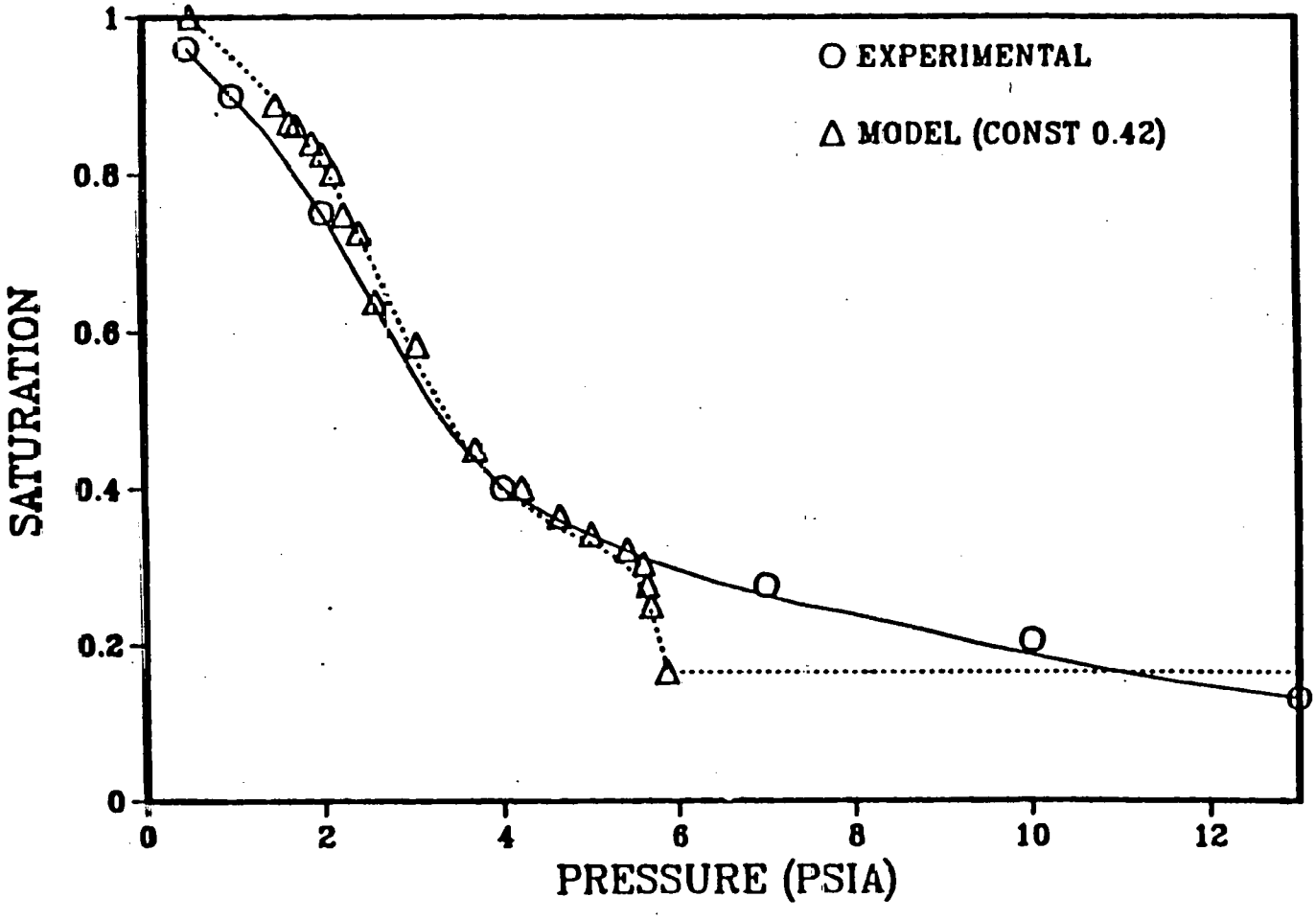

Figure 39: Equilibrium desaturation curve for −32 mesh coal Cake formed with MIBC 1000 ppm

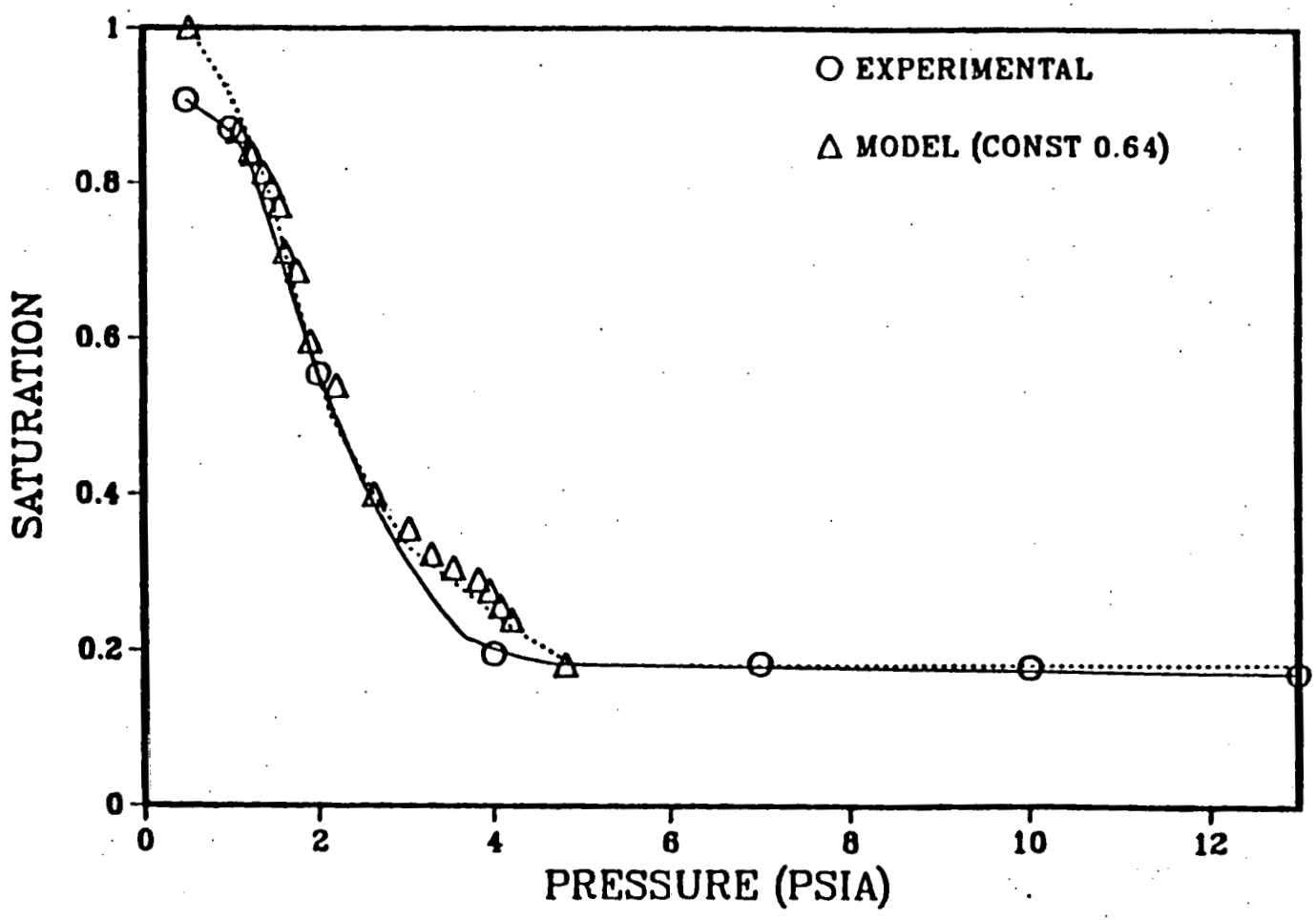

Figure 40: Equilibrium desaturation curve for −32 mesh coal Cake formed with Triton/Floc. 30 ppm

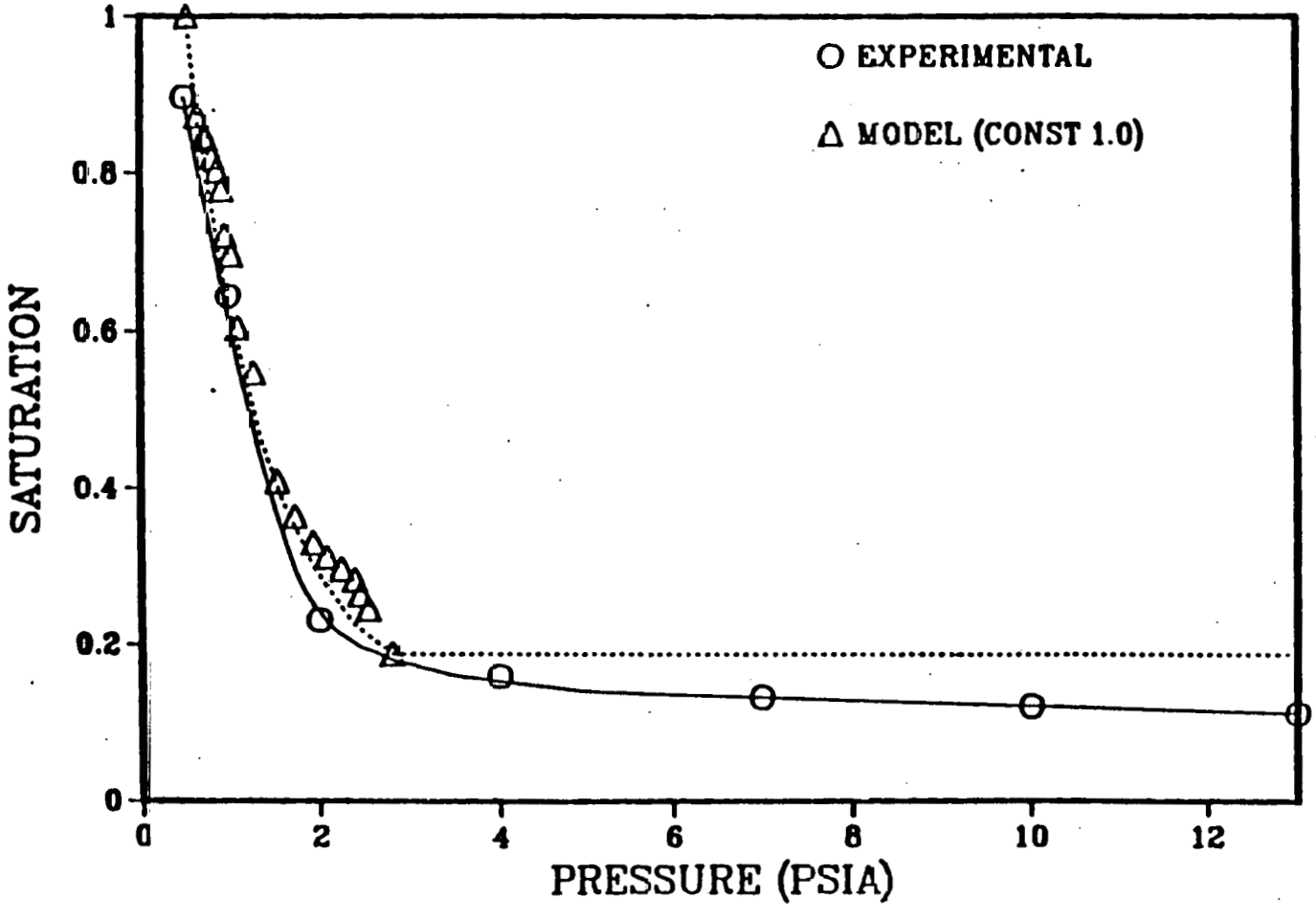

Figure 41: Equilibrium desaturation curve for −32 mesh coal Cake formed with Triton/Floc. 125 ppm

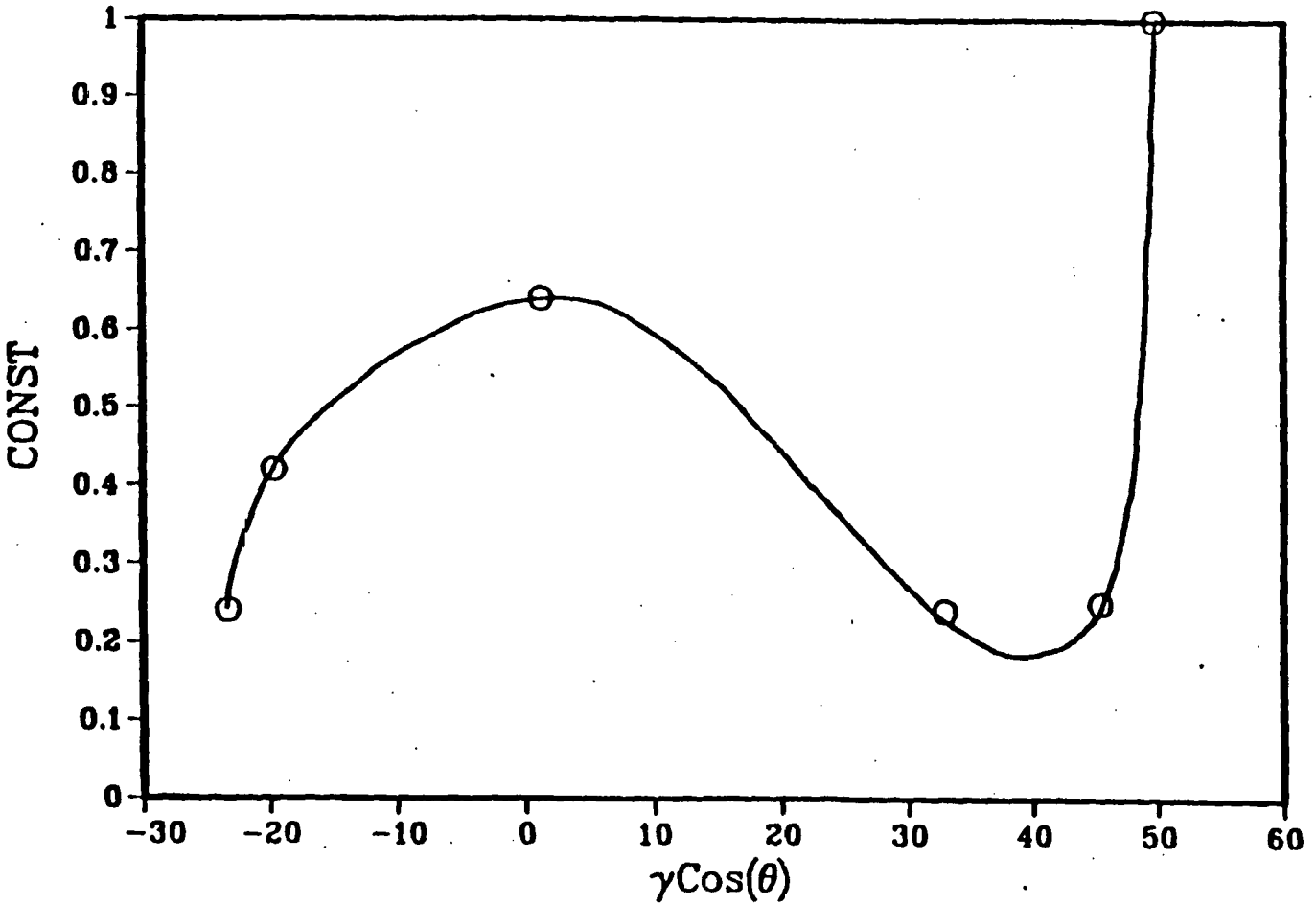

Figure 42: Correlation between modified entry diameter constant (for surfactant cakes) and experimental surface tension and contact angle values

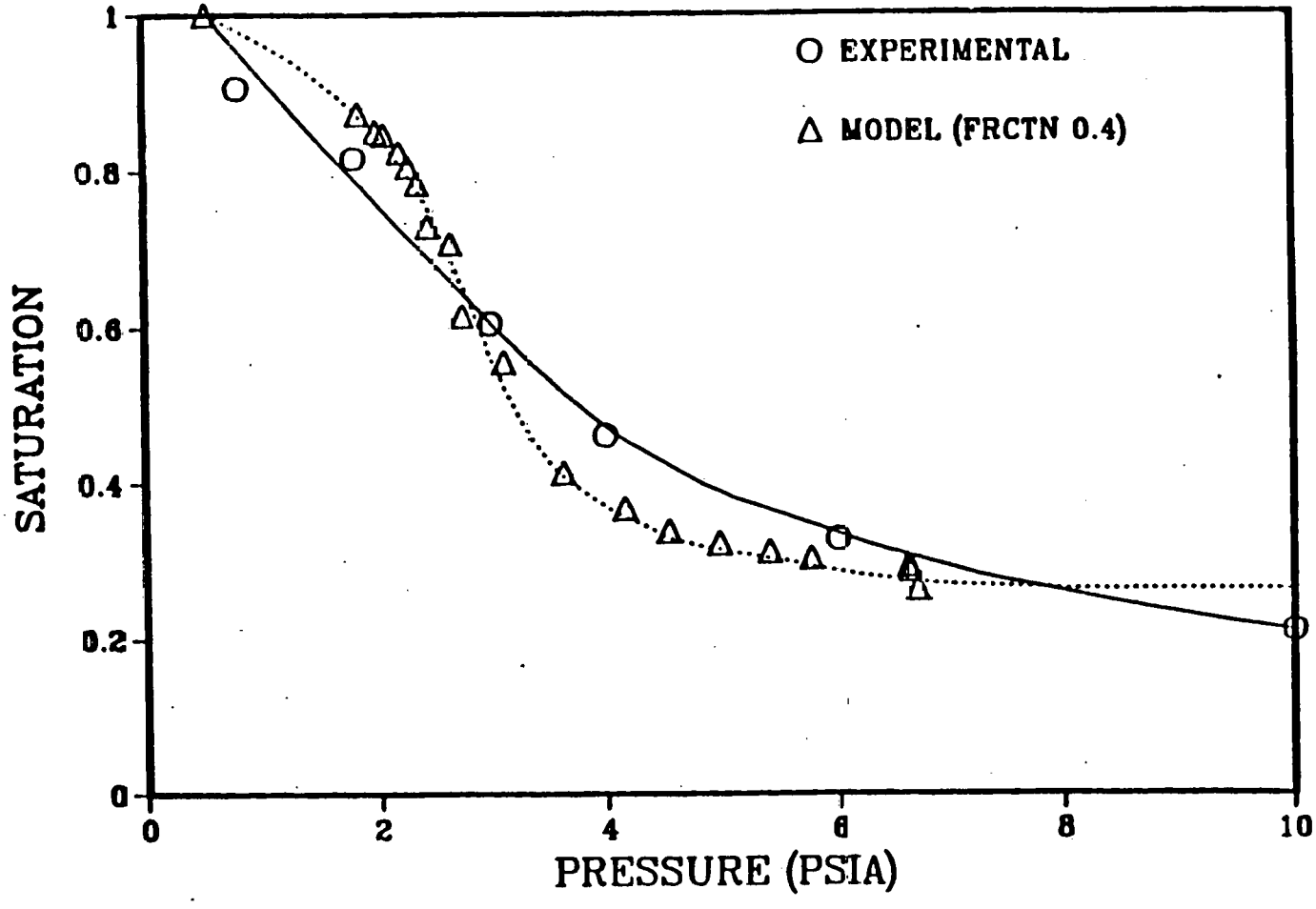

Figure 43: Equilibrium desaturation curve for −32 mesh coal when pore size distribution is estimated from dispersed particle size distribution

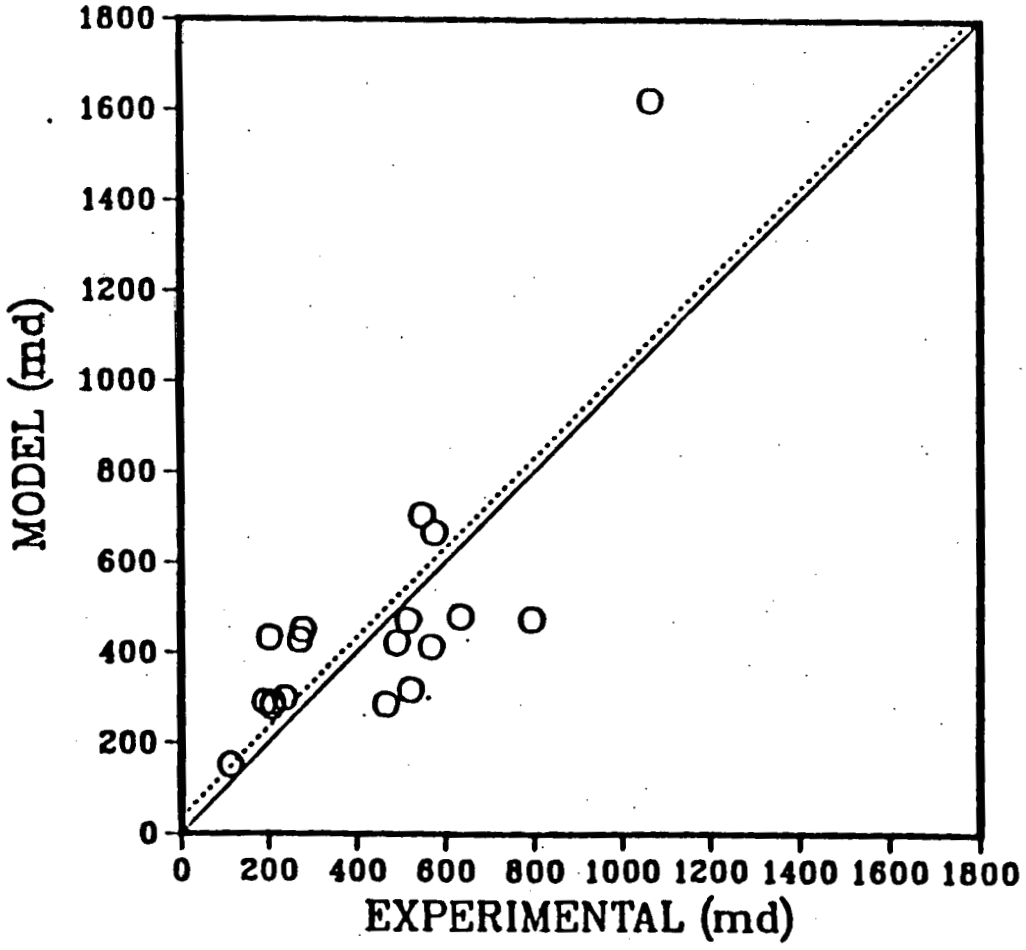

Figure 44: Comparison of the Experimental and Predicted Single Phase Permeabilities using Bond–Flow Correlated Network

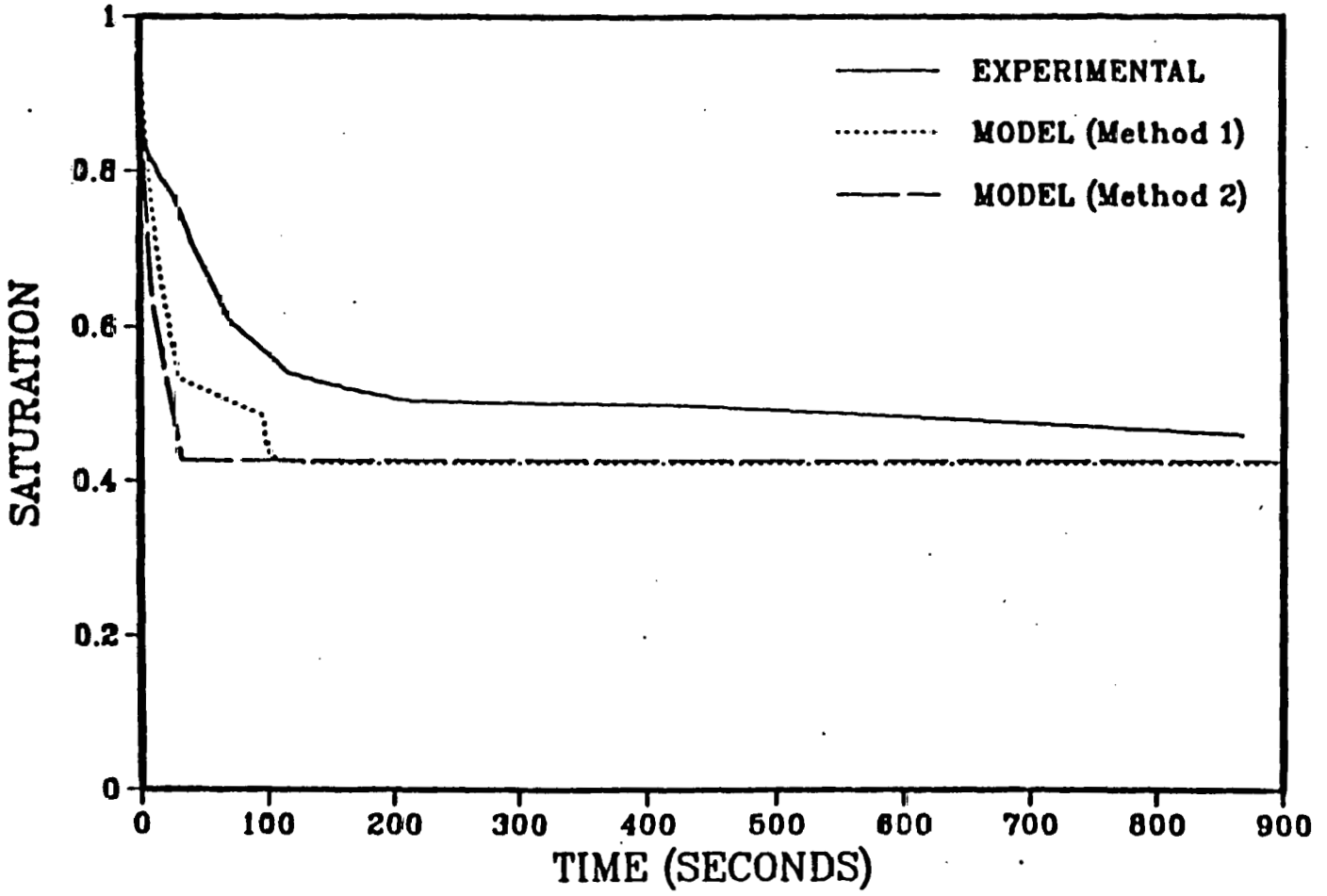

Figure 45: Comparison of the calculated and experimental dewatering curvs for −32 mesh coal (Cake F63)

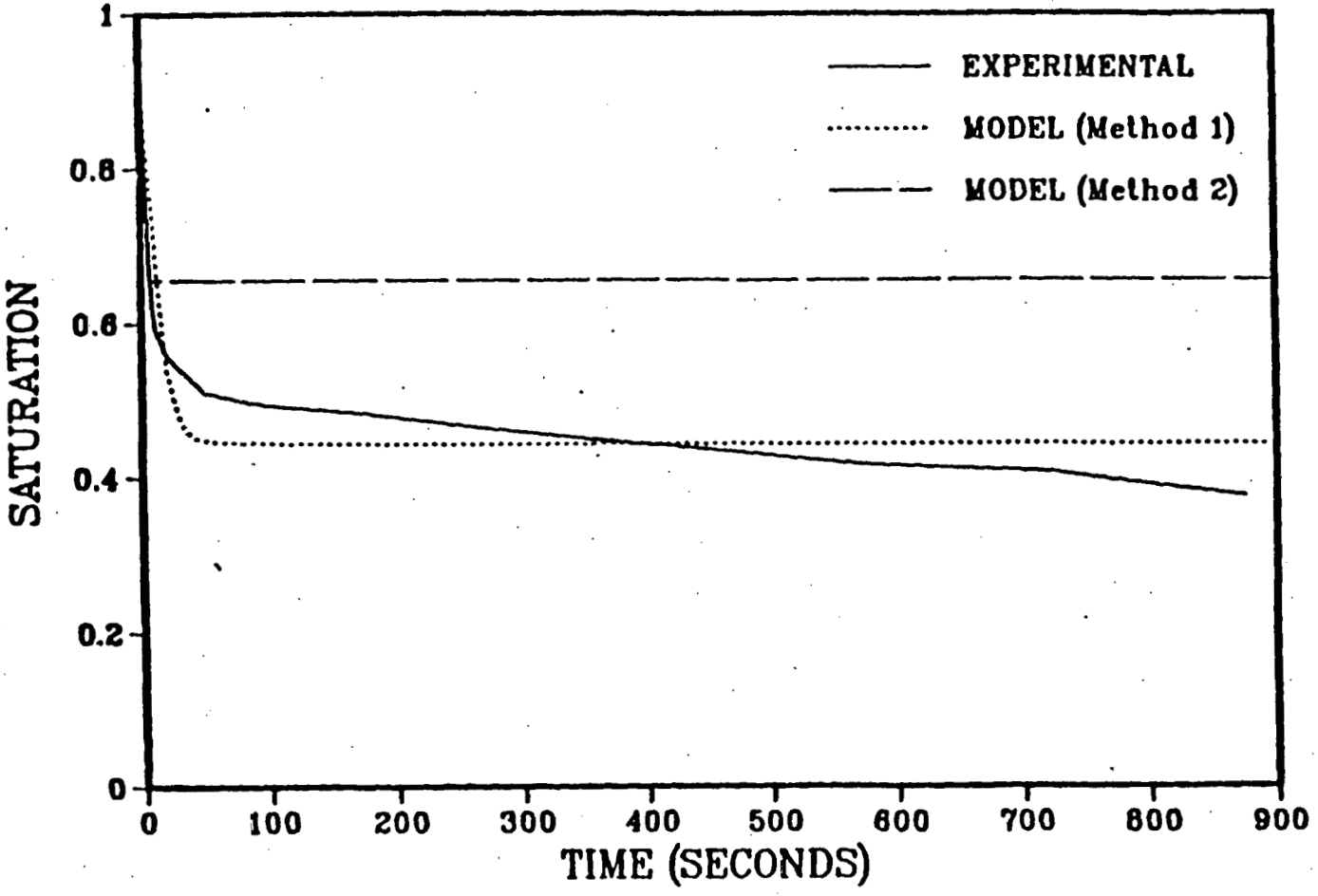

Figure 46: Comparison of the calculated and experimental dewatering curves for −32 mesh coal (cake F67)

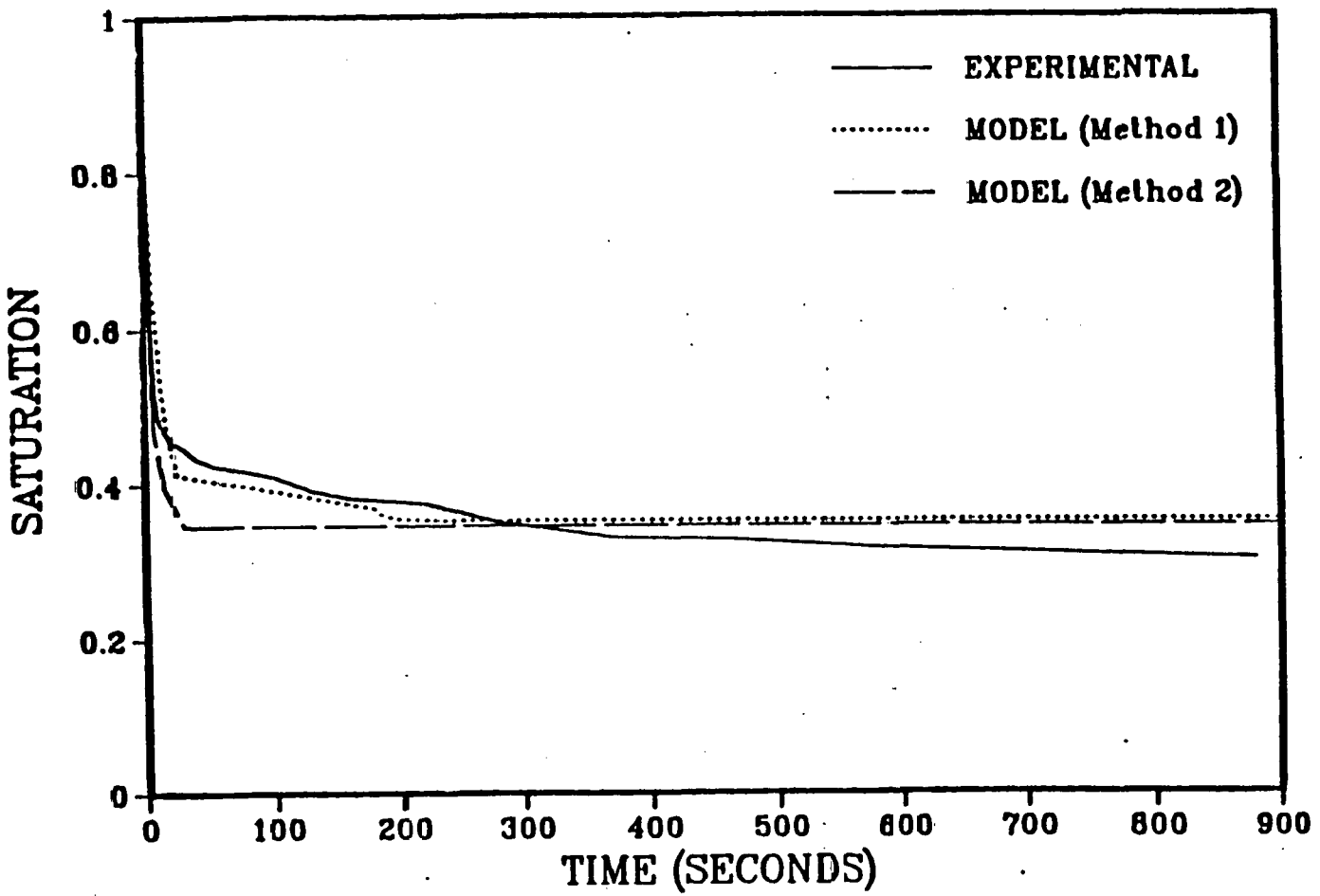

Figure 47: Comparison of the calculated and experimental dwatering curves for −32 mesh coal (cake F68)

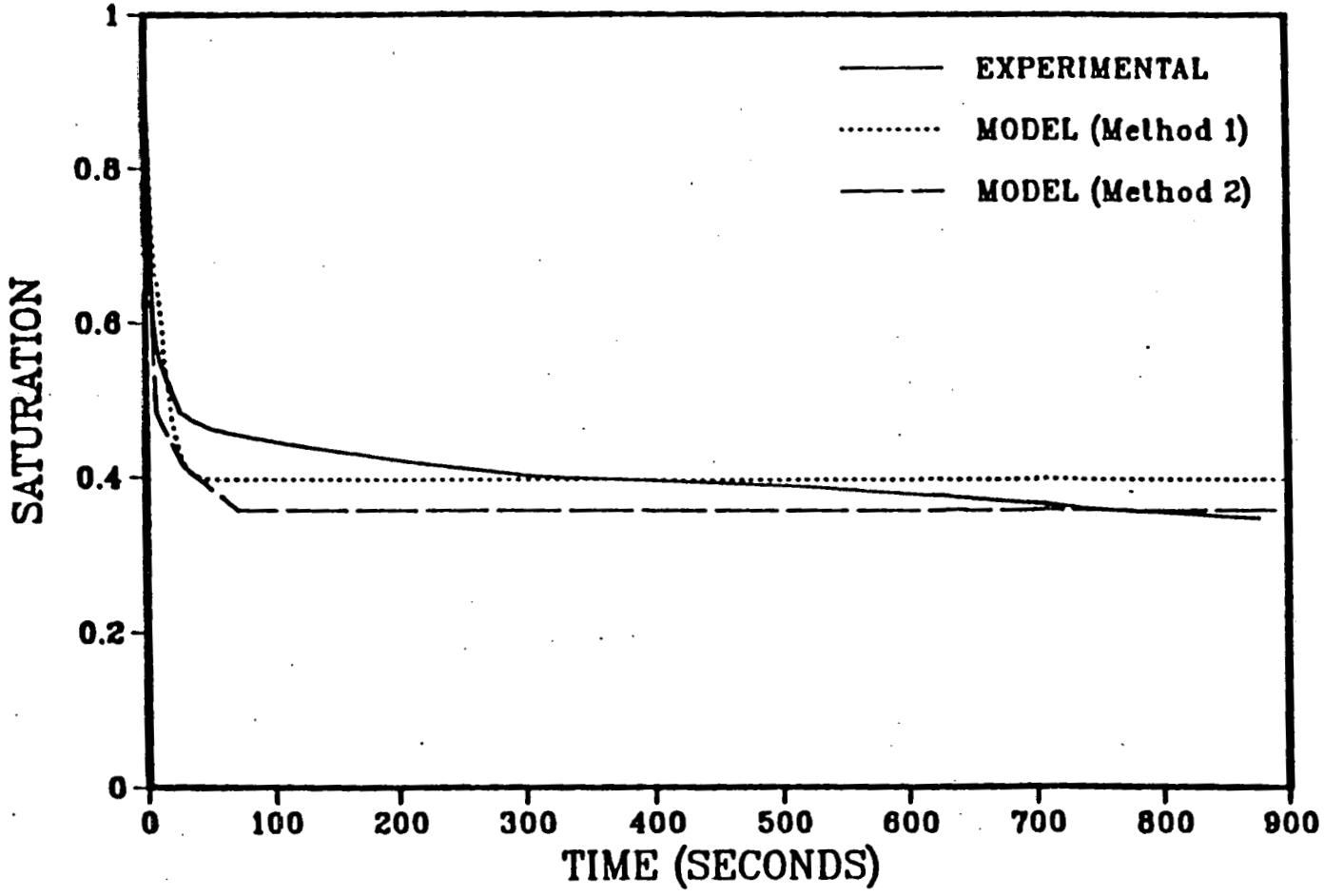

Figure 48: Comparison of the calculated and experimental dewatering curves for −32 mesh coal (cake F69)

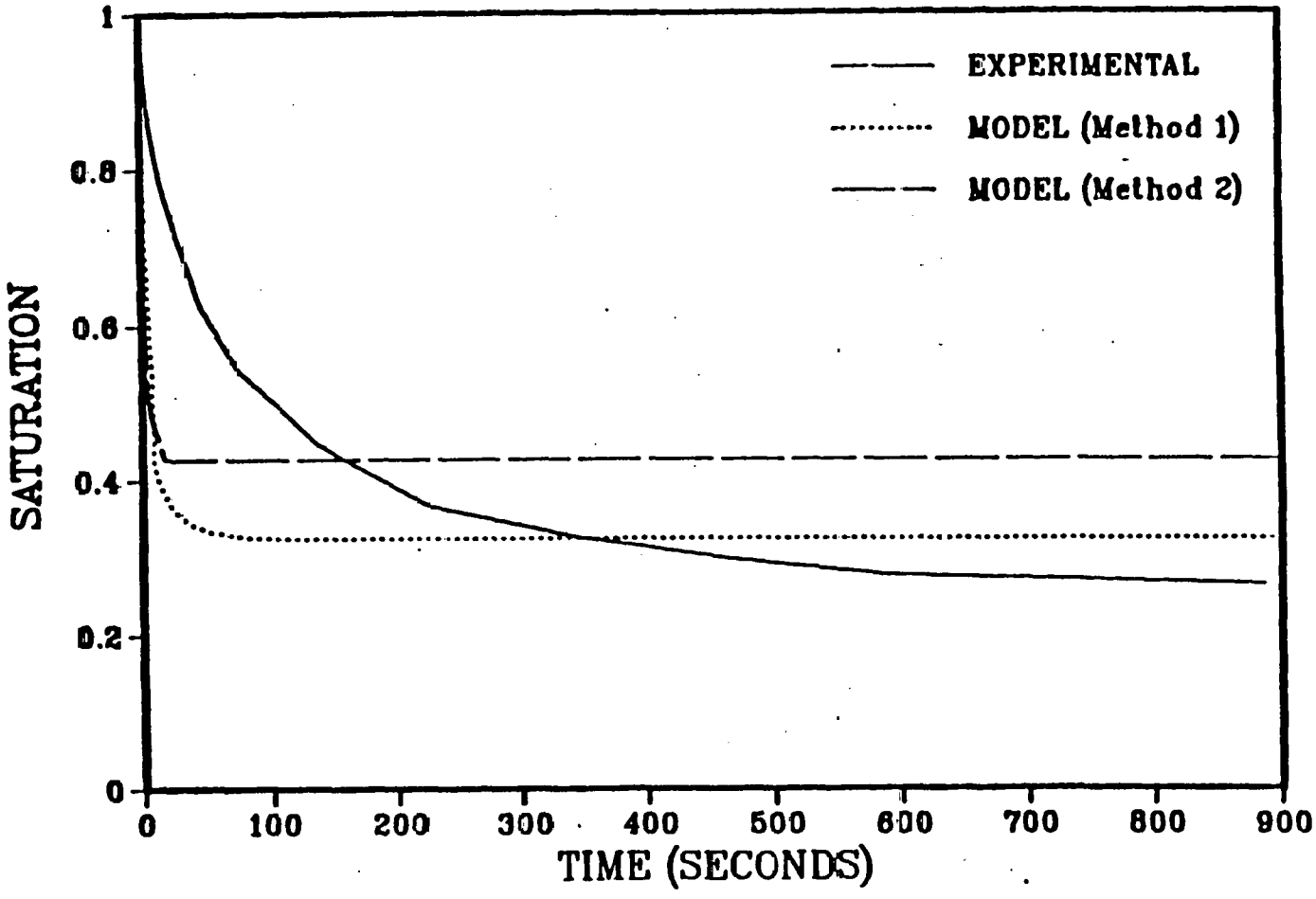

Figure 49: Comparison of the calculated and experimental dewatering curves for −100+200 mesh coal (cake F119)

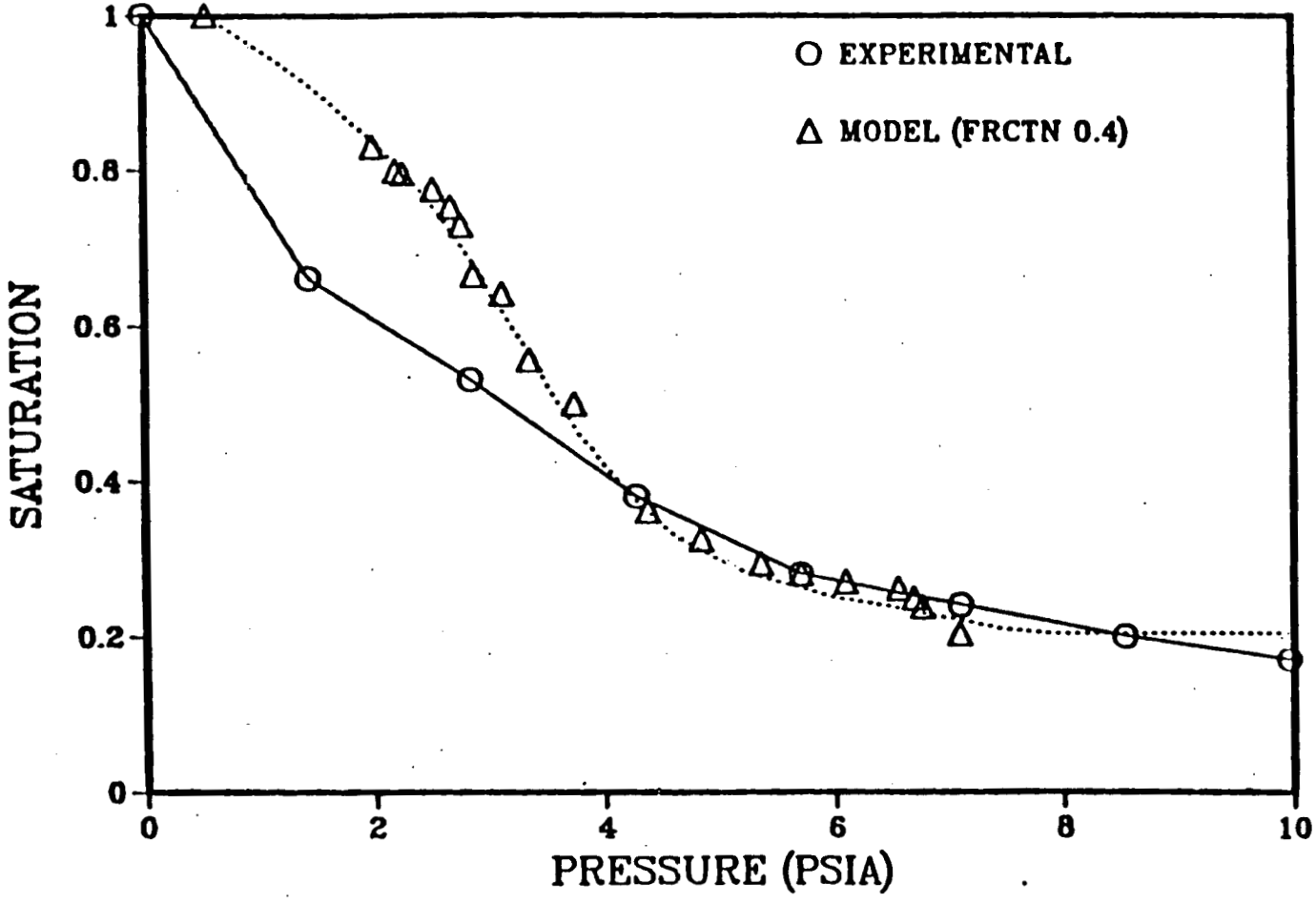

Figure 50: Comparison of calculated and experimental equilibrium desaturation curves for −30 mesh Betteshanger coal (from Gray)

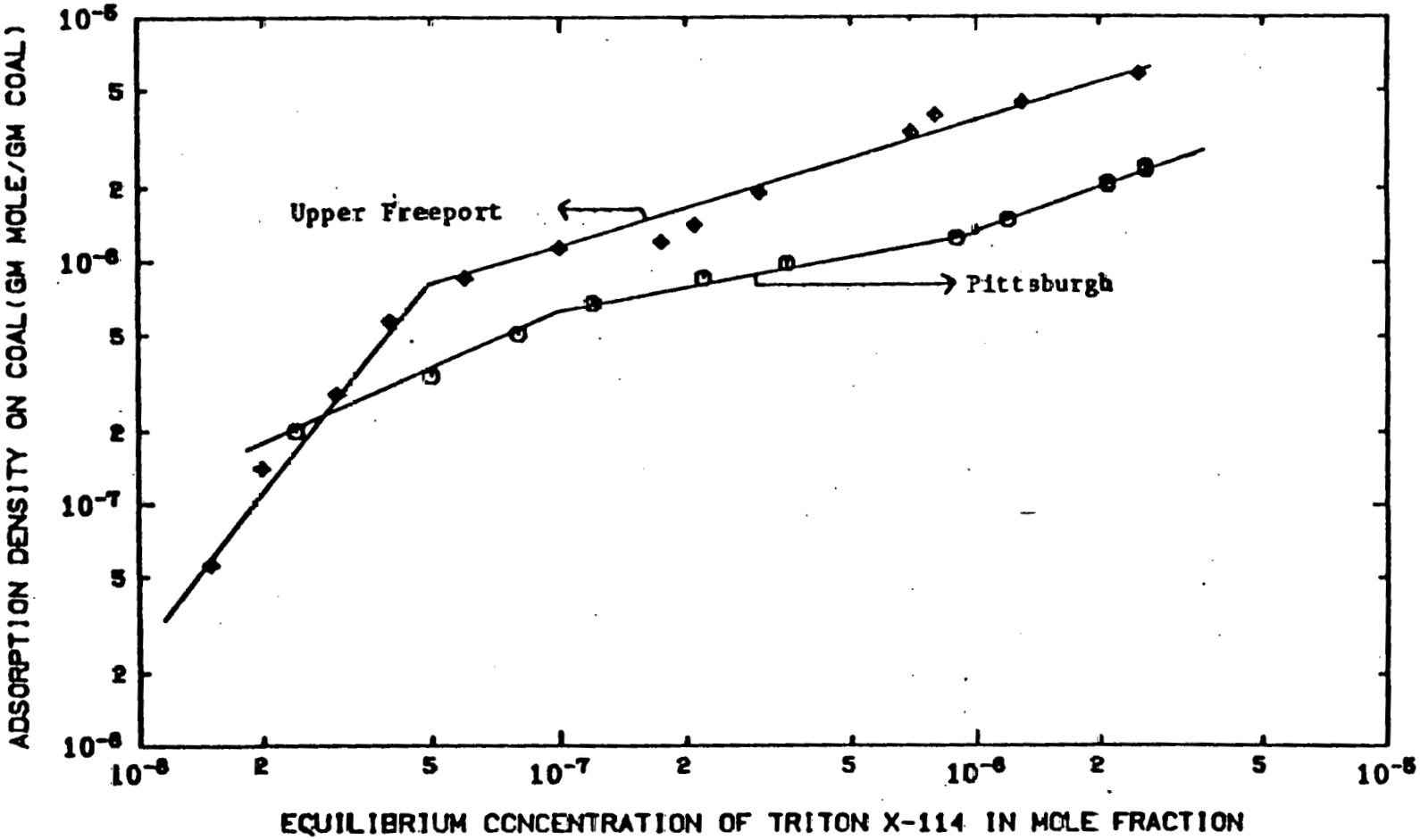

Figure 51: Comparison of Adsorption Isotherms of Triton X-114 on -32 Mesh Pittsburgh and -32 Mesh Upper Freeport Coals.

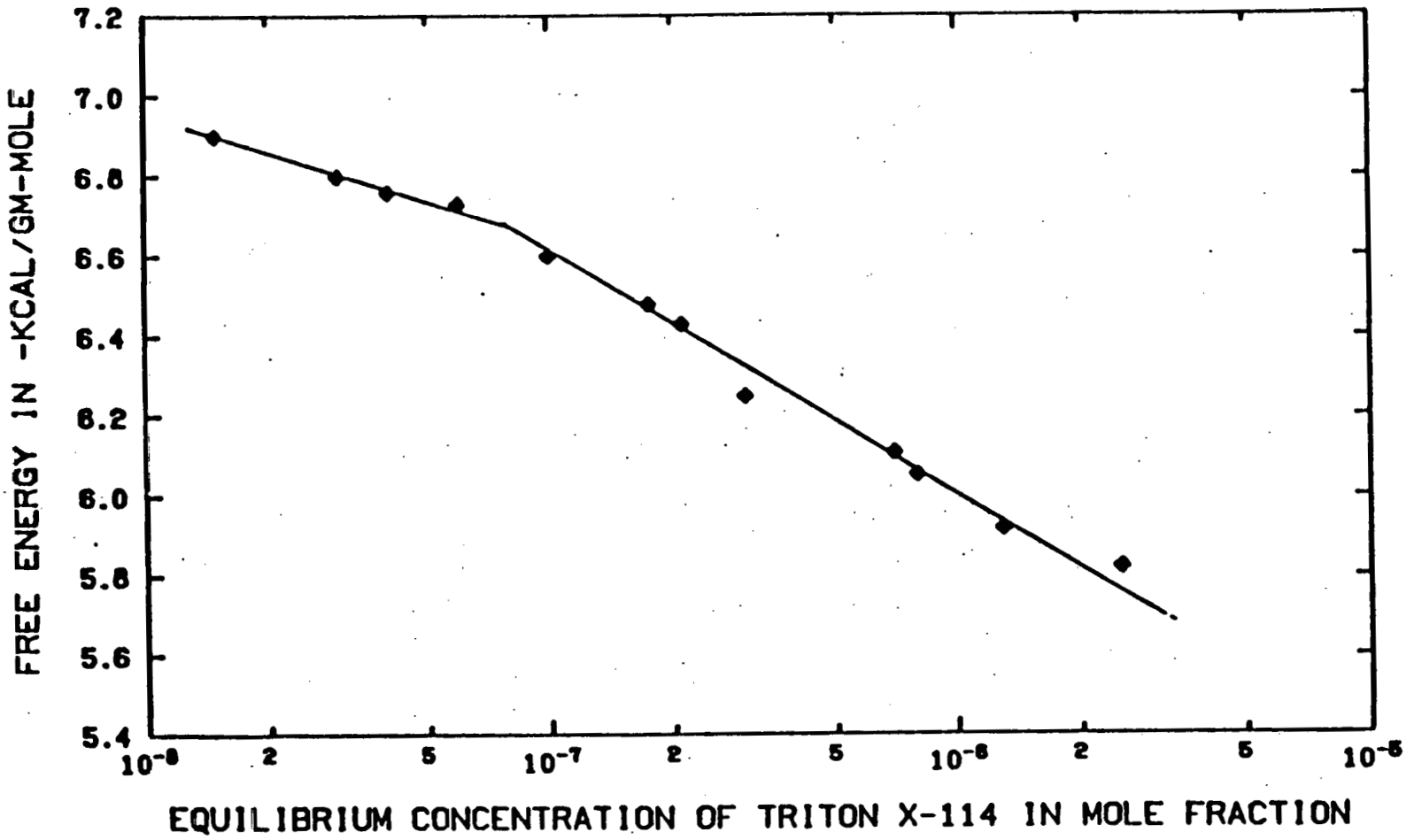

Figure 52: Free Energy Curve for Triton X-114 on Upper Freeport Coal.

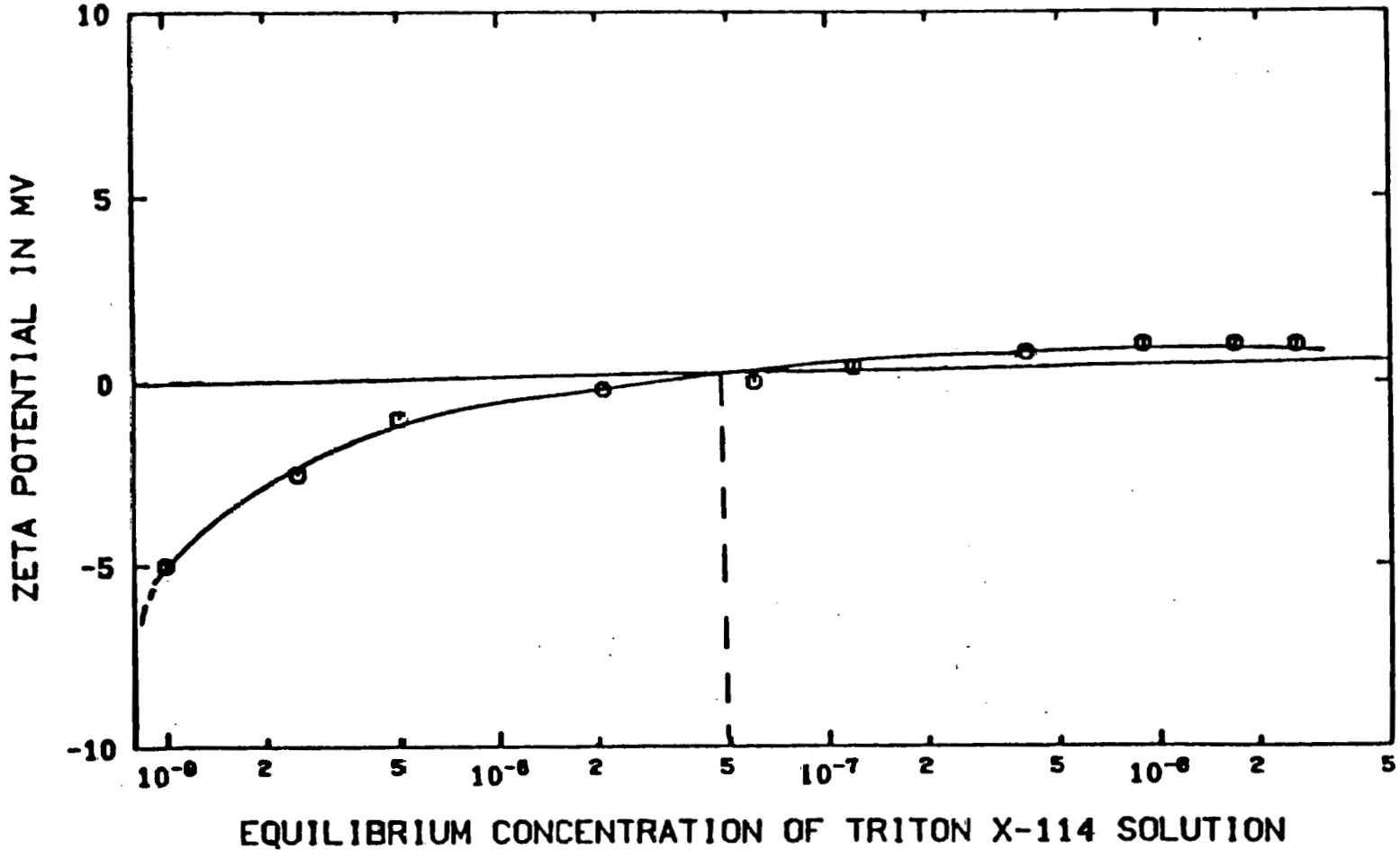

Figure 53: Zeta Potential as Function of Concentration for Triton X-114.

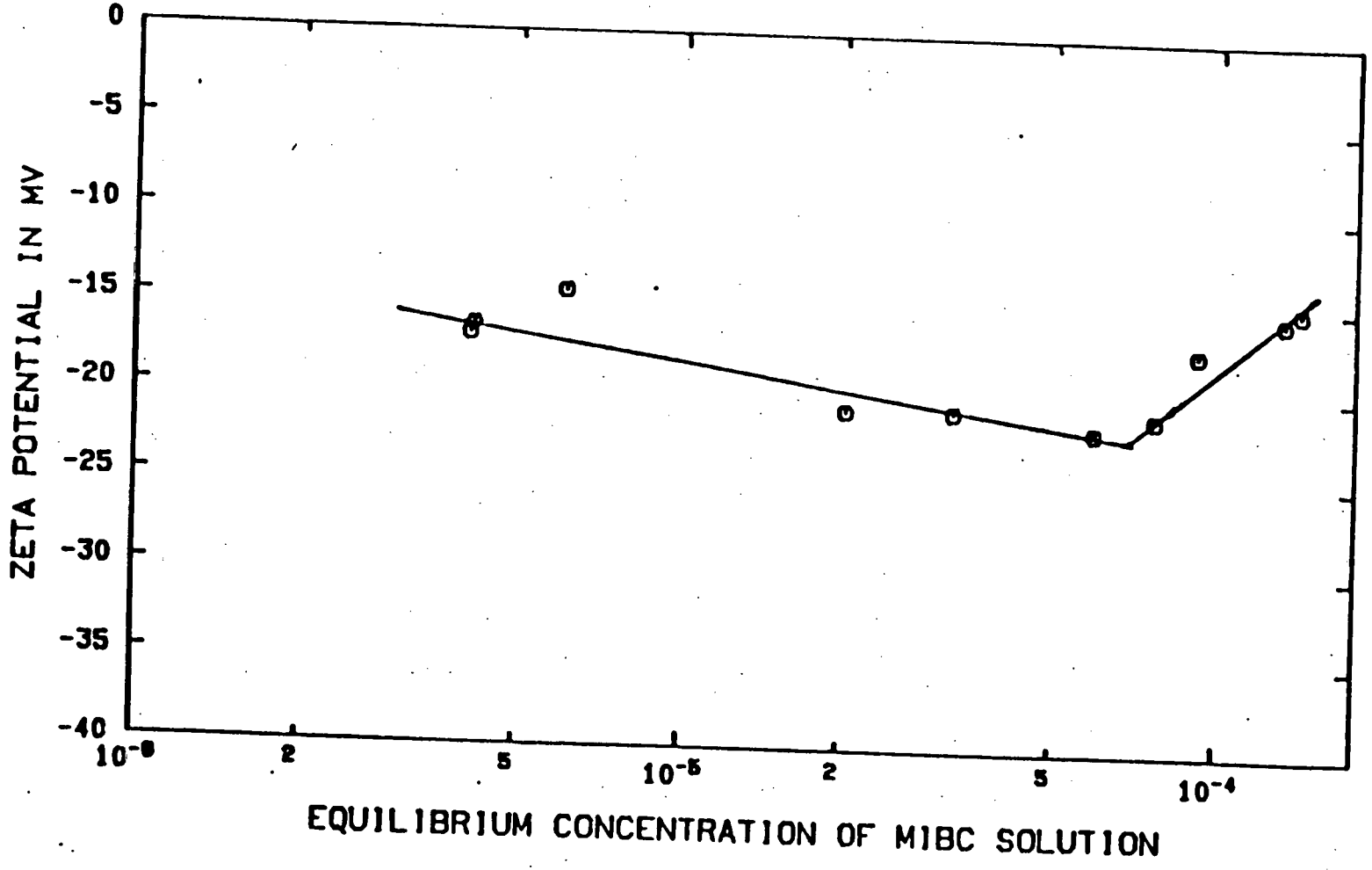

Figure 54: Zeta Potential as Function of Concentration for MIBC.

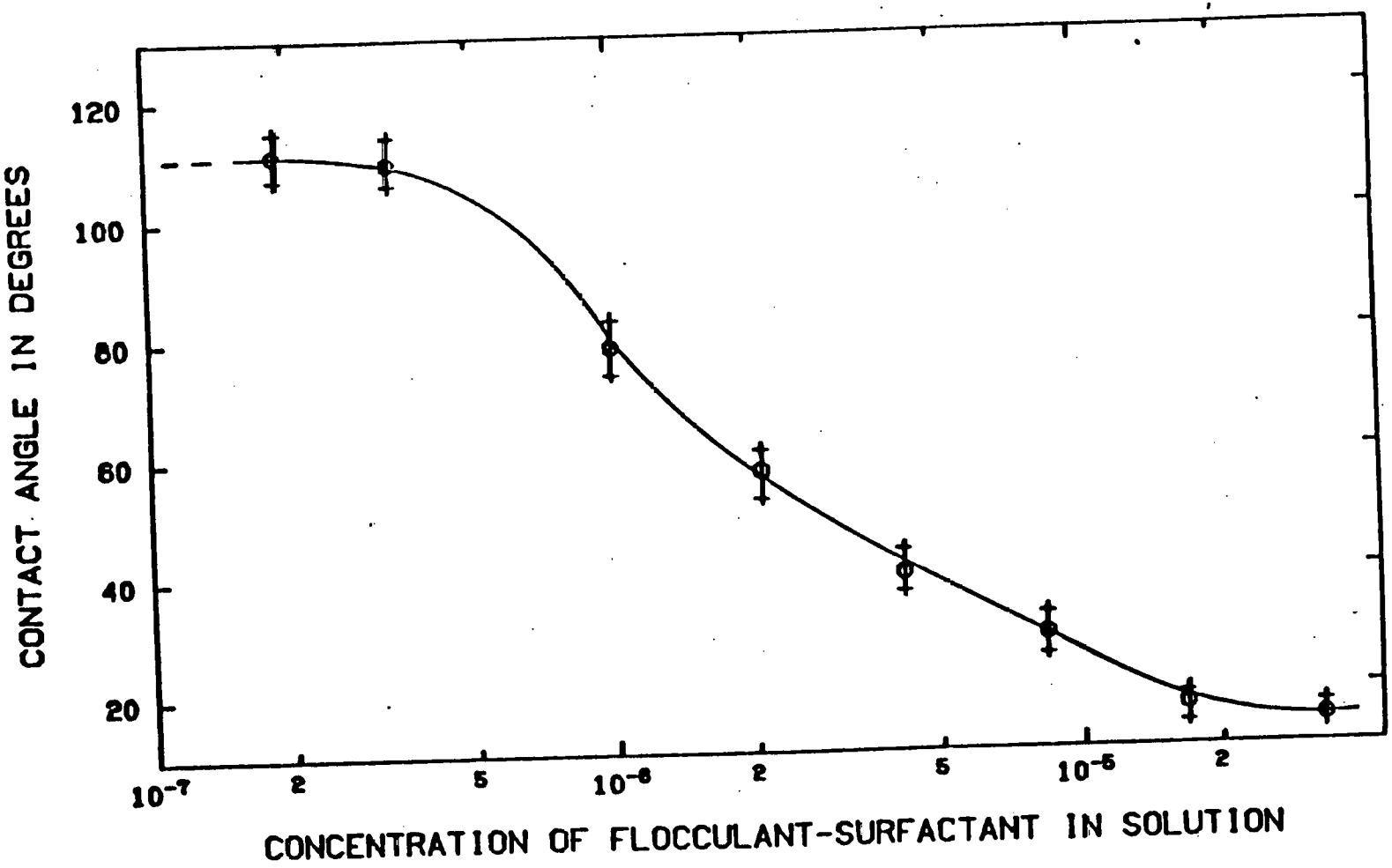

Figure 55: Contact Angle as Function of Flocculant/Surfactant Concentration on -32 Mesh Coal Pellets.

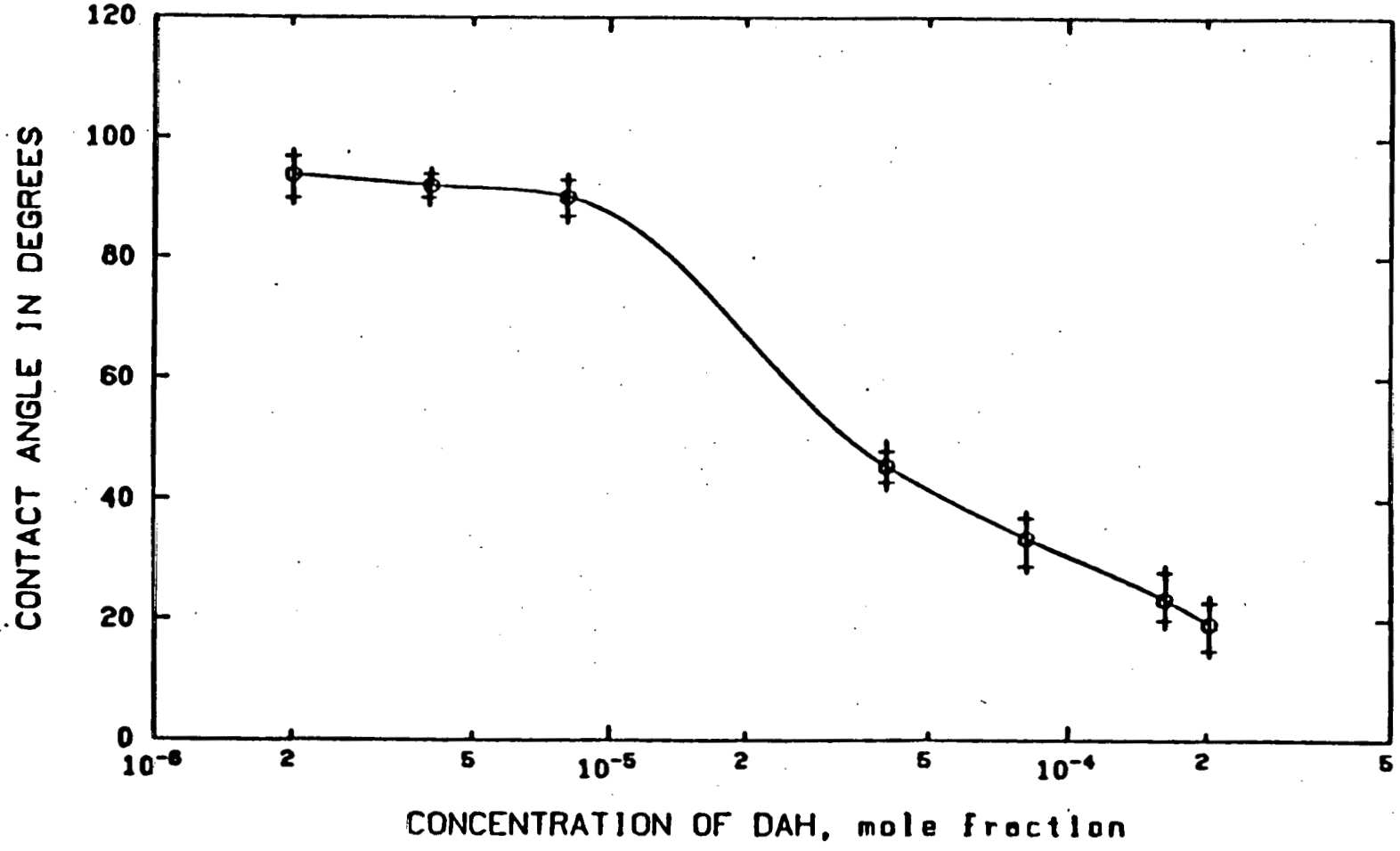

Figure 56: Contact Angle as Function of DAH Concentration on -32 Mesh Coal Pellets

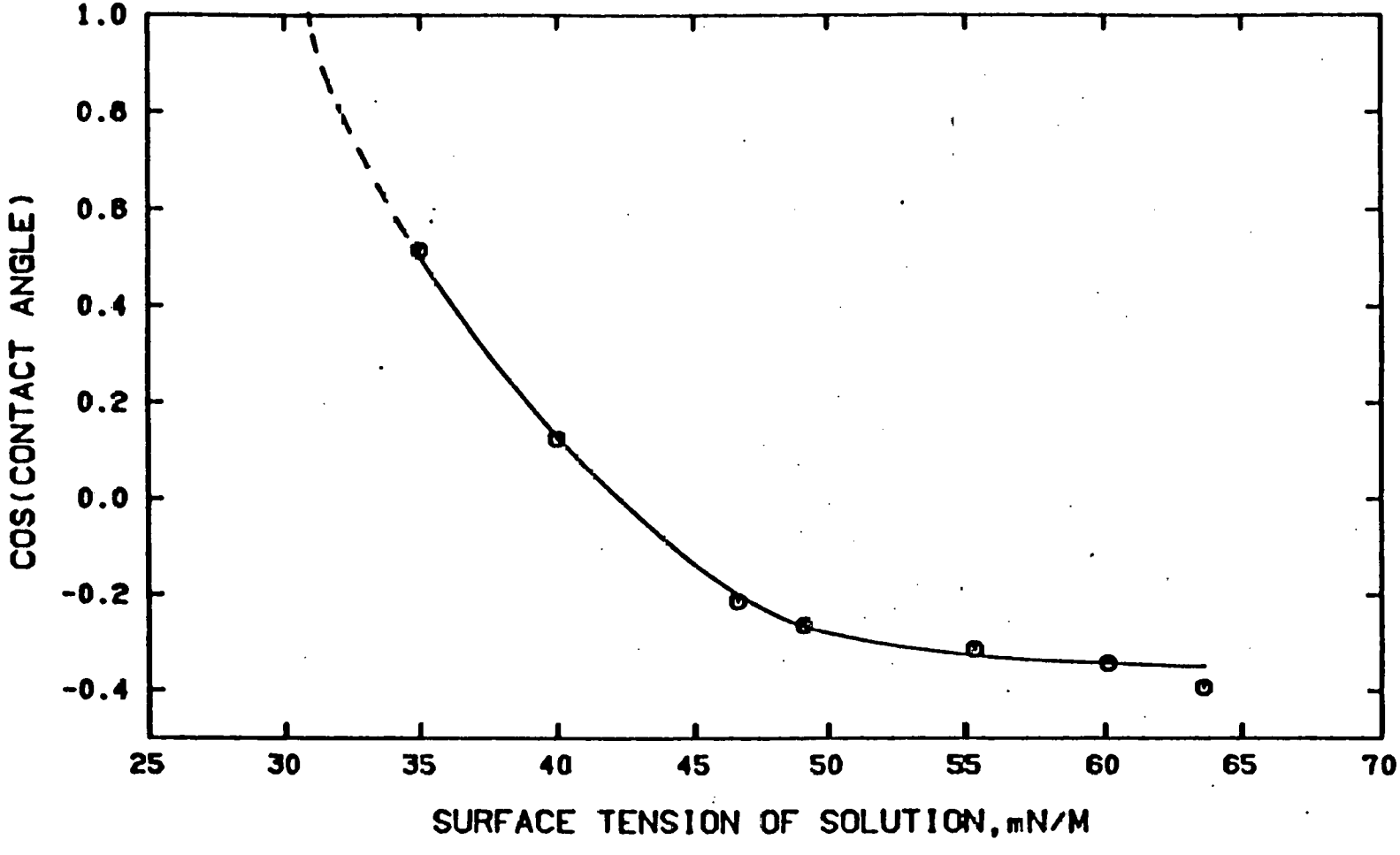

Figure 57: Typical Zisman Plot to Determine the "Critical" Surface Tension of MIBC

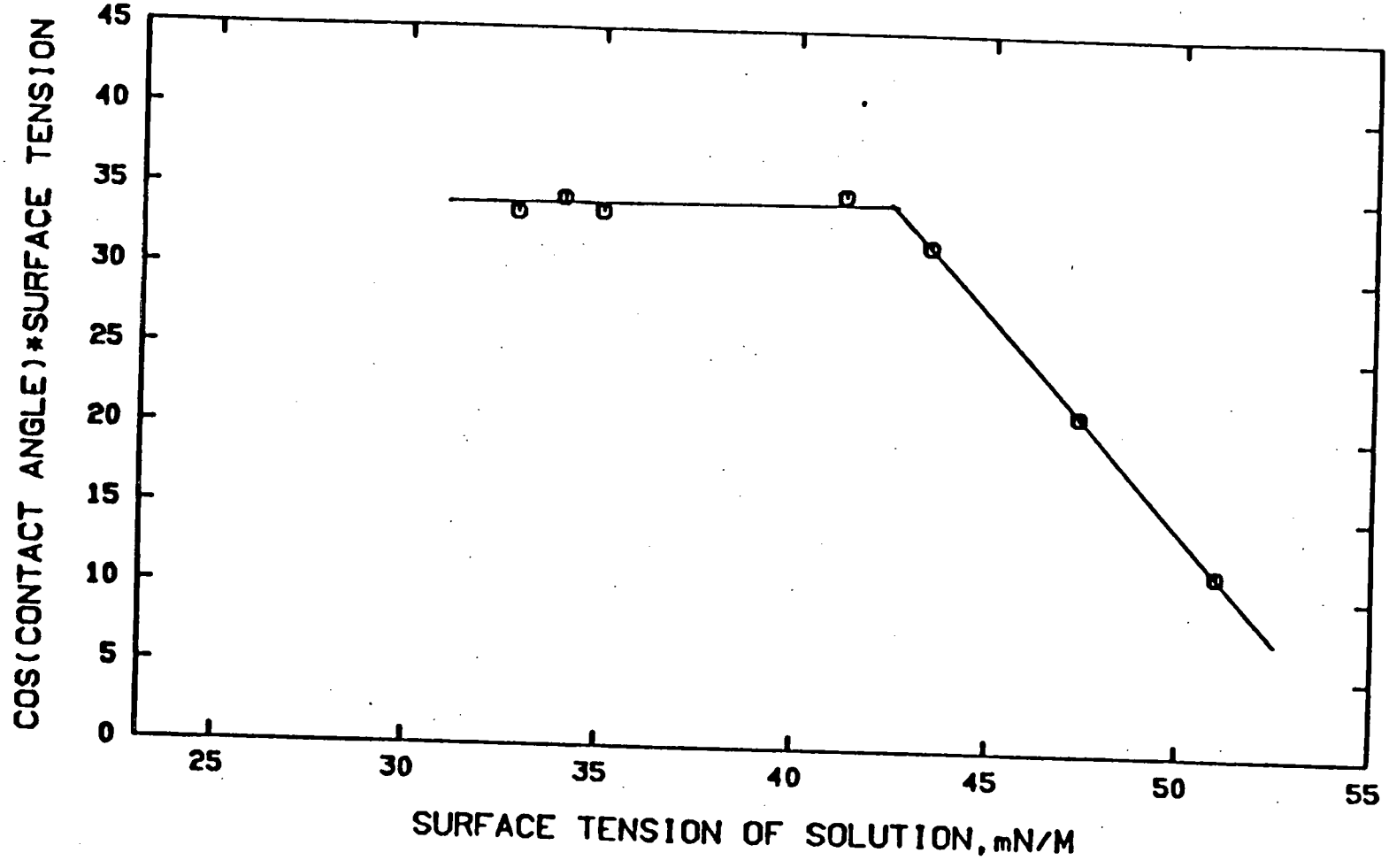

Figure 58: Adsorption Characteristics by the Method of Slopes for Aerosol-OT Solutions.

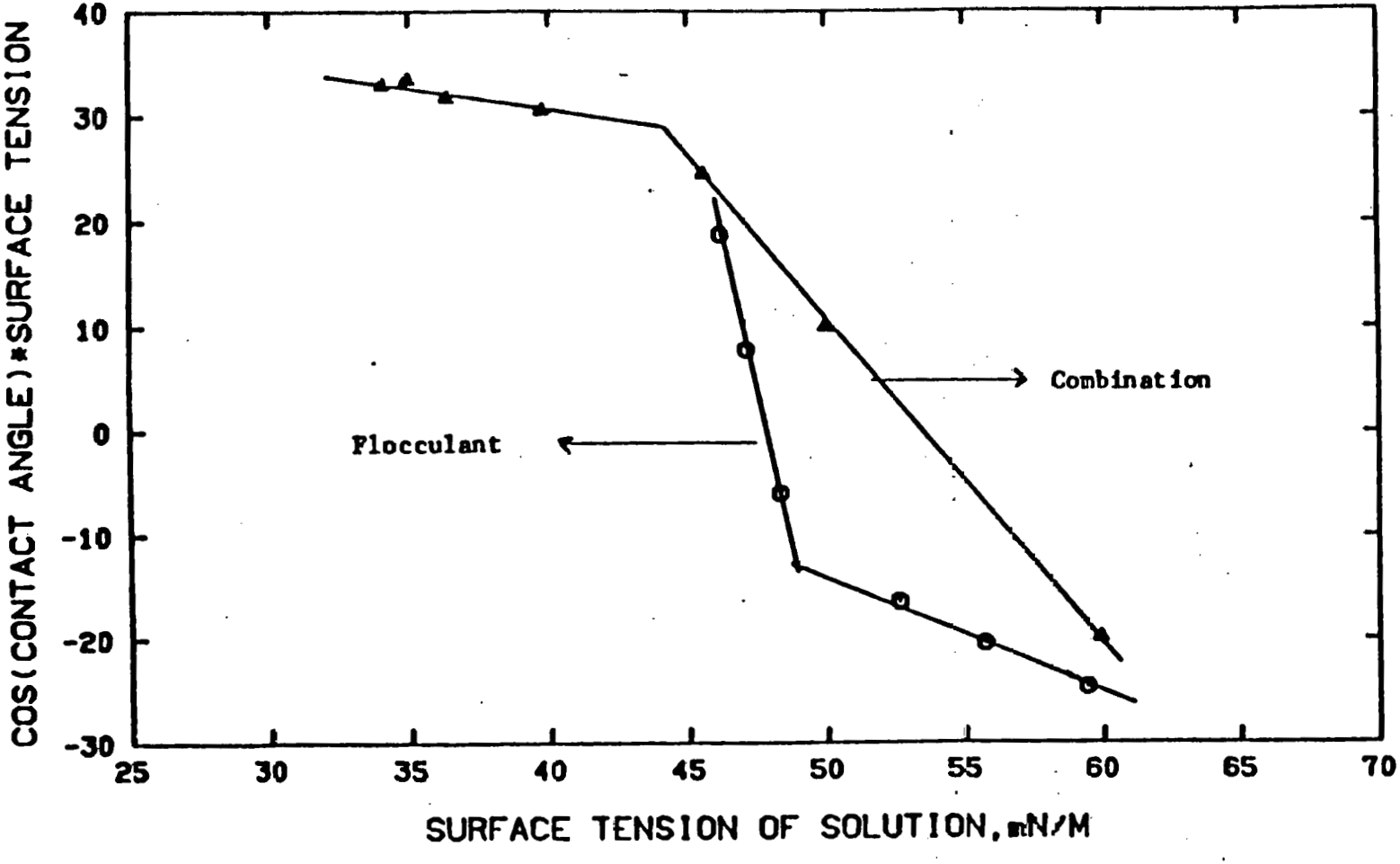

Figure 59: Adsorption Characteristics by the Method of Slopes for Flocculant and Combination of Flocculant/Surfactant Solutions.

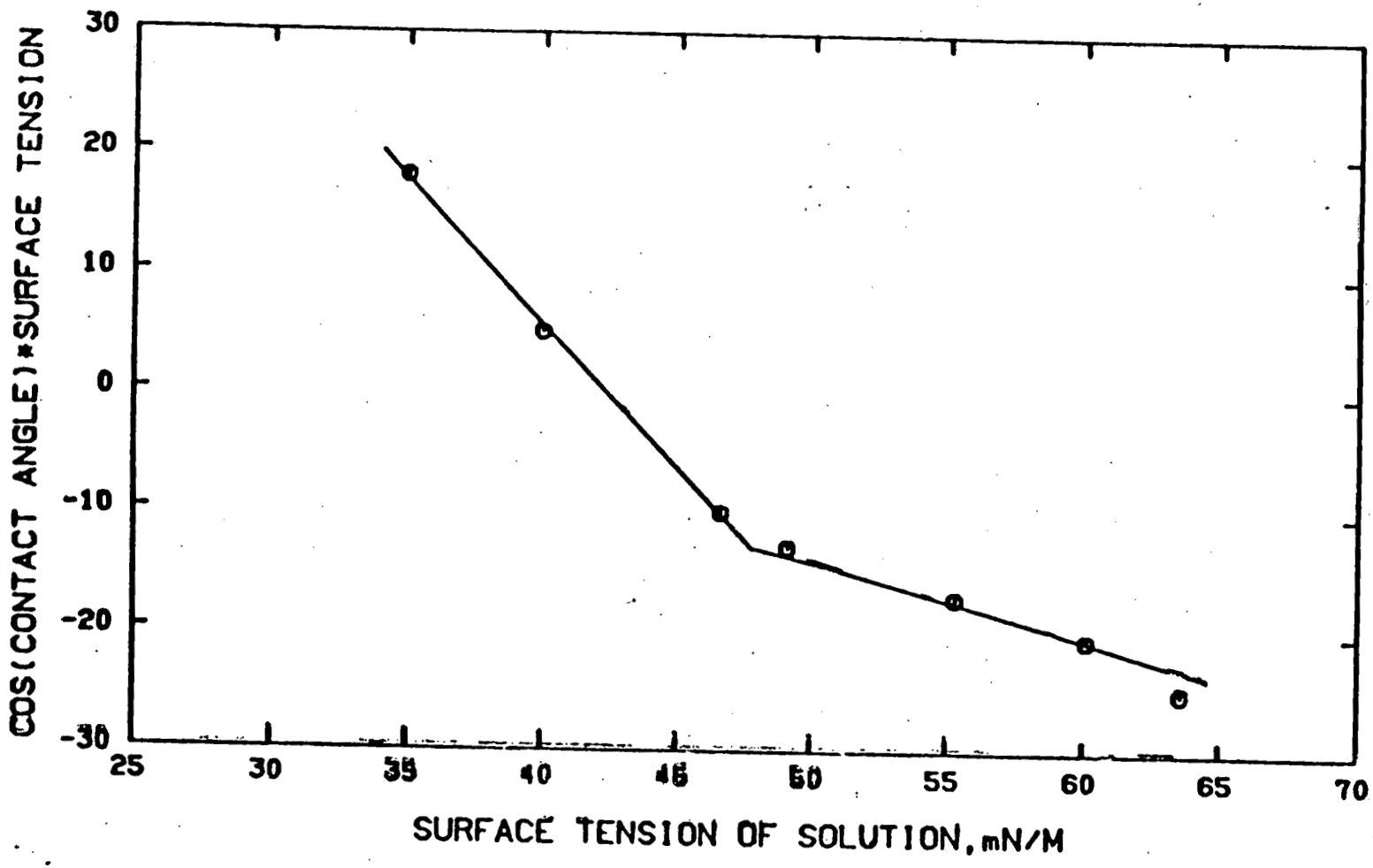

Figure 60: Adsorption Characteristics by the Method of Slopes for MIBC Solutions.

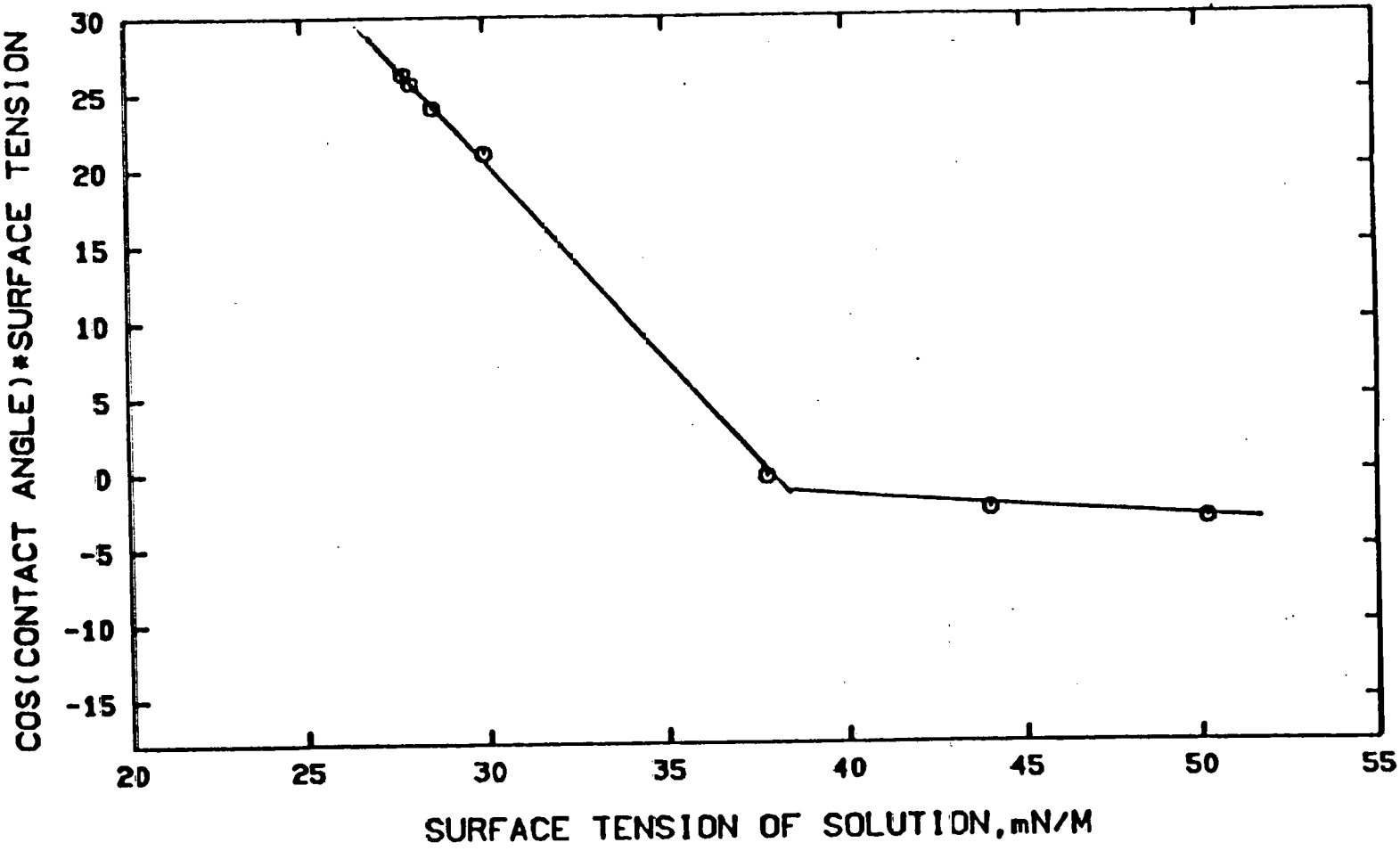

Figure 61: Adsorption Characteristics by the Method of Slopes for DAll Solutions.

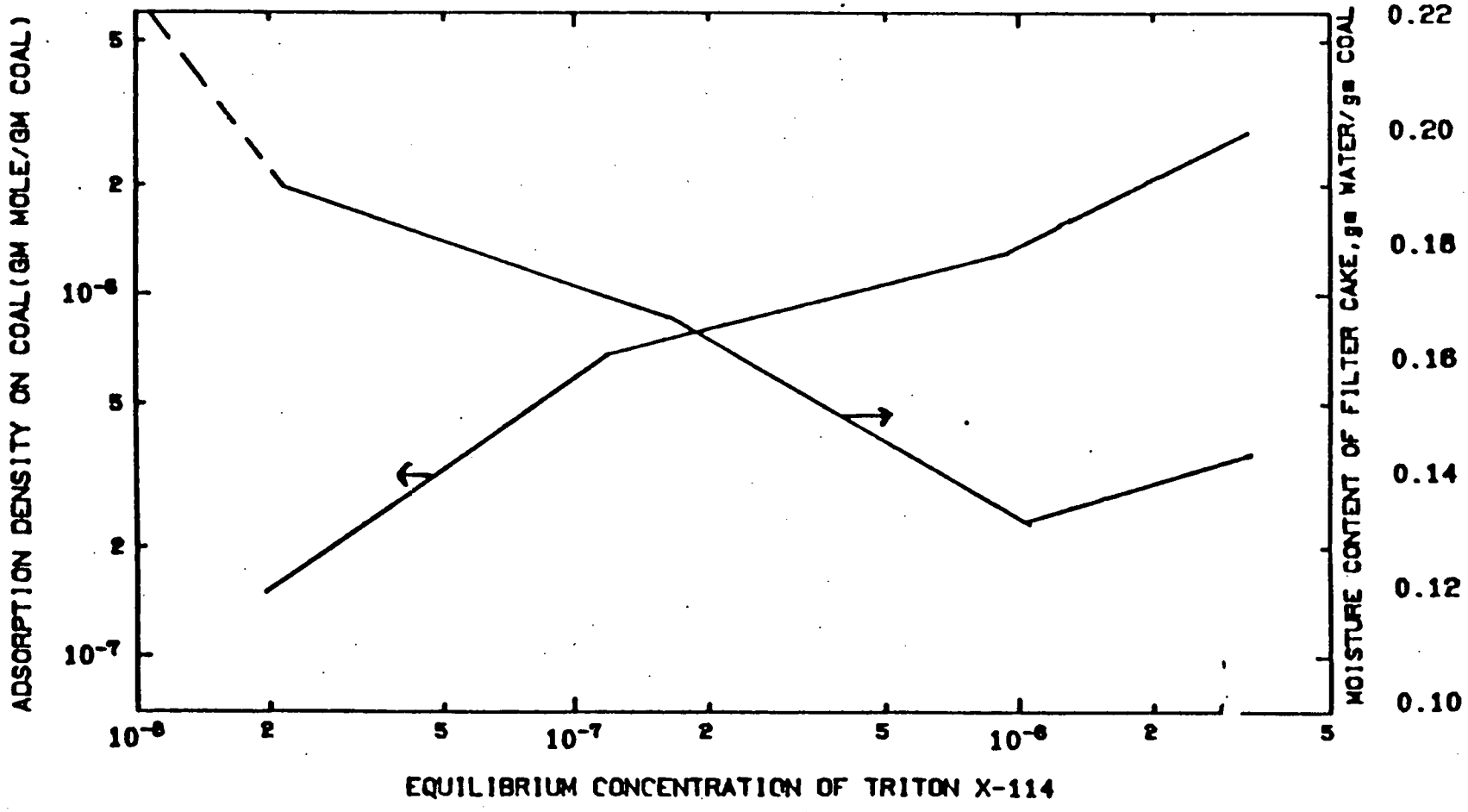

Figure 62: Comparison of Adsorption Isotherm and Moisture Content for Triton X-114 Solutions.

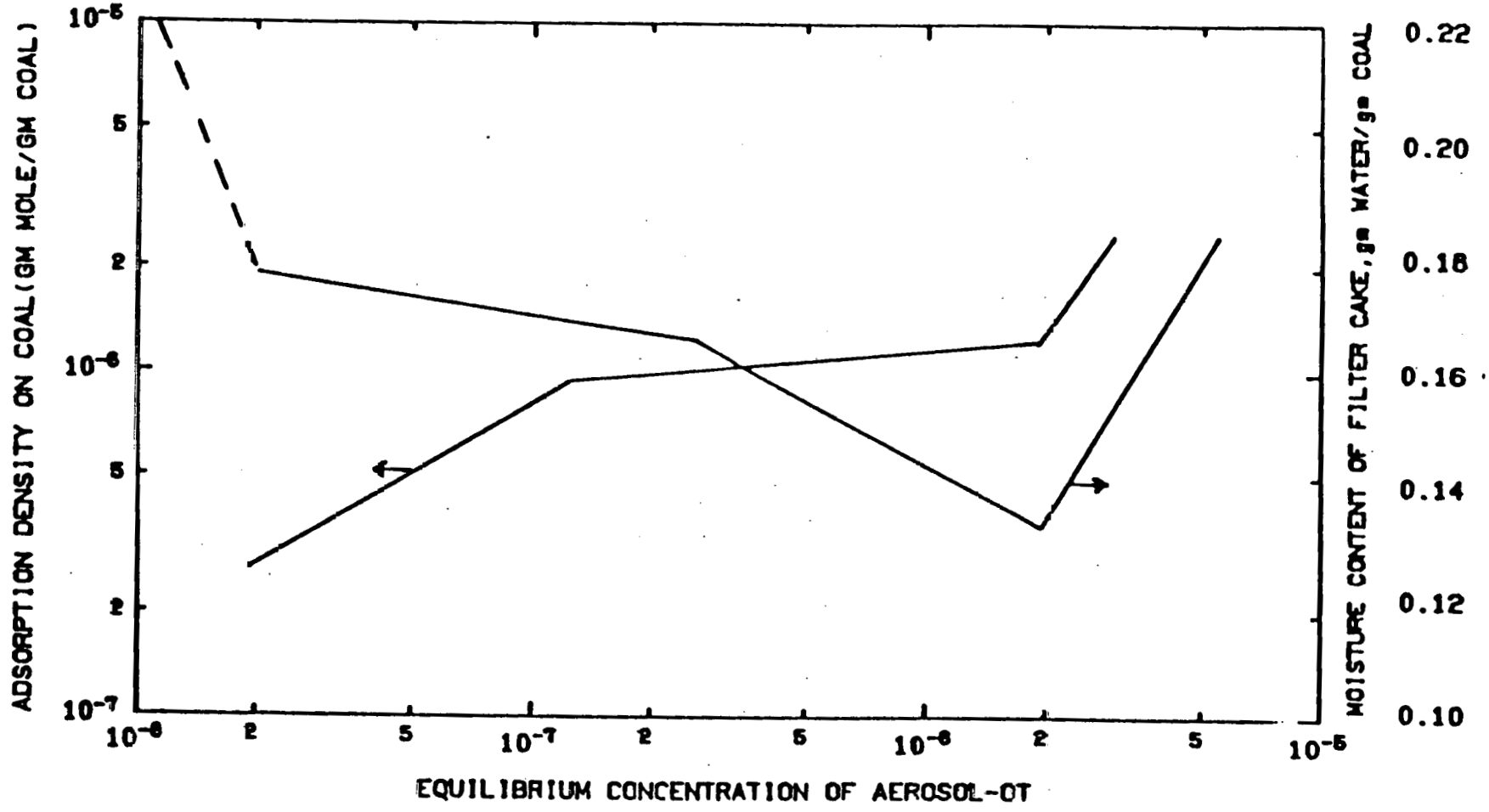

Figure 63: Comparison of Adsorption Isotherm and Moisture Content for Aerosol-OT Solutions.

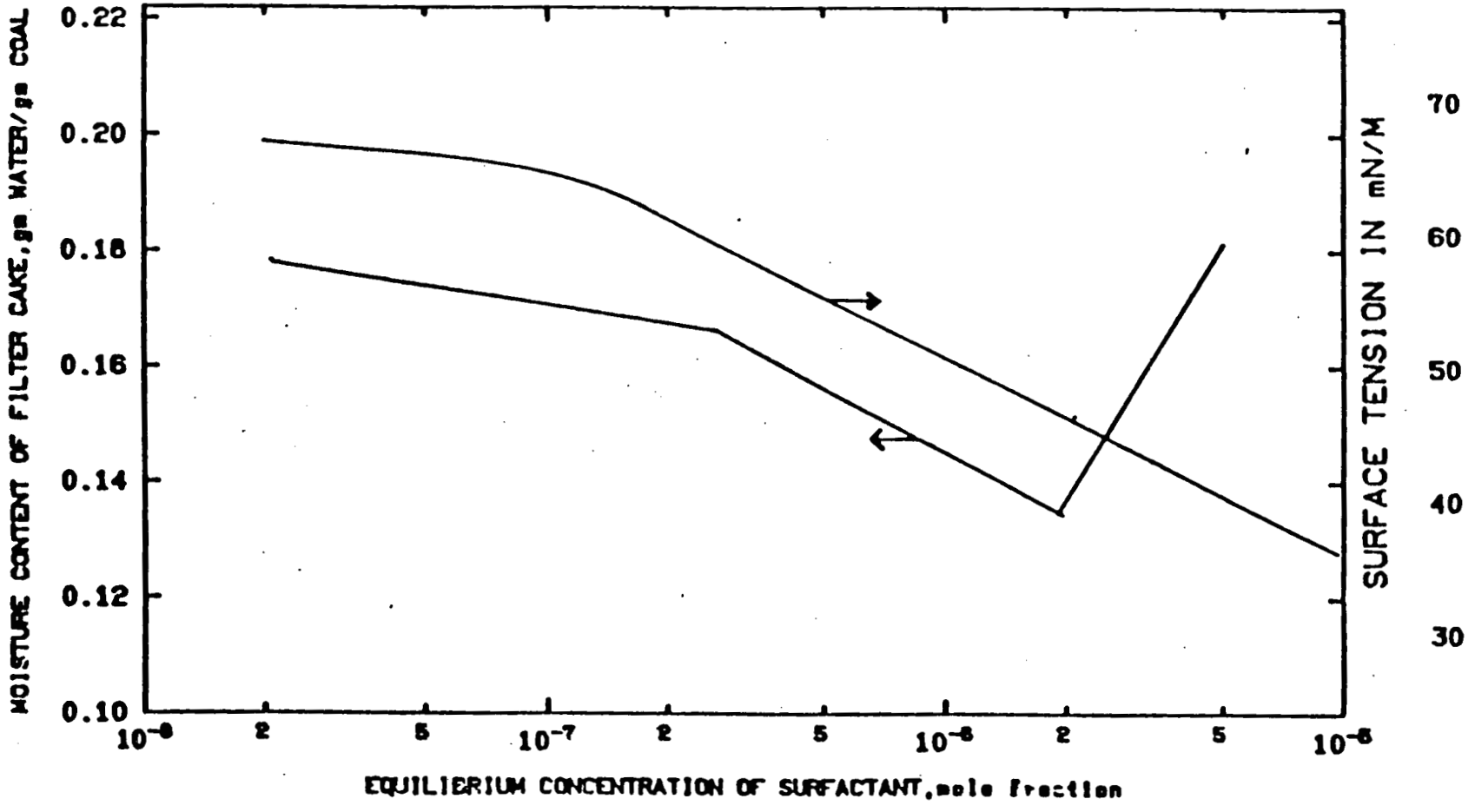

Figure 64: Comparison of Moisture Content and Surface Tension Characteristics for Aerosol-OT.

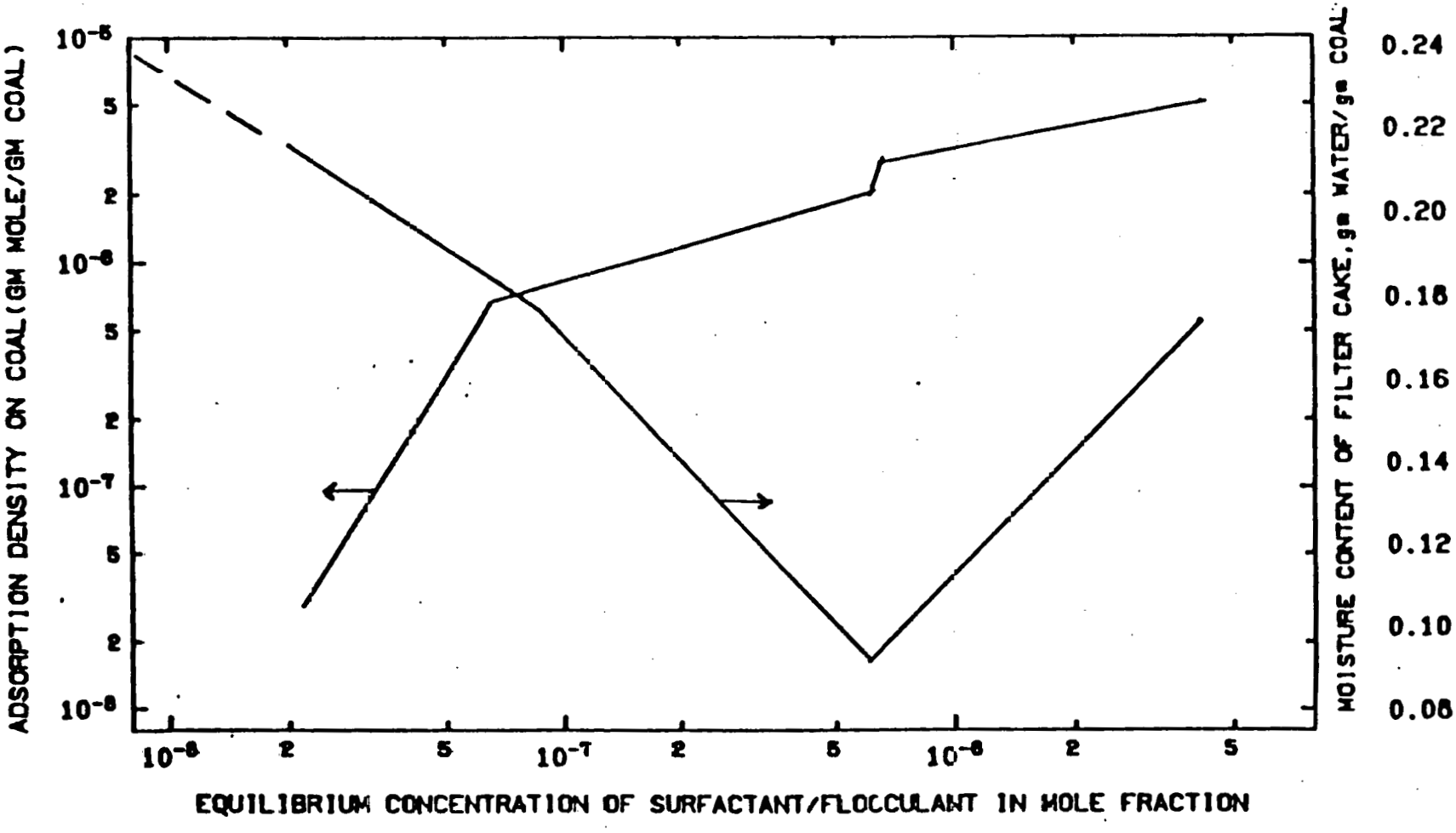

Figure 65: Comparison of Adsorption Isotherm and Moisture Content for Premixed Combination of Flocculant/Surfactant.

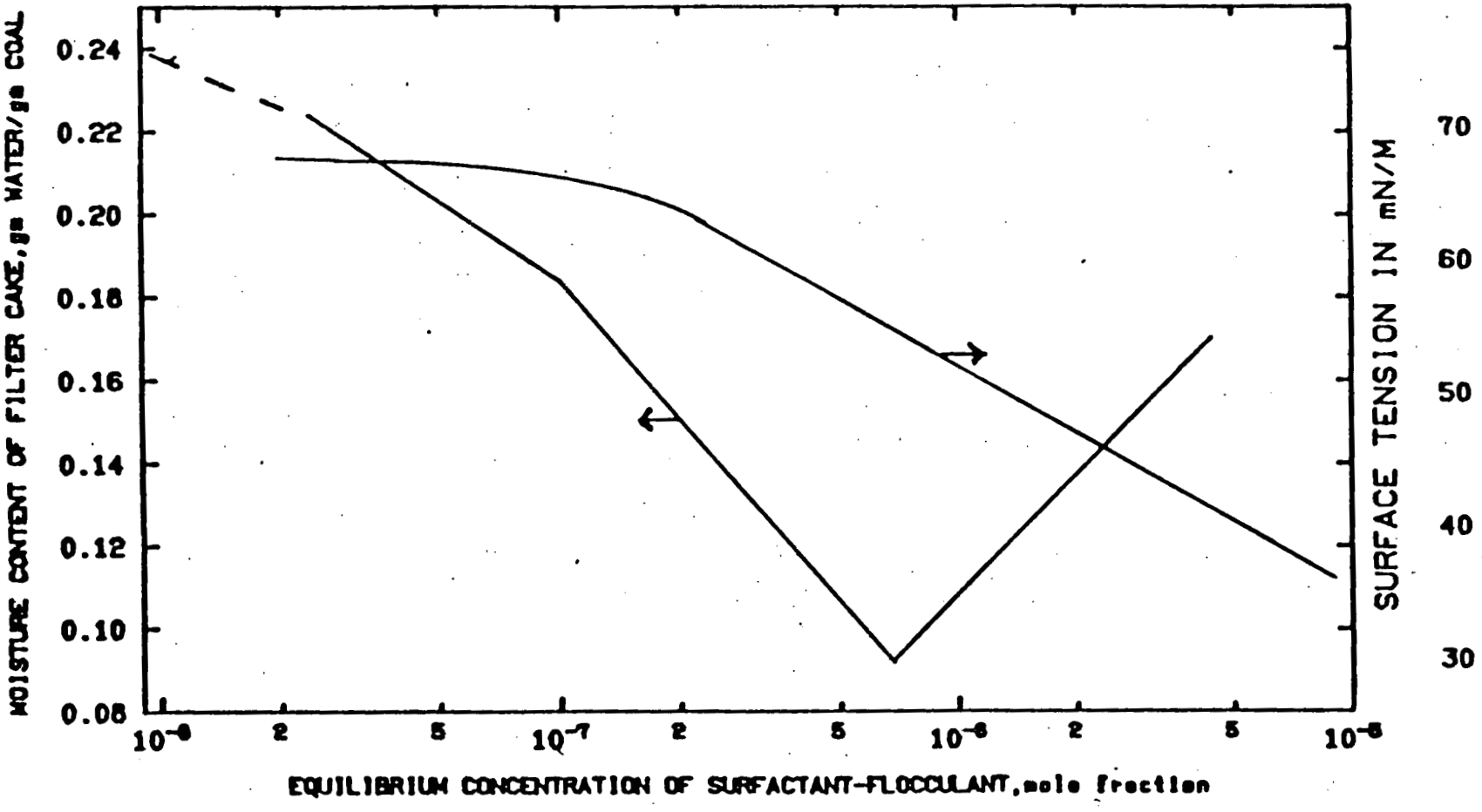

Figure 66: Comparison of Moisture Content and Surface Tension Characteristics for Premixed Combination of Flocculant/Surfactant.

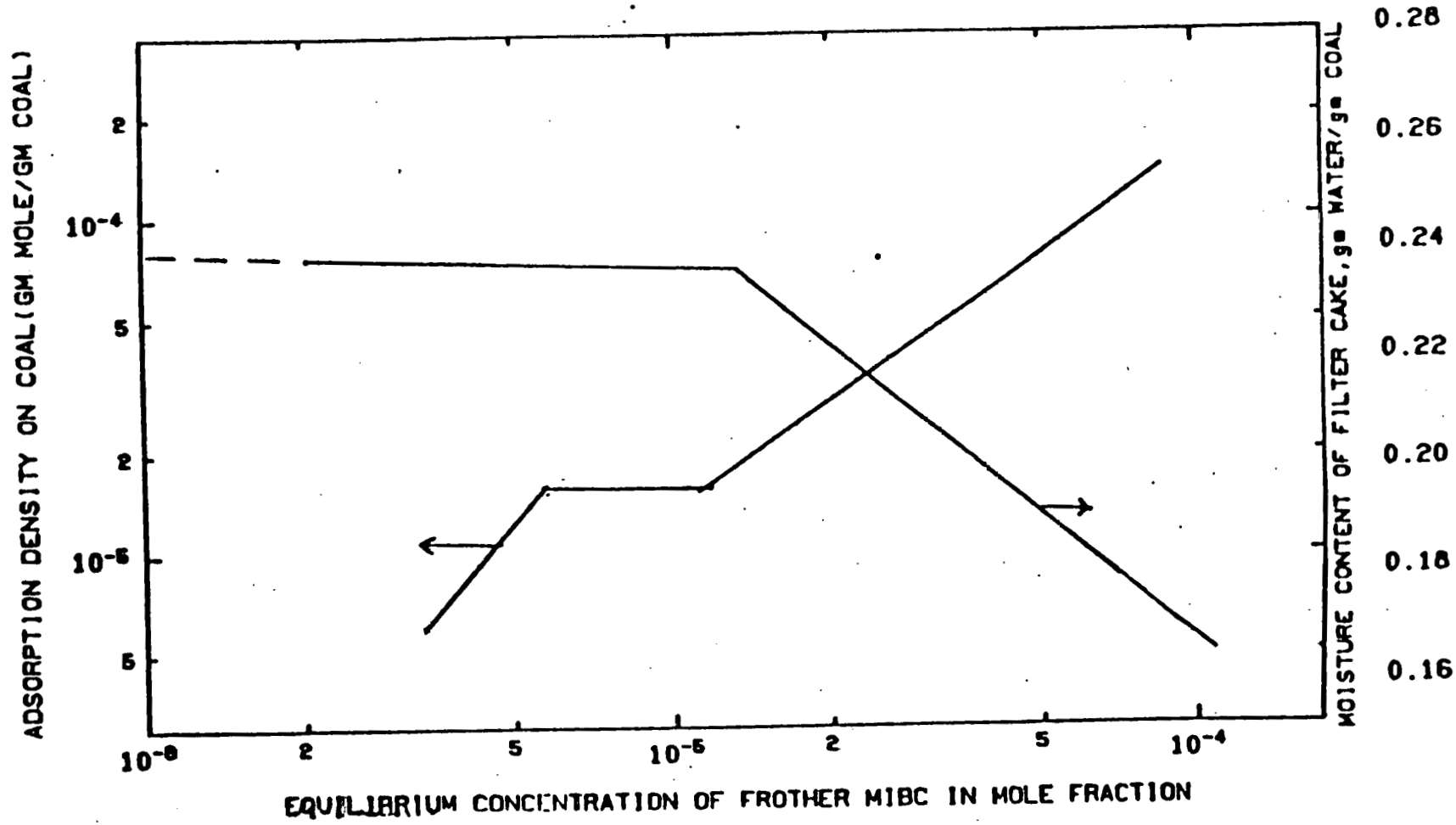

Figure 67: Comparison of Adsorption Isotherm and Moisture Content for MIBC Solutions

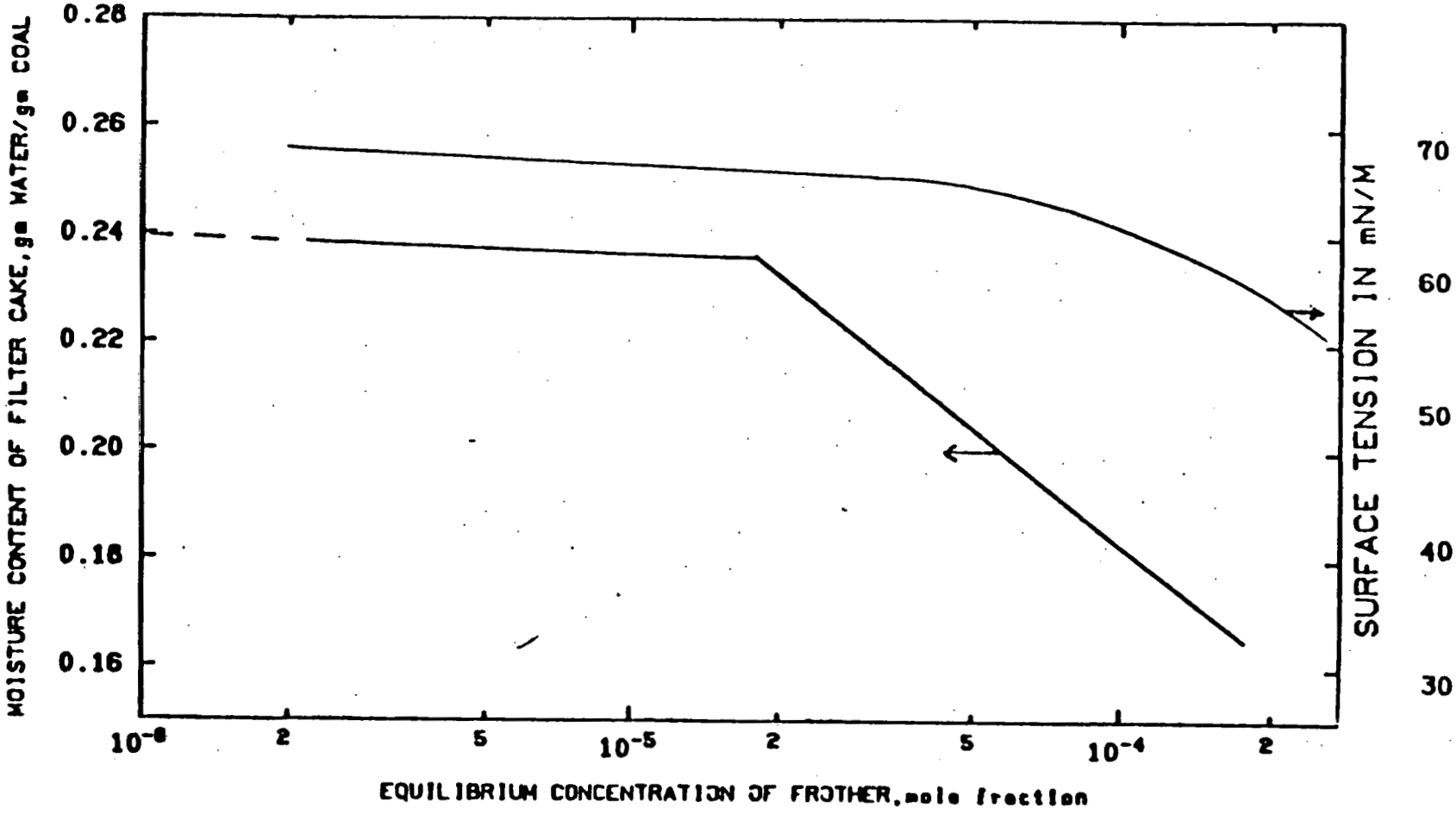

Figure 68: Comparison of Moisture Content and Surface Tension for MIBC Solutions

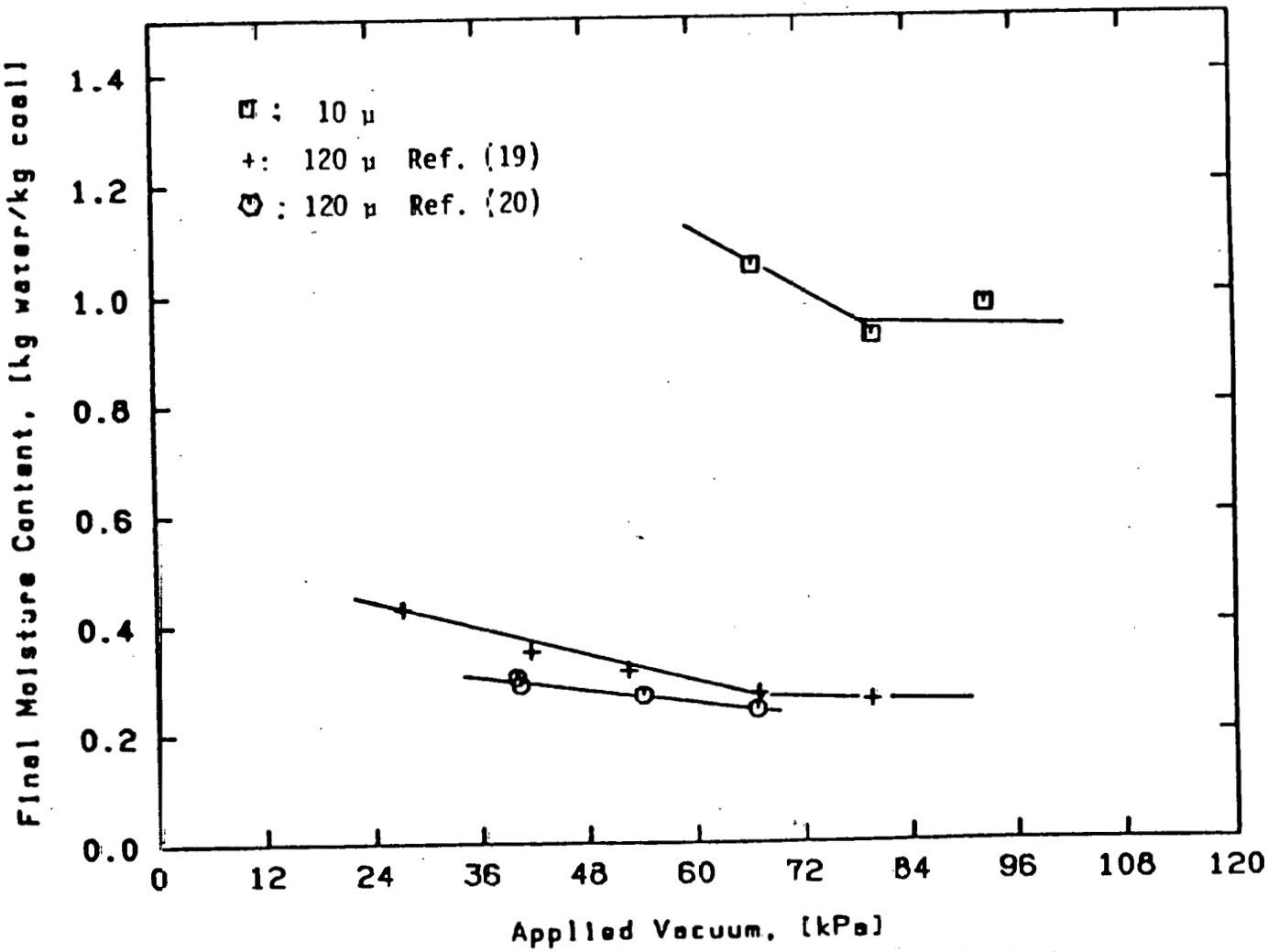

Figure 69: Effect of Applied Vacuum on the Moisture Content

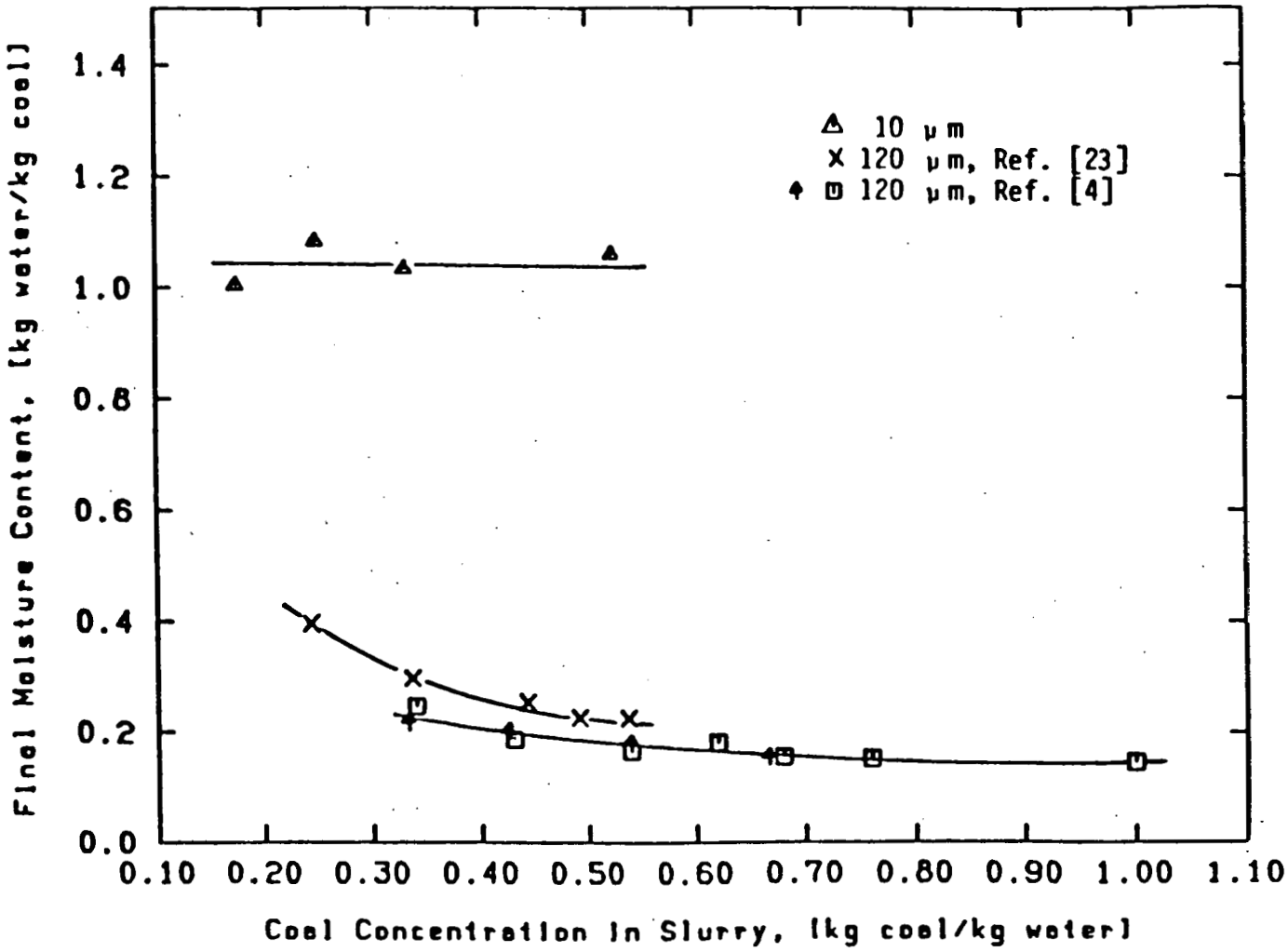

Figure 70: Effect of Solid Concentration on the Cake Moisture Content

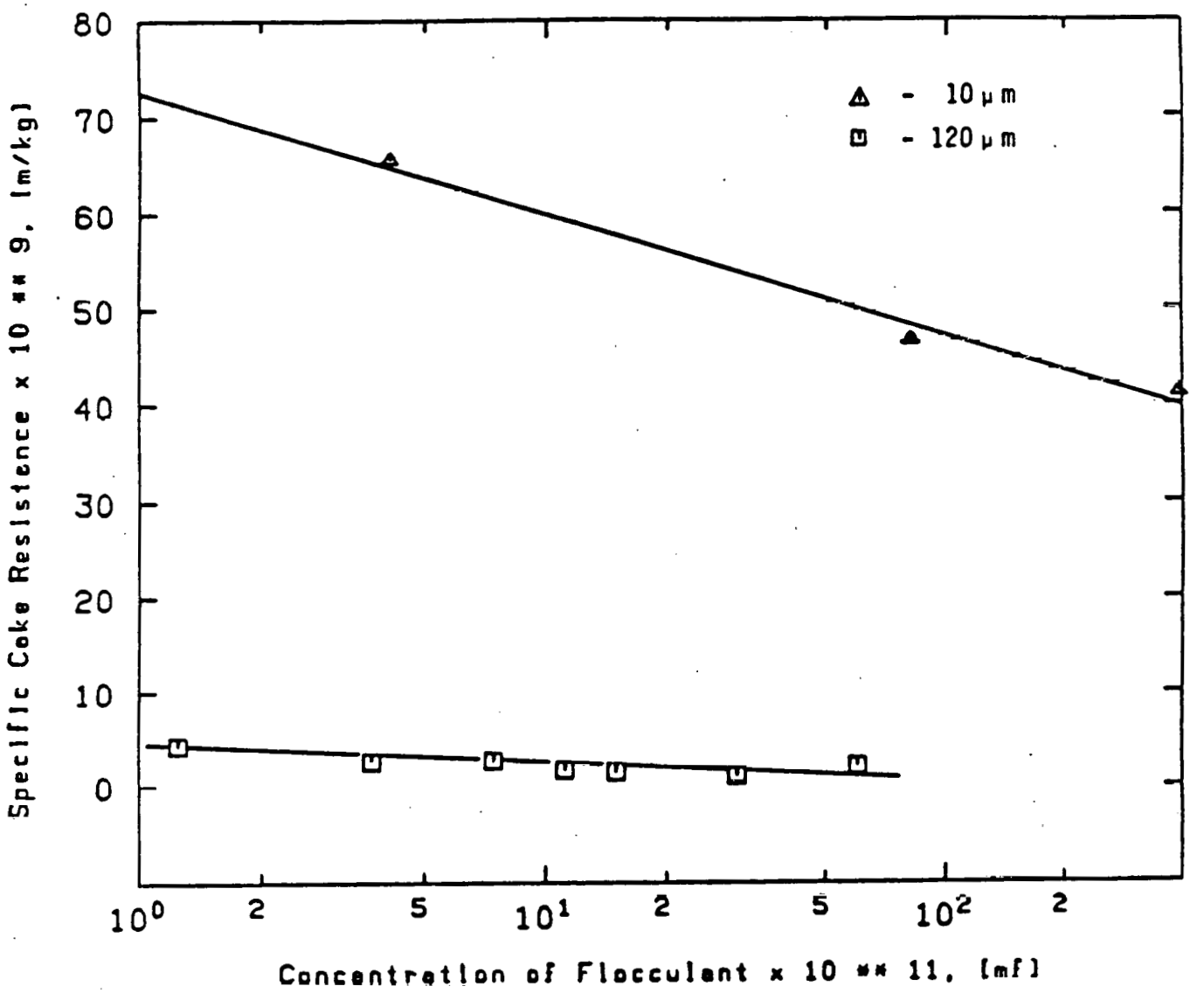

Figure 71: Effect of Flocculation on the Specific Cake Resistance

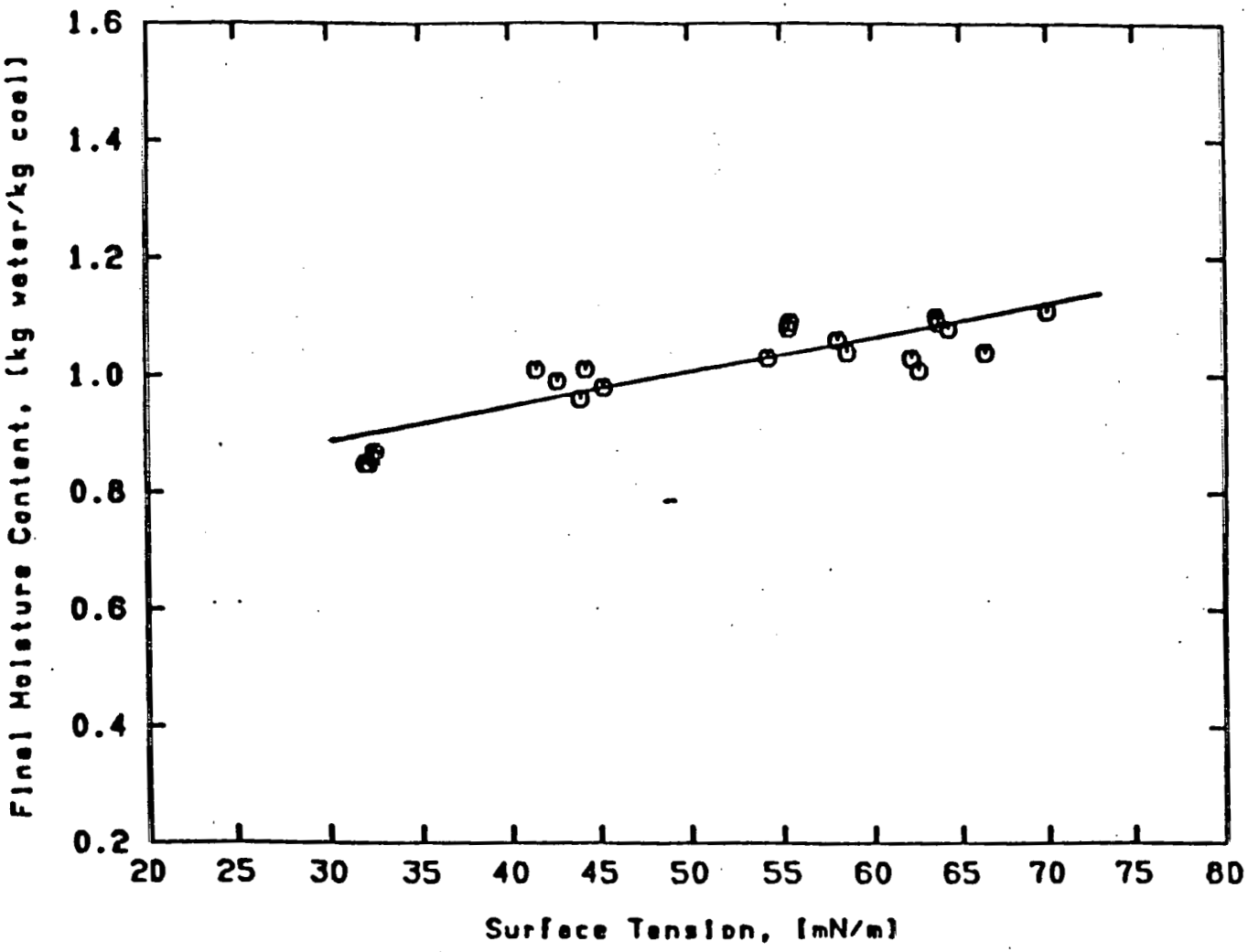

Figure 72: Effect of Surface Tension on the Cake Moisture

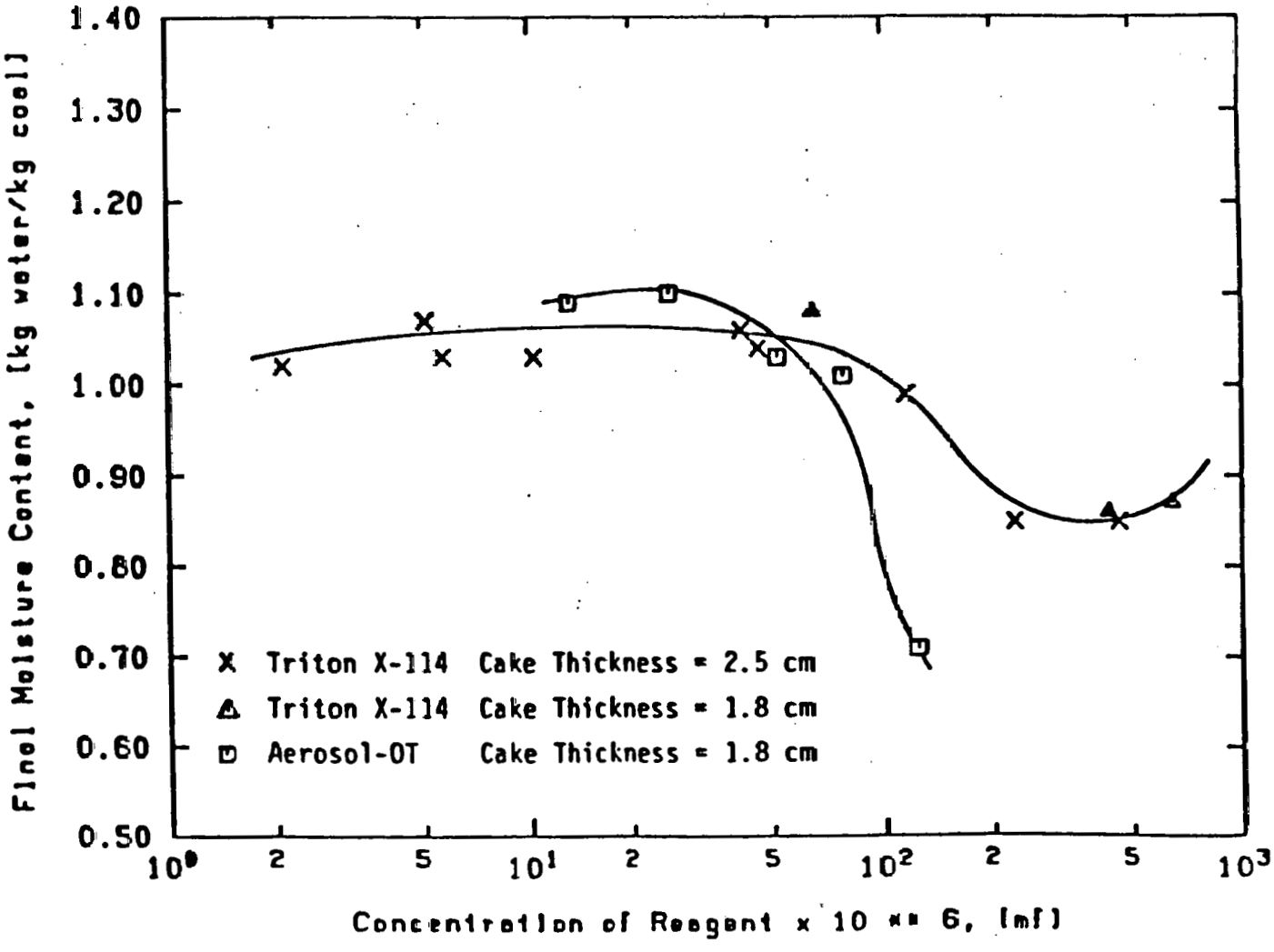

Figure 73: Effect of the Initial Concentration of Surfactant on the Cake Moisture

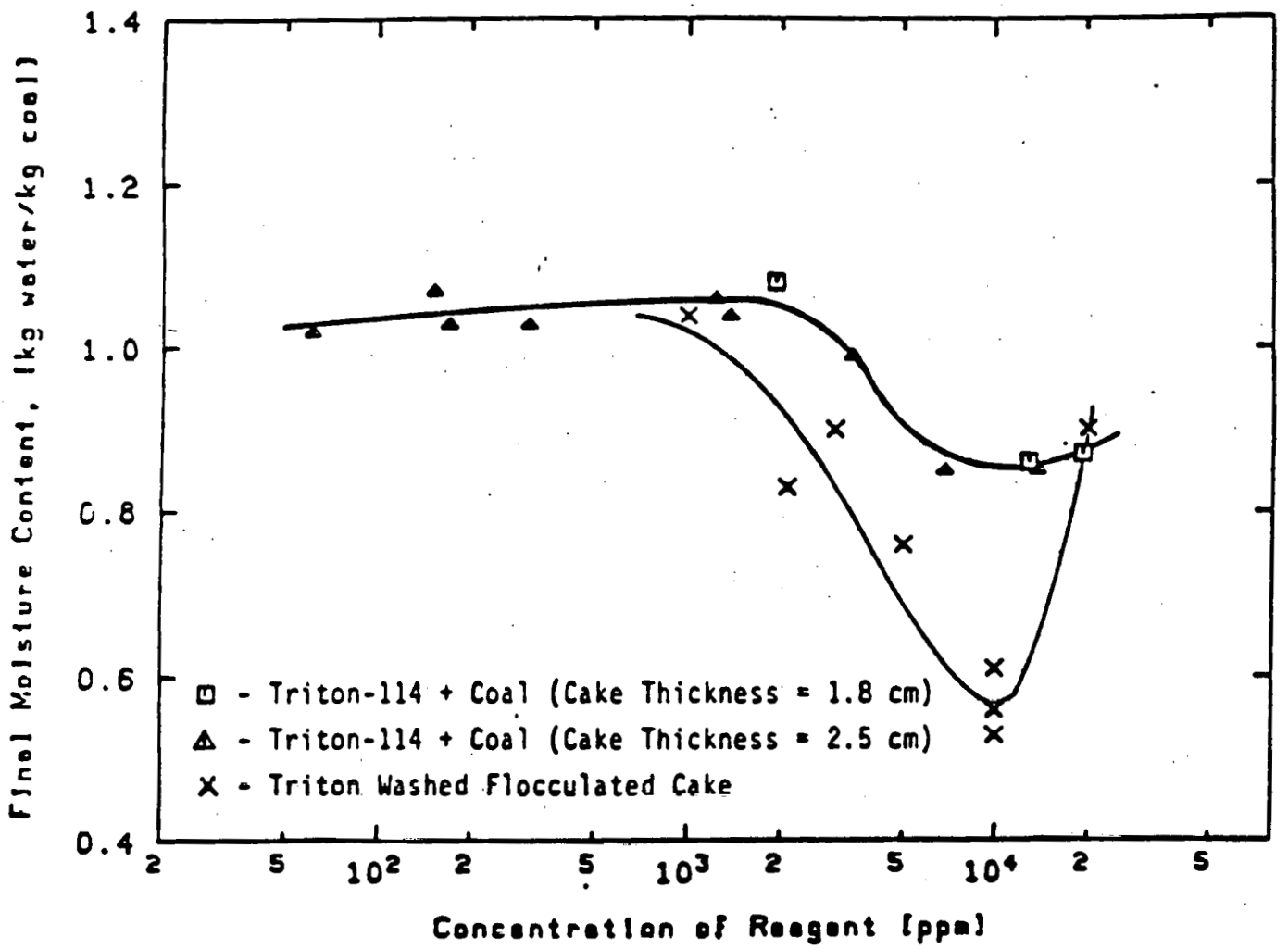

Figure 74: Comparison Between Pretreatment and Combined Pretreatment - Post-treatment Processes

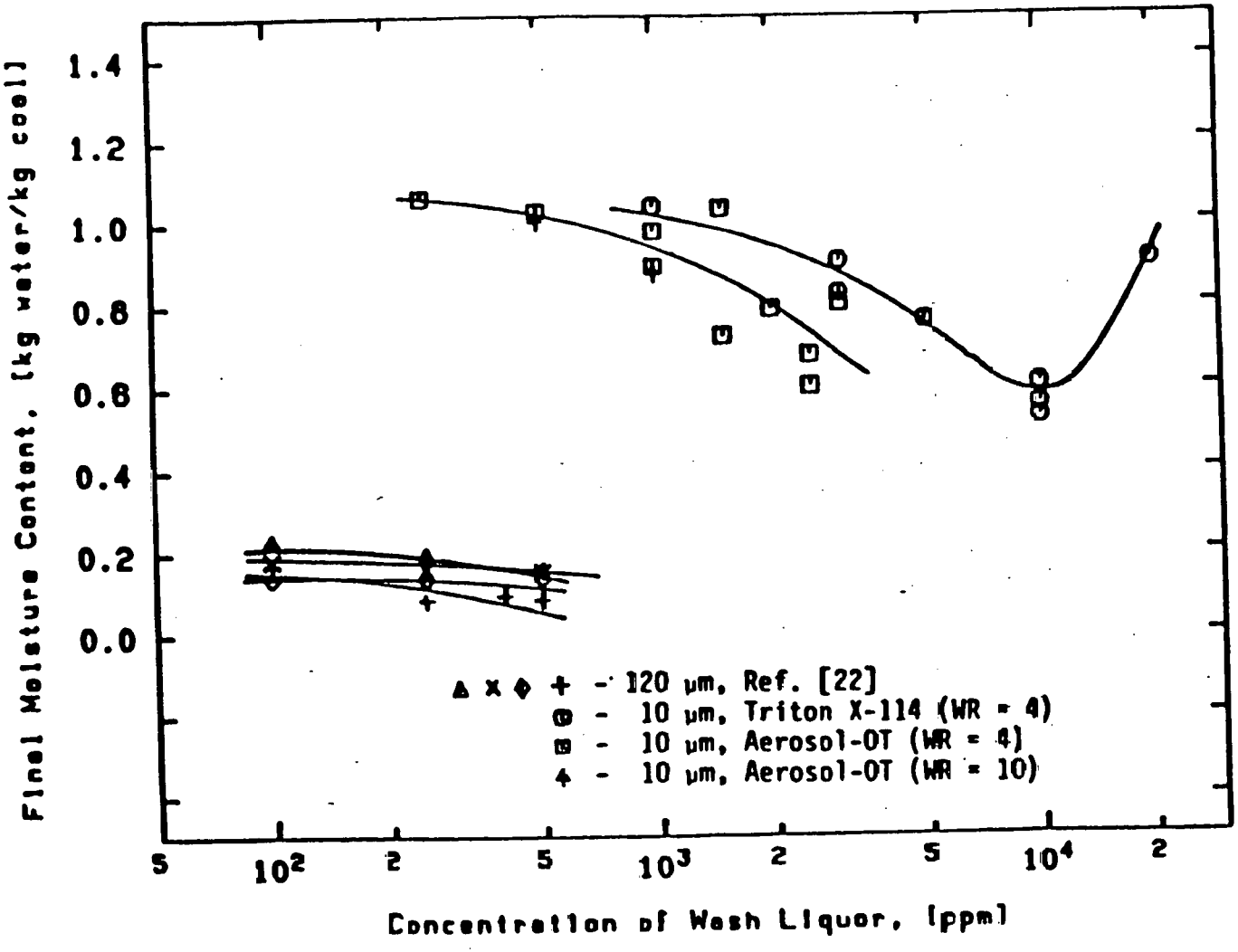

Figure 75: Effect of Concentration of Wash Liquor on the Cake Moisture